NTNU – Trondheim
Norwegian University of
Science and Technology

Symplectic integration of a one-dimensional Hamiltonian system of permanent magnets oscillating in a gravitational field.

A mechanical analogue to a thermodynamic system.

Sigve Karolius

Chemical Engineering and Biotechnology
Submission date: June 2014
Supervisor: Tore Haug-Warberg, IKP
Co-supervisor: Pablo Bouza, IKP
Thomas Jefferson Wilcox, Retired

Norwegian University of Science and Technology
Department of Chemical Engineering

Summary

The objective of this work was to analyze a mechanical analogue to a thermodynamic system. The main goal was to investigate the temperature distribution in a vertical system of oscillating magnets in a gravitational field and assess whether the system could be used as a model of an atmosphere of an ideal gas. In order to answer this question it was necessary to integrate the equations of motion over a long time interval. The reason for this is that the thermodynamic interpretation reduced the mechanical phase space for each magnet to a common statistical interpretation. The long time interval guaranteed that a truly thermodynamic system of magnets would have enough time to occupy each state at least once.

Most of the work considered integration methods that ensured the integration remained on the energy surface throughout the interval, known as symplectic integration methods. A total of seven methods of different order and properties were derived, implemented and compared. The low order methods were used to study general properties of symplectic methods on the simple harmonic oscillator. It was shown that even though the symplectic methods conserved the phase space trajectory they caused the Hamiltonian (i.e. the total energy) to oscillate. Based on the simulations it was concluded that as long as the Hamiltonian was conserved to the fifth decimal place the symplectic method reproduced the analytical phase space trajectory. This was supported by the long-time simulations that were performed using a linear system of interacting ODEs with oscillatory solutions to compare the remaining six methods. It was found that the order of the numerical method is significant when considering oscillatory systems, i.e. adding symplectic property to a method will not compensate for the increased accuracy of a higher order method. The superior method was a third order symplectic Runge-Kutta-Nyström method (STRKN) that was designed to exactly integrate linear oscillatory systems. Furthermore, the method was superior to a fourth order Runge-Kutta-Nyström method; this implies that fitting the numerical method a-priori to the form of the solution of the system has a significant impact on the accuracy of the integration.

The simulations of the magnets showed that the probability density concerning the displacement of the velocity for all the magnets in the system could be described using the same Maxwell-Boltzmann density function. From this result it was conclude that, analogue to a thermodynamic system, the temperature was constant throughout. Additionally, the results showed that the probability density concerning the position displacement of each magnet around static equilibrium depends on the index of the magnet in the stack. The width of the density function, which describes the amplitude of the oscillations, increased towards the top of the stack. The thermodynamic analogue to this result is the density, which consequently decreases along the height. Subsequent simulations of systems with equal initial conditions but different total energy showed that the force of the system on the environment, analogue to the pressure, increased linearly. Based on the statistical analysis of the thermodynamic analogue of the results it was concluded that the system of magnets could be used as a model of an atmosphere of an ideal gas.

Sammendrag

Formålet med dette arbeidet var å gjennomføre en analyse av hvordan et mekanisk system tilsvarer et termodynamisk system. Hovedspørsmålet var å undersıke temperaturfordelingen i et vertikalt system av oscillerende magneter i gravitasjonsfeltet og vurdere om modellen kunne brukes til å illustrere en atmosfœre bestående av en ideell gass. For å svare på dette spørsmålet var det nødvendig å integrere bevegelsesligningene over et langt tidsintervall, da den termodynamiske tolkningen reduserer det mekaniske tilstandsrommet for hver magnet til én statistisk fordeling som felles for alle magnetene. Intensjonen med det lange tidsintervallet var å garantere at magnetene fikk nok tid til å besøke hele tilstandsrommet minst minst én gang i løpet av integrasjonen dersom systemet var termodynamisk.

Mesteparten av arbeidet i dette prosjektet bestod i å vurdere integrasjonsmetorder som garanterer at de numeriske oppdateringene forblir på energimanifoldet gennom hele integrasjonsintervallet, kjent som symplektiske integrasjonsmetoder. Syv forskjellige metoder med forskjellige egenskaper og orden ble utledet, implementert og sammenlignet. Metodene med lav orden ble brukt til å integrere en harmonisk oscillator for å vise karakteristiske trekk symplektiske metoder. Det ble vist at selv om metodene bevarte det mekaniske tilstandsrommet førte de til at verdien av Hamiltonfunksjonen (dvs. den totale energien) begynte å oscillere. På bakrunn av simuleringene ble det konkludert med at den analytiske løsningen ble tilnrmet nøyaktig reprodusert dersom verdien av Hamiltonfunksjonen var knstant til femte desimal. Simuleringene over lange tidsintervall, som ble gjennomført på et system bestende sammenhengende hamoniske oscillatorer, støttet også denne observasjonen. Disse simuleringene viste også at orden på den numeriske metoden spiller en viktig rolle når man jobber med svingesystemer. Dette vil si at det å gjøre en metode symplektisk vil ikke alene være nok til å kompensere for lavere numerisk orden. Den beste metoden var en symplectisk Runge-Kutta-Nyström metode av orden tre (STRKN) som var tilpasset slik at den integrerte et lineœrt oscillatorisk system eksakt. Denne metoden var også bedre enn en fjerde orden Runge-Kuttas-Nyström-metode. Dette resultatet støttet konklusjonen om at å a-priori tilpasse en numerisk metode til å integrere en basisfunksjon med samme form som løsningen fører til betydelig økt nøyaktighet.

Simuleringene av magnetsystemet viste at sannsynlighetstettheten for hastighetene til hver magnet kunne bli erstattet med én Maxwell-Boltzmann-funksjon. Fra dette resultatet ble det konkludert at, sammenlignet med et termodynamisk system, var temperaturen konstant. I tillegg viste resultatene at sannsynlighetstettheten for posisjonen til hver magnet var sentrert rundt den statiske likevektsposisjonen. Bredden på tetthetsfunksjonen, som beskriver amplituden av svingningene, økte mot toppen av systemet. Den termodynamiske analog til dette resultatet er tettheten, som dermed minsker langs høyden. Det ble også gjenomført simuleringer med forskjellig total energi, men samme startbetingelser, som viste at kraften på den øverste magneten økte lineœrt med energien i systemet. Den termodynamiske analogien til kraften på den øverste magneten er trykk. Basert på resultatene ble det konkludert med at systemet med magneter kan brukes som en modell for en atmosfœre av en ideell gass.

Preface

This work is dedicated to everyone that has made the past five years an unforgettable experience. I am grateful and consider myself lucky to have a family that supports me and is patient with my behavior during periods of high work load.

The thesis would never have been possible without the guidance and encouragement of my main supervisor, Tore Haug Warberg. Additionally I have been lucky to have two excellent co-supervisors; Pablo Bouza and Thomas Jefferson Wilcox, they have both been important sources of knowledge, experience and motivation. This made it possible for me to complete this work without having any prerequisite experience from many of the main subjects in this work. My girlfriend Brittany Hall has also been astonishingly patient and I am grateful for her direct contribution of proof reading this thesis, all imperfections are undoubtably my own doing.

Declaration of compliance
I declare that this is an independent work according to the exam regulations of the Norwegian University of Science and Technology (NTNU).

Place and date: Signature:

Trondheim 23.06.2014

Table of Contents

List of Tables

List of Figures

List of symbols

Latin symbols

$a_{ij}, \bar{a}_{ij}$	inner weight in Runge-Kutta-Nyström method	
$b_i, \bar{b}_i$	weight in Runge-Kutta-Nyström method	
c_i	node in Runge-Kutta-Nyström method	
c	force of fully compressed spring (Hooke's law)	$[kgms^{-2}]$
$\mathcal{F}$	force	$[N]$
F	generating function	$[Js]$
g	gravitational constant	$[ms^{-2}]$
G	unspecified function (with continuous second derivative)	$[Js]$
h	numerical step size	
$\mathcal{H}$,$\tilde{\mathcal{H}}$	Hamiltonian, canonically transformed Hamiltonian	$[J]$
k	"spring constant" (Hooke's law)	$[kgs^{-2}]$
k_m	magnetic force field constant	$[kgm^3s^{-2}]$
L	length	$[m]$
$\mathcal{L}$,$\tilde{\mathcal{L}}$	Lagrangian, canonically transformed Lagrangian	$[J]$
m	mass	$[kg]$
n	number of components in a system	
$\mathcal{O}$	algebraic error	
p,p_i/P_i	canonical momentum / canonically transformed momentum	$[Nm]$
q,q_i/Q_i	generalized position / canonically transformed position	$[m]$
$\dot{q}$,$\dot{q}_i$	generalized velocity	$[ms^{-1}]$
$\mathcal{S}$,$\tilde{\mathcal{S}}$	action, canonically transformed action	$[Js]$
T	kinetic energy	$[J]$
U	potential energy	$[J]$
t	time	$[s]$
x, y	cartesian position	$[m]$
z	coefficient used for exponential fitting of Runge-Kutta-Nyström	

Greek symbols

$\bar{\alpha}_{ij}$	inner weight in exponentially fitted Runge-Kutta-Nyström method
$\beta_i, \bar{\beta}_i$	weight in exponentially fitted Runge-Kutta-Nyström method
ζ_i	element in the transformed canonical coordinate vector
η_i	element in the canonical coordinate vector
λ	scaling constant in canonical transformations
λ_i	eigenvalue
μ	scaling constant (restricted canonical transformations)
ν	scaling constant (restricted canonical transformations)
φ	probability density
Φ	cumulative probability
ω_0	constant used to scale equations of motion for a system

Mathematical symbols

$\mathbf{A}^{-1}$	inverse of matrix A	
$f(x)\Big\vert_{x=0}$	function $f(x)$ evaluated at $x = 0$	
$df(x, y, z)$	total derivative of the function f	$df = f_x dx + f_y dy + f_z dz$
δy	variational quantity	$\delta y \equiv \frac{\partial y}{\partial x}\Big\vert_0 dx$
U_t	partial derivative of U wrt. t	
y'	"Newtonian" derivative notation	$y'(x) = \frac{dy}{dx}$
$\dot{y}, \ddot{y}$	time derivative	$\frac{dy}{dt}, \frac{d^2y}{dt^2}$
$\det \lvert\mathbf{A}\rvert$	determinant of a matrix	

Matrices and vectors

$\mathbf{A}$	coefficient matrix	
$\mathbf{M}$	symplectic matrix	
$\mathbf{T}$	tridiagonal matrix	
$\mathbf{J}$	anti-symmetric matrix	
$\mathbf{S}$	eigenvector matrix	
$\mathbf{\Lambda}$	eigenvalue matrix	
$\boldsymbol{\eta}$	vector of canonical coordinates	$[q_i \dots q_n, p_i \dots p_n]^T$
$\boldsymbol{\zeta}$	vector of transformed canonical coordinates	$[Q_i \dots Q_n, P_i \dots P_n]^T$
$\mathbf{\Theta}'$	numerical flow jacobian	

List of Acronyms

ODE	ordinary differential equation
RK	Runge-Kutta
RKN	Runge-KuttaNyström
ERKN	exponential Runge-KuttaNyström
SRKN	symplectic Runge-KuttaNyström
SERKN	symplectic and exponential Runge-KuttaNyström

Chapter 1

Introduction

1.1 Background and motivation

The background of this work is a question that is asked in the article Coombes and Laue (1985). It concerns the temperature a vertical column that is filled with in a gas and isolated from its surroundings, i.e. it is an adiabatic system.
The question is as follows:

> *If a vertical column of air which is adiabatically enclosed is in thermal equilibrium, is the temperature the same throughout the column or is there a temperature gradient along the direction of the gravitational field?*

The article suggests this question as an interesting teaching exercise for statistical mechanics, however it can also be used in classical thermodynamics as well. While the question may seem trivial at first, it creates an apparent paradox where two answers, which each individually seem reasonable, contradict one another:

1. *There is no temperature gradient because a system which is in thermal equilibrium has the same temperature throughout.*
2. *The temperature decreases as one goes up the column for the following reasons:*
   (a) *Energy conservation implies that every molecule looses kinetic energy as it travels upward, so that the average kinetic energy of all molecules decreases with height.*
   (b) *Temperature is proportional to the average molecular kinetic energy.*

The answers both seem satisfactory but there is a fundamental assumption hidden in answer $(2a)$. At first glance this might seem to be the most convincing argument for as-

suming that answer (2) is correct; what happens if the number of particles decreases along the height of the column. In fact this is the essence of the answer that is given in Coombes and Laue (1985), that the gravitational force does not decrease the kinetic energy of the particles in the top of the column, but rather the number of particles. This way the mean kinetic energy and consequently the temperature remains constant along the height of the column.

While the answer was presented here as a simple logical argument, it can also be treated rigorously as shown in Velasco et al. (1996) using statistical mechanics. In fact, the logical argument is based on the assumption that the Boltzmann equation is valid such that the Maxwell-Boltzmann probability distribution is valid for each particle in the column. This statement has a much deeper impact than the sentence above implies and understanding the fundamental theory requires insight beyond what most people are ever going to need to learn. However, if this can be visualized it would be a wonderful tool to illustrate the thermodynamic properties of the ideal gas.

Similar systems have been studied in the past, in the article Ibsen et al. (1997) a mechanical system of hard rods stacked vertically in the presence of a gravitational field. This work will use a similar system of idealized dipole magnets which will naturally have a static equilibrium distribution where the separation between the magnets will increase along the height of the column. If the system shows ideal gas behavior the kinetic energy of the top and bottom magnet should be equal. Moreover, the amplitude of the magnets can be used to illustrate that the density of the system decreases along the height. This would be a visual way of illustrating the temperature and density dependence of height of an atmosphere of an ideal gas. A less visual but important property is the pressure dependence with respect to energy, which will be the force exerted on the top of the stack.

This motivates the study to check wether the mechanical system can be used as a model of a thermodynamic atmosphere of an ideal gas.

1.2 Objective and scope of the work

The objective of this work is to perform a complete analysis of an analytical description of a simple mechanical analogue to a general thermodynamic system. Specifically, a system of small permanent magnets oscillating in a gravitational field will be simulated. The simulation incorporates several classical topics from physics such as: Dynamics of oscillatory mechanical systems, symplectic numerical integration, and the statistical interpretation of thermodynamic variables. The theoretical scope of this work is limited to classical mechanics and symplectic integration whereas the statistical interpretation will be considered using well known results from statistical mechanics without further theoretical consideration.

As a fundamental approximation it is assumed that the behavior of the magnets is comparable to that of ideal dipoles. This assumption results in a simple power law model describing the potential energy of the magnets; being proportional to the inverse of the distance between the dipoles. A linear description of the system is obtained by linearizing the potential energy around the static equilibrium distribution of the magnets. The linear model can subsequently be analyzed using eigenvalue / eigenvector decomposition of the coupling matrix describing the system.

The numerical implementation is performed such that the integration steps are guaranteed to remain on the energy surface, i.e. symplectic integration. This part of the work account for the largest work load of the thesis and several integration methods are derived and tested in order to consider which method is best suited for the system of magnets. The reason why it is desirable to use symplectic integration methods is that they prevent numerical diffusion of potential energy to kinetic or gravitational energy. A special type of integration meted that is of particular interest is fitted to linear oscillatory systems (i.e. it exactly integrates systems whose solutions are trigonometric functions). The different integration methods are tested in order to study the importance of the different properties when applied to a linear system of oscillatory ODEs.

One important result of the simulation is the probability density concerning the displacement and velocity of each magnet in the system. The ultimate question is whether or not the probability density of the velocity depends on the absolute position of the magnet. The analogue to real thermodynamic systems is e.g. the question of whether the temperature of the atmosphere is constant or varies with altitude.

1.3 Structure of the thesis

The thesis is divided into four main chapters where the first two contains the major theoretical work. The main goal of these chapters is to introduce physical mechanics and symplectic integration on a level such that it is within the technical level of anyone with a background from basic university level mathematics. Chapter (2) introduces the basic theory of physical mechanics. The introduction starts at the Lagrangian formulation, introduces the Hamiltonian representation through the Legendre transformation and ends up at the canonically transformed representations of the Hamiltonian representation. The last topic is particularly important in the context of this work since it is used as the basis for understanding symplectic integration methods. This chapter is supported by appendix (B) and (C), respectively, considering calculus of variations and a rigorously derived relation which proves that the Hamiltonian for the systems in this work is equal to the total energy.

Researching, understanding, deriving and implementing numerical integration methods accounts for approximately half of the time spent working on this thesis. Chapter (3) is therefore of considerable size and much time and effort has been spent trying to tie the symplectic integration methods to the concept of canonical transformations from chapter (2). The reason for the focus on integration methods is that temporal integration of oscillatory systems is a challenge that requires special methods that guarantee that the numerical trajectory remains on the energy manifold throughout. Additionally, the statistical interpretation of the results also render commercial multistep methods, such as $ode45$, impractical compared with an explicit fixed step size methods. The literature study revealed that the available articles are mathematically dense and hard to understand, therefore the derivation of all the methods is considered in detail in this work; however, the methods themselves were originally proposed elsewhere. A straight forward implementation of the methods is shown in appendix (E). However, the methods were implemented in MatLab and the implementation in the appendix is consequently computationally slow compared with the speed implementation of the built in MathWorks methods. The version of the methods that was used in this work is consequently scripted such that the speed was increased. This implementation along with all the additional functions can be found in Karolius (2014); however with respect to the integration methods, the clarity of the script is compromised in the latter implementation.

A total of seven methods were derived and compared in this work. The numerical experiments in chapter (4) compare the methods using the simple harmonic oscillator and a chain of interacting oscillators, both of which are first order homogeneous ODEs. It is undoubtable a drawback that the methods are not studied using a nonlinear system; however, lack of experience in the analysis of nonlinear dynamics made it necessary to limit the experiments to the linear case. The comparison of the models was performed based on the solution of the linear system using eigenvector/eigenfunction expansion in appendix (D). This allowed the initial conditions to be estimated based on the numerical solution at every numerical time step.

The model of a system consisting of seven vertically stacked magnets in a gravitational field was introduced and simulated in chapter (5). The groundwork for the development of

the nonlinear and linearized model was originally performed in Warberg (2013), however a derivation that includes several intermediate steps and mathematical details was performed in appendix (A). The model validation focused on validating the static equilibrium conditions and the diffusion of kinetic energy for low total energy simulations where the model logically could be assumed to be linear. The statistical interpretation of the simulations was performed in the last sections of the chapter. The interpretations used the velocity displacement probability distribution to consider the mean kinetic energy, analogous to the thermodynamic temperature. The absolute force exerted on the top magnet was also studied, analogous to the pressure, as a function of the total energy in the system. The validity of the statistical interpretation was also considered by investigating the ergodic behavior of the system.

The final two chapters (6) and (7) respectively discusses the results, suggests topics for expanding this work and finally provides a brief and concise conclusion.

Chapter 2

Classical Mechanics

This chapter introduces conventional terminology and concepts from classical mechanics, which will be used throughout this work. The theory from the chapter is relevant in order to understand the derivation of mechanical equations of motion and it also serves as the foundation on which the understanding of symplectic integration is based.

The chapter is divided into sections that provides a brief introduction into the basic concepts before an example applies the concept. The systems that are considered in the examples are shown in figure (2.1).

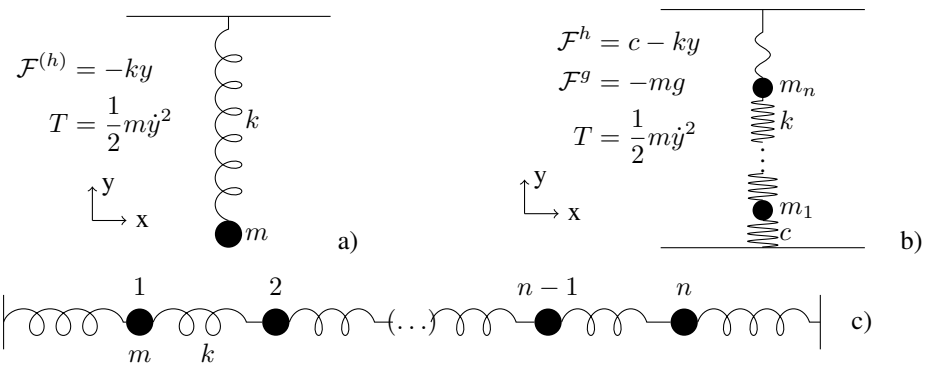

Figure 2.1: a) Harmonic oscillator b) Chain of harmonic oscillators in a gravitational field ,c) Chain of harmonic oscillators

2.1 Lagrangian Mechanics

This section defines a scalar function known as the Lagrangian as the origin of classical mechanics. The purpose of this section is to serve as an introduction to Hamiltonian mechanics in section (2.2).

2.1.1 The Lagrangian function

The Lagrangian ($\mathcal{L}$) is a scalar function that is defined as the difference between the kinetic ($\mathbf{T}$) and potential ($\mathbf{U}$) energy as shown in equation (2.1).

$$\mathcal{L}(\mathbf{q}, \dot{\mathbf{q}}) = \mathbf{T}(\dot{\mathbf{q}}) - \mathbf{U}(\mathbf{q}) \tag{2.1}$$

Where the $\mathbf{q}$ and $\dot{\mathbf{q}}$ represent the position and its time derivative, i.e. the velocity.

The systems in this work all have second order dependence with respect to velocity in the kinetic energy; they can all be described using the following expression:

$$T = \sum_{\forall i} \frac{1}{2} m \dot{q}_i^2$$

The analytic expression for the potential energy, however, is formulated from the force fields as shown below.

$$U - U^o = -\int_0^q \mathcal{F}(\gamma) d\gamma$$

Where the initial potential energy U^o can be chosen to present the results in an intuitive way, e.g. using the static equilibrium values of the potential energy. The potential energy for larger systems is found by summing up the contributions from all the elements in the system as follows:

$$U - U^o = \sum_{\forall i} U_i - U_i^o$$

The systems in this work can all be expressed based on the general form of the Lagrangian shown in equation (2.2).

$$\mathcal{L} = \sum_{\forall i} \frac{1}{2} m \dot{q}_i^2 - \sum_{\forall i} U_i \tag{2.2}$$

The examples at the end of the section shows how the different force potentials in the systems in figure (2.1) is used to determine the potential energy and the Lagrangian functions for the systems.

Another variable that is derived from the Lagrangian function is the momentum.

$$p_i \hat{=} \frac{\partial \mathcal{L}}{\partial \dot{q}_i} = m \dot{q}_i \tag{2.3}$$

All of the systems in this work have potential energy that is independent of the velocity; this means that the form of the momentum in equation (2.3) is common for all of the systems in this work.

This example shows how the different force models for the systems systems in figure (2.1) can be used to derive the potential energy and formulate the Lagrangian.

Harmonic oscillator

The simple harmonic oscillator in system a) in the figure and the potential energy becomes:

$$U = -\int_0^y -k\gamma d\gamma = \frac{1}{2}ky^2$$

The Lagrangian function can now be formulated from the definition.

$$\boxed{\mathcal{L}(\mathbf{q}, \dot{\mathbf{q}}) = \frac{1}{2}m\dot{q}^2 - \frac{1}{2}kq^2}$$

Chain of harmonic oscillators

The total potential energy for the chain of harmonic oscillator (c) is formulated by summing the contributions from each mass point.

$$U^{(h)} = -\sum_{i=0}^{n} \frac{1}{2}k(x_{i+1} - x_i)^2$$

Note that the walls are included in the summation, however since they do not move they must satisfy boundary conditions: $\dot{x}_0 = \dot{x}_{n+1} = 0$. The Lagrangian function becomes:

$$\boxed{\mathcal{L}\left(\mathbf{x}, \dot{\mathbf{x}}\right) = \frac{1}{2}\sum_{j=1}^{n} m\dot{x}_j^2 + \frac{1}{2}\sum_{j=0}^{n} k(x_{j+1} - x_j)^2}$$

Chain of harmonic oscillators in a gravitational field

The potential energy due to the spring takes the following form:

$$U^{(h)} = -\int_0^y c - k\gamma d\gamma = -cy_i + \frac{1}{2}ky_i^2 = \sum_{i=0}^{n} \frac{k}{2}(y_{i+1} - y_i)^2 - c(y_{i+1} - y_i)$$

However, in contrast to the horizontal chain this system also includes the gravitational potential.

$$U^{(g)} = \sum_{i=0}^{n} m_i g y_i$$

The Lagrangian can finally be formulated as:

$$\boxed{\mathcal{L}\left(\mathbf{y}, \dot{\mathbf{y}}\right) = \frac{1}{2}\sum_{i=1}^{n} m\dot{y}_i^2 + \sum_{i=0}^{n} c(y_{i+1} - y_i) - \frac{1}{2}k(y_{i+1} - y_i)^2 - mgy_i}$$

2.1.2 The Lagrange equations of motion

In order to derive the Lagrange equations of motion, a new quantity known as the action ($\mathcal{S}$) is needed. The action is defined as the integral of the Lagrangian over a path from time a to b. While initially there is no limit to which path that is considered in the action integral, the interesting path is the one that minimizes the action, i.e. obeys equation (2.4).

$$\min_{q_i(t)} \mathcal{S}[\mathbf{q}(t)] = \min_{q_i(t)} \int_a^b \mathcal{L}(\mathbf{q}, \dot{\mathbf{q}}, t)dt = 0 \tag{2.4}$$

This path will be referred to as the trajectory and it represents the path of least resistance, i.e. the natural path that the system will follow. The idea that the trajectory follows the path of minimized action is known as Hamilton's principle and since it is a fundamental assumption, it must be obeyed by both the Lagrangian and Hamiltonian representations.

The mathematical formulation of Hamilton's principle is shown in equation (2.5) and it is a direct result of the minimization problem in equation (2.4). Appendix (B) considers the minimization of simple functionals and shows how the Euler-Lagrange equations and Hamilton's principle as a general mathematical result.

$$\frac{\delta \mathcal{S}}{\delta \mathbf{q}(t)} = 0 \quad ; \mathbf{q} = [q_1 \ \dots \ q_n]^T \tag{2.5}$$

The minimization does not result in an analytic expression for the trajectory of the system but a requirement, known as the Euler-Lagrange equation, that the trajectory of the system must fulfill in order to obey Hamilton's principle. All the systems in this work have the same form of the Lagrangian and the Euler-Lagrange equation (2.6) can therefore be used in order to obtain the equations of motion for all the systems.

$$\frac{d\mathcal{L}}{dq_i} - \frac{d}{dt}\left[\frac{\partial \mathcal{L}}{\partial \dot{q}_i}\right] = 0 \quad ; i = [1 \dots n] \tag{2.6}$$

There is one Euler-Lagrange equation for each displacement degree of freedom in the system, i.e. a one-dimensional system of n elements also has n Euler-Lagrange equations. The equations of motion are second order ODEs of the form shown in equation (2.7).

$$m\ddot{\mathbf{q}} + \boldsymbol{\mathcal{F}} = 0 \quad ; \mathcal{F} = \frac{\partial \mathcal{L}}{\partial q_i} \tag{2.7}$$

There is one equation of motion per Euler-Lagrange equation because they are second order and thus require twice as many initial conditions. The system of second order equations can also be written as a system of first order equations. This is considered in section (2.2.2) where they are compared with the canonical Hamiltonian equations of motion.

The following example considers the derivation of the Lagrangian equations for the systems whose Lagrangian function was derived in the example in the previous section.

This example is concerned with obtaining the Lagrange equations of motion for the systems from the example in section (2.1.1). The Euler-Lagrange equation (2.6) from this section is used for all the cases.

Harmonic oscillator

$$\boxed{\ddot{q} = -\omega_0^2 q \quad ; \omega_0 = \sqrt{\frac{k}{m}}}$$

Chain of harmonic oscillators

The chain of harmonic oscillators follows the same steps as the harmonic oscillator. The differentiation below is performed in one step and results in n Euler-Lagrange equations.

$$\begin{aligned}
\ddot{x}_j &= \frac{k}{m}(x_2 - x_1) - \frac{k}{m}(x_1 - x_0) \\
\ddot{x}_j &= \frac{k}{m}(x_{j+1} - x_j) - \frac{k}{m}(x_j - x_{j-1}) \quad ; j = 2 \ldots n-1 \\
\ddot{x}_j &= \frac{k}{m}(x_{n+1} - x_n) - \frac{k}{m}(x_n - x_{n-1})
\end{aligned}$$

Note that one must use some care when performing the differentiation because of the summation over the different oscillators in the chain. The resulting ODE for one oscillator in the chain is shown below.

$$\boxed{\begin{aligned}
&\ddot{\mathbf{x}} = -\omega_0^2 \mathbf{T}\mathbf{x} + \omega_0^2(x_0\mathbf{e}_1 + x_{n+1}\mathbf{e}_n) \quad ; \omega_0 = \sqrt{\frac{k}{m}} \\
&\mathbf{e}_1 = [1\ 0\ \ldots]^T \quad \mathbf{e}_n = [0\ \ldots\ 1]^T \quad \mathbf{y} = [y_1\ \ldots\ y_n]^T
\end{aligned}}$$

Chain of harmonic oscillators in a gravitational field

The derivation of the Lagrangian equations of motion for the follows the same procedure as the harmonic chain.

$$\begin{aligned}
\ddot{y}_1 &= -g - \frac{c}{m} + \frac{k}{m}(\ y_2\ -\ y_1\ ) + \frac{c}{m} - \frac{k}{m}(y_1 - y_0) \\
\ddot{y}_j &= -g - \frac{c}{m} + \frac{k}{m}(y_{j+1} - y_j) + \frac{c}{m} - \frac{k}{m}(y_j - y_{j-1}) \quad ; j = 2, \ldots, n-1 \\
\ddot{y}_n &= -g - \frac{c}{m} + \frac{k}{m}(y_{n+1} - y_n) + \frac{c}{m} - \frac{k}{m}(y_n - y_{n-1})
\end{aligned}$$

In contrast to the harmonic chain this is not derived in deviation variables and further analysis is necessary in order to remove the q_0 and q_1 terms.

$$\boxed{\begin{aligned}
&\ddot{\mathbf{y}} = -\omega_0^2 \mathbf{T}\mathbf{y} + \omega_0^2(y_0\mathbf{e}_1 + y_{n+1}\mathbf{e}_n) - g\mathbf{e} \quad ; \omega_0 = \sqrt{\frac{k}{m}} \\
&\mathbf{e} = [1\ \ldots\ 1]^T \quad \mathbf{e}_1 = [1\ 0\ \ldots]^T \quad \mathbf{e}_n = [0\ \ldots\ 1]^T \quad \mathbf{y} = [y_1\ \ldots\ y_n]^T
\end{aligned}}$$

2.1.3 Determining the static equilibrium distribution

The systems in this work are all described by Lagrangian equations of motion of the form shown in equation (2.7). This sections shows how the static equilibrium of the Lagrangian equations of motions can be used in order to determine the static equilibrium positions for the systems in this work. Moreover it will be shown how the solution can be used in order to turn the inhomogeneous second order ODEs from the example in the previous section into a homogeneous system. Static equilibrium implies that the time derivative in equation (2.7) is equal to zero, i.e. the forces balance exactly as shown in equation (2.8).

$$\boldsymbol{\mathcal{F}}(\mathbf{x}^0) = 0 \quad ; \mathcal{F} = \frac{\partial \mathcal{L}}{\partial q_i} \tag{2.8}$$

The section will use the horizontal harmonic chain, whose static equilibrium is shown below, to outline the general strategy if determining the static equilibrium positions.

$$-\mathbf{T}\mathbf{x}^0 + x_0^0\mathbf{e}_1 + x_{n+1}^0\mathbf{e}_n = 0 \Leftrightarrow \mathbf{x}^0 = x_0\mathbf{T}^{-1}\mathbf{e}_1 + x_{n+1}\mathbf{T}^{-1}\mathbf{e}_n$$

Next the position of the system is defined to be 0 at the left wall and L at the right:

$$x_0^0 = 0 \qquad x_{n+1}^0 = L$$

The static equilibrium equations of motion can now be written in the following way:

$$\mathbf{T}\mathbf{x}^0 = L\mathbf{T}^{-1}\mathbf{e}_n \quad ; \mathbf{T} = \begin{bmatrix} 2 & -1 & & \\ -1 & 2 & -1 & \\ & \ddots & \ddots & \ddots \\ & & -1 & 2 \end{bmatrix}$$

The following explicit formulae for the inverse of a tridiagonal matrix with constant coefficients was verified by performing numerical inversions.

$$T_{ij}^{-1} = \begin{cases} \frac{1}{N+1}(N+1-i)j & \text{if } i \geq j \\ \frac{1}{N+1}(N+1-j)i & \text{otherwise} \end{cases}$$

By multiplying the inverse matrix by unity vectors of different forms the following recursive expressions was found:

$$\begin{aligned} \mathbf{T}^{-1}\mathbf{e}_1 &= \frac{i}{N+1}N & ; \mathbf{e}_1 &= [1\ 0\ \ldots]^T \\ \mathbf{T}^{-1}\mathbf{e} &= \frac{Ni + i - i^2}{2} & ; \mathbf{e} &= [1\ \ldots\ 1]^T \\ \mathbf{T}^{-1}\mathbf{e}_n &= \frac{i}{N+1} & ; \mathbf{e}_n &= [0\ \ldots\ 1]^T \end{aligned} \tag{2.9}$$

The bottom expression in equation (2.9) can be used in order to formulate an analytic recursive expression for the static equilibrium positions shown in equation (2.10).

$$\mathbf{x}^0 = L\frac{i}{N+1} \quad ; i = 1 \ldots n \tag{2.10}$$

Note that the length of the chain must be chosen and the recursive relation will thereafter distribute the mass points from left to right. The static equilibrium distribution can be studied in order to determine if the behavior of the system is reasonable. In the case of the horizontal harmonic chain, equation (2.10) suggests that the distance between the mass points is equal. This is a reasonable result since each mass point is affected by the same force throughout the length of the chain.

An even more useful property is to introduce a new variable based on the static distribution. The new variable describes the position relative to the equilibrium position, i.e. the deviation from the static equilibrium.

$$\mathbf{q} \hat{=} \mathbf{y} - \mathbf{y}^0$$

When the deviation variable ($\mathbf{q}$) is in the equations of motion they take the following form:

$$\ddot{\mathbf{q}} = -\omega_0^2 \mathbf{T}\mathbf{q} + \omega_0^2 \mathbf{T}(\underbrace{x_0 \mathbf{T}^{-1}\mathbf{e}_1 + x_{n+1}\mathbf{T}^{-1}\mathbf{e}_n}_{\mathbf{x}^0} - \mathbf{x}^0)$$

The expressions in the parenthesis cancels and the equations of motion becomes homogeneous.

$$\boxed{\ddot{\mathbf{q}} = -\omega_0^2 \mathbf{T}\mathbf{q}}$$

This example considers the static equilibrium of the vertical chain of oscillators. The goal is to show that the static equilibrium is dependent on the height and that when the gravitational potential is used to determine the static equilibrium the equations of motion are independent.
The solution of the static equations of motion of the vertical chain with becomes:

$$\mathbf{y}^0 = y_0 \mathbf{T}^{-1}\mathbf{e}_1 + y_{n+1}\mathbf{T}^{-1}\mathbf{e}_n - \frac{g}{\omega_0^2}\mathbf{T}^{-1}\mathbf{e}$$

When the analytical expression fro the inverse of the tridiagonal matrix from equation (2.9) is used and the position of the bottom and top of the chain is set respectively to 0 and L the recursive analytical expression for the static equilibrium becomes:

$$\boxed{\mathbf{y}_i^0 = L\frac{i}{N+1} - \frac{g}{\omega_0^2}\frac{Ni + i - i^2}{2}} \tag{2.11}$$

Introducing the deviation variable ($\mathbf{q}$) into the equations of motion it can be shown that the resulting second order ODE is homogeneous. From the recursive relation it can be seen that the distance between the mass points varies along the height of the system. Moreover, as shown below, introducing the deviation variable ($\mathbf{q}$) into the equations of motion proves that the equations of motion become insensitive to the gravitational constant.

$$\ddot{\mathbf{q}} = -\omega_0^2 \mathbf{T}\mathbf{q} + \omega_0^2 \mathbf{T}(\underbrace{y_0 \mathbf{T}^{-1}\mathbf{e}_1 + y_{n+1}\mathbf{T}^{-1}\mathbf{e}_n - \frac{g}{\omega_0^2}\mathbf{T}^{-1}\mathbf{e}}_{\mathbf{y}^0} - \mathbf{y}^0)$$

2.1.4 Cyclic Coordinates

A coordinate, q_i, is said to be cyclic if the Lagrangian function does not depend explicitly on the coordinate itself but on the corresponding velocity. At first glance it is not clear why this is useful, however it provides a nice transition to the section introducing Hamiltonian mechanics and it can also be used to understand the canonical integration techniques in section (3.1).

First, Imagine a Lagrangian that is only dependent on the velocity:

$$\mathcal{L} = \mathcal{L}(\dot{q}_1 \dots \dot{q}_n) \tag{2.12}$$

The equations of motion are obtained using the Euler-Lagrange equation.

$$\frac{d}{dt}\frac{\partial \mathcal{L}}{\partial \dot{q}_j} - \cancelto{0}{\frac{\partial \mathcal{L}}{\partial q_j}} = 0$$

The differential equation describing the trajectory is second order. However, it becomes first order if the canonical momentum from equation (2.3) is used.

$$\frac{d}{dt}\frac{\partial \mathcal{L}}{\partial \dot{q}_j} = \frac{dp_j}{dt} = 0$$

Integrating the first order equation that describes the momentum reveals that it is simply equal to a constant (α_j). The Hamiltonian representation for the Lagrangian in equation (2.12) is only a function of the canonical momentum, which was just shown to be a constant. The Hamiltonian function shown in equation (2.13) is therefore also a constant.

$$\mathcal{H} = \mathcal{H}(\alpha_1 \dots \alpha_n) \tag{2.13}$$

This is difficult to see without knowing how the Hamiltonian function is generated, which is introduced in section (2.2). The reason why this is introduced prematurely is that the Hamilton equations of motion are first order and as shown below they will be particularly useful for solving problems involving cyclic coordinates.

$$\dot{q}_j = \frac{\partial H}{\partial p_j} = \frac{\partial H}{\partial \alpha_j} = \omega_j$$
$$\dot{p}_j = -\frac{\partial H}{\partial q_j} = 0$$

Section (2.2.2) shows that the system of first order ODEs known as the Hamilton equations of motion are equivalent to the Lagrange equations. For the case of cyclic coordinates, it is clear that the Hamilton equations are superior to the Lagrange. The reason for this is that the differential equation describing the position is simply equal to the constant ω_j. This equation is separable and first order; the solution is shown in equation (2.14).

$$q_j(t) = \omega_j t + \beta_j \tag{2.14}$$

This illustrates why choosing a convenient set of generalized coordinates can significantly simplify an otherwise complex problem. Furthermore, if the canonical equations of motion are both equal to zero, the trajectory is equal to a constant.

2.2 Hamiltonian Mechanics

Hamiltonian mechanics is a reformulation of the Lagrangian description. The term reformulation implies that even though the Lagrangian is transformed to a new function, the physics on which the Lagrangian remains unchanged. The ultimate goal of this section is to introduce a more abstract representation of Hamiltonian mechanics using canonical transformations. This concept and the terminology that goes along with it will become the bedrock of chapter (3).

2.2.1 Generating the Hamiltonian

This section introduces the process of generating the Hamiltonian using the Legendre transformation. The starting point is the total differential of the Lagrangian function in equation (2.15).

$$d\mathcal{L} = \frac{\partial \mathcal{L}}{\partial q_i} dq_i + \frac{\partial \mathcal{L}}{\partial \dot{q}_i} d\dot{q}_i \tag{2.15}$$

Note that the summation over the subscript (i) is intentionally left out in order to show the concepts more clearly throughout the section. The partial derivatives can be replaced by introducing the canonical momentum from the definition in equation (2.3).

$$d\mathcal{L} = \dot{p}_i dq_i + p_i d\dot{q}_i \tag{2.16}$$

The goal is to derive a function with variables that are not related through differentiation with respect to time. This can be accomplished using the following Legendre transform. There are several Legendre transforms, as anyone with a background from thermodynamics will know, but the transform in equation (2.17) defines the Hamiltonian function.

$$\mathcal{H}(\mathbf{q}, \mathbf{p}, t) \hat{=} \dot{q}_i p_i - \mathcal{L}(\mathbf{q}, \dot{\mathbf{q}}) \tag{2.17}$$

Differentiating the transformation equation and the variable $\dot{q}_i$ cancels, as shown below.

$$\begin{aligned} d\mathcal{H} &= d(\dot{q}_i p_i) - d\mathcal{L}(\mathbf{q}, \dot{\mathbf{q}}, t) \\ d\mathcal{H} &= \dot{q} dp_i + \cancel{p_i d\dot{q}_i} - \cancel{p_i d\dot{q}_i} - \dot{p} dq_i \end{aligned} \tag{2.18}$$

The result of the Legendre transform is a new representation of energy known as the Hamiltonian function as shown in equation (2.19). The equivalency between equations (2.19) and the total derivative of the Hamiltonian means that $2n$ relations must be defined. These relations are the Hamilton equations of motion which will be discussed in section (2.2.2).

$$d\mathcal{H} = \dot{q}_i dp_i - \dot{p}_i dq_i \tag{2.19}$$

The equations above show that the set of variables making up the Hamiltonian is $\mathbf{q}, \mathbf{p}$, i.e. position and momentum.

The systems in this work are simple enough such that the Hamiltonian can be formulated directly as shown in equation (2.20).

$$\mathcal{H} = \frac{1}{2m}\sum_{\forall i} p_i^2 + U(\mathbf{q}) \tag{2.20}$$

In addition to this, appendix (C) shows that the Hamiltonian for the systems in this work can be interpreted as the total energy of the system.

$$\mathcal{H} = T(\dot{\mathbf{q}}) + U(\mathbf{q}) \tag{2.21}$$

This work will use this form form of the Hamiltonian shown in equation (2.21), however the following example uses the formulation in equation (2.20) in order to be consistent with theory.

This example derives the Hamiltonian for the systems that have been studied throughout this chapter.

Harmonic oscillator

The Hamiltonian for the harmonic oscillator is obtained immediately as:

$$\boxed{\mathcal{H} = \frac{1}{2m}p^2 + \frac{1}{2}kq^2}$$

Chain of harmonic oscillators

Just as the the Legendre transform yields:

$$\mathcal{H} = \sum_{i=0}^{n} p_i\dot{q}_i - \frac{1}{2}\Big[\sum_{i=0}^{n} m\dot{q}_i^2 + \sum_{i=0}^{n} k(q_{i+1} - q_i)^2\Big]$$

The final expression for the hamiltonian is obtained just as easily as for the harmonic oscillator.

$$\boxed{\mathcal{H} = \frac{1}{2m}\sum_{i=0}^{n} p_i^2 + \frac{k}{2}\sum_{i=0}^{n}(q_{i+1} - q_i)^2}$$

Chain of harmonic oscillators in a gravitational field

Starting at the Lagrangian function:

$$\mathcal{L} = \frac{1}{2}\sum_{i=0}^{n} m\dot{y}_i^2 - 2gmy_i + 2c(y_{i+1} - y_i) + k(y_{i+1} - y_i)^2$$

The Legendre transform is defined as: $\mathcal{H} = \dot{\mathbf{q}}\mathbf{p} - \mathcal{L} \quad ; \dot{q}_i = mp_i$. From the Legendre transfer it is found that this Hamiltonian also has the expected form.

$$\boxed{\mathcal{H} = \frac{1}{2m}\sum_{i=1}^{n} p_i^2 + \sum_{i=0}^{n} c(y_i - y_{i+1}) + \frac{k}{2}(y_{i+1} - y_i)^2 + mgq_i}$$

2.2.2 The Hamilton Equations of Motion

The Hamilton equations of motion are the relations connecting equation (2.19) and and the total differential of the Hamiltonian function. They consists of a system of $2n$ ODEs that can be expressed as shown in equation (2.22) for the systems in this work.

$$\begin{aligned} \dot{\mathbf{q}} &= \frac{\partial \mathcal{H}}{\partial \mathbf{p}} = \frac{1}{m}\mathbf{p} \\ \dot{\mathbf{p}} &= -\frac{\partial \mathcal{H}}{\partial \mathbf{q}} = -\mathcal{F}(\mathbf{q}) \quad ; \mathcal{F} = \frac{\partial \mathcal{L}}{\partial \mathbf{q}} \end{aligned} \tag{2.22}$$

The equivalency between the Hamiltonian equations of motion and the Lagrange can be seen by expressing the Lagrangian equations of motion as the system of first order ODEs in equation (2.23).

$$\begin{aligned} \dot{\mathbf{q}} &= \mathbf{v} \quad ; \mathbf{v} = \dot{\mathbf{q}} \\ \dot{\mathbf{v}} &= -\frac{1}{m}\frac{\partial \mathcal{L}}{\partial \mathbf{q}} \quad ; \dot{\mathbf{v}} = \ddot{\mathbf{q}} \end{aligned} \tag{2.23}$$

The equivalency can be seen by using the definition of the canonical momentum and its time derivative shown below.

$$\mathbf{p} = m\mathbf{v} \qquad \dot{\mathbf{p}} = m\dot{\mathbf{v}}$$

The geometry of the canonical equations of motion is the property that is used in the symplectic integration methods in section (3.2). The notation that is used in the derivation of the symplectic requirements in section (2.2.4) is based on expressing the geometry of the equations of motion using the anti-symmetric matrix matrix $\mathbf{J}$ as shown below.

$$\begin{gathered} \dot{\boldsymbol{\eta}} = \mathbf{J}\frac{\partial H}{\partial \boldsymbol{\eta}} \quad ; \mathbf{J} = \begin{bmatrix} \mathbf{0}_n & \mathbf{I}_n \\ -\mathbf{I}_n & \mathbf{0}_n \end{bmatrix} \\ \Updownarrow \\ \begin{bmatrix} \dot{q_1} \\ \dot{q_2} \\ \dot{p_1} \\ \dot{p_2} \end{bmatrix} = \begin{bmatrix} 0 & 0 & 1 & 0 \\ 0 & 0 & 0 & 1 \\ -1 & 0 & 0 & 0 \\ 0 & -1 & 0 & 0 \end{bmatrix} \begin{bmatrix} -\dot{p_1} \\ -\dot{p_2} \\ \dot{q_1} \\ \dot{q_2} \end{bmatrix} \end{gathered}$$

The symplectic property is a geometric property that characterizes a system of ODEs. This means that even though the symplectic notation is expressed with respect to the canonical variables it can also be used for the system in equation (2.23).

When this work refers to integration of Hamiltonian systems it consequently refers to any system of ODEs that possess the geometric properties of a real Hamiltonian system. The framework of canonical transformations that is developed in the final two subsections in this section are designed to preserve the geometry of Hamiltonian systems.

This example considers the derivation of the canonical equations of motion for the Hamiltonian functions obtained in the example in section (2.2.1).

Harmonic oscillator

There are two canonical equations of motion for the harmonic oscillator. One describing the trajectory and the other the canonical momentum.

$$\begin{aligned}\dot{q} &= \frac{\partial H}{\partial p} = \frac{1}{m}p \\ \dot{p} &= -\frac{\partial H}{\partial q} = -kq\end{aligned}$$

The equations of motion can be written using matrix notation as follows:

$$\boxed{\begin{bmatrix}\dot{q} \\ \dot{p}\end{bmatrix} = \begin{bmatrix}0 & m^{-1} \\ -k_m & 0\end{bmatrix}\begin{bmatrix}p \\ q\end{bmatrix}}$$

Chain of harmonic oscillators

The Hamiltonian has the following form when the deviation from the static equilibrium positions:

$$\mathcal{H} = \frac{1}{2m}\sum_{i=1}^{n} p_i^2 + \sum_{i=0}^{n}\frac{k}{2}(q_i - q_{i+1})^2 \qquad ; q \hat{=} x - x^0$$

The matrix representation of the canonical equations of motion leads to the following system:

$$\boxed{\begin{aligned}\dot{\mathbf{q}} &= \frac{\partial \mathcal{H}}{\partial p_j} = m^{-1}\mathbf{p} \\ \dot{\mathbf{p}} &= -\frac{\partial \mathcal{H}}{\partial q_j} = -k\mathbf{T}\end{aligned}}$$

Note that the deviation from the static equilibrium distribution from the example in section (2.1.3) must be used for the ODEs describing the position.

Chain of harmonic oscillators in a gravitational field

The Hamiltonian for the chain of harmonic oscillator has the following form:

$$\mathcal{H} = \frac{1}{2m}\sum_{i=1}^{n} p_i^2 + \sum_{i=0}^{n} c(q_i - q_{i+1}) + \frac{k}{2}(q_i - q_{i+1})^2 + mgq_i \qquad ; q \hat{=} y - y^0$$

The canonical equations of motions obtained from the Hamiltonian are as follows:

$$\boxed{\begin{aligned}\dot{\mathbf{q}} &= \frac{\partial \mathcal{H}}{\partial p_j} = \frac{1}{m}\mathbf{p_i} \\ \dot{\mathbf{p}} &= -\frac{\partial \mathcal{H}}{\partial y_j} = -k_m\mathbf{T}\mathbf{q} - g\mathbf{e}\end{aligned}}$$

Note that the deviation from the static equilibrium distribution from the example in section (2.1.3) must be used in the ODEs describing the position.

2.2.3 Canonical Transformations using generating functions

This section methodically goes through the process of how the canonical transformation is produced using generating functions. The goal is to create a new Hamiltonian function $\tilde{\mathcal{H}}$, which is equal to the original but where each new variable is now a function of the original variables. The example at the end of this section is meant to show why this is clever; however, the full power of this method becomes very clear in section (3.1).

The transformation is initiated by defining the new coordinates $\mathbf{Q}, \mathbf{P}$ as functions of the original. This is shown in equation (2.24) for one pair of transformed coordinates Q_i, P_i. The relations in this equation will later be referred to as the transformation equations.

$$\begin{aligned} Q_i &= Q_i(\mathbf{q}, \mathbf{p}) \\ P_i &= P_i(\mathbf{q}, \mathbf{p}) \end{aligned} \tag{2.24}$$

The idea is to use the transformed coordinates as the variables in a new Hamiltonian ($\tilde{\mathcal{H}}$), and thereafter use Hamilton's principle to ensure that it is equal to the original Hamiltonian. This ensures that the structure of the canonical equations and the physics is conserved in the transformation.

$$\tilde{\mathcal{H}} = \tilde{\mathcal{H}}(\mathbf{Q}, \mathbf{P}) \tag{2.25}$$

In order to ensure that the Hamiltonian functions represent the same physics, they must both obey Hamilton's principle. This can de done using the reverse Legendre transform in equation (2.26) and (2.27).

$$\delta \int_{t_1}^{t_2} \Big[P_i \dot{Q}_i - \tilde{\mathcal{H}}(\mathbf{Q}, \mathbf{P}) \Big] dt = 0 \tag{2.26}$$

$$\delta \int_{t_1}^{t_2} \Big[\ p_i \dot{q}_i - \ \mathcal{H}(\mathbf{q}, \mathbf{p}) \Big] dt = 0 \tag{2.27}$$

Once again it is important to bare in mind that the integrand are functionals and simply demanding equivalency of the integrands is not a sufficient requirement. In Goldstein et al. (2014) it can be found that equation (2.28) does just that. The reason for this must be understood based on calculus of variations in appendix (B).

First consider the action integral for some modified Lagrangian written as $\tilde{\mathcal{L}} = \lambda L + F(t)$.

$$\tilde{\mathcal{S}} = \int_{t_1}^{t_2} \tilde{\mathcal{L}} d\tau = \lambda \int_{t_1}^{t_2} \mathcal{L} d\tau + \int_{t_1}^{t_2} F(\tau) d\tau = \lambda \mathcal{S} + \int_{t_1}^{t_2} F(\tau) d\tau$$

It is clear that when this functional is minimized with respect to a generalized coordinate q_i the function $F(t)$ will simply disappear t the end points of the integration. Any function that is independent of the path can be added to the functional without changing the extrema of the functional. However, if the function is chosen cleverly, i.e. ensuring that total derivative with respect to time is independent of the path, the action integral of the modified Lagrangian can also be written as shown below.

$$\tilde{\mathcal{S}} = \int_{t_1}^{t_2} \tilde{\mathcal{L}} d\tau = \lambda \int_{t_1}^{t_2} \mathcal{L} d\tau + \frac{dF}{dt} = \lambda \mathcal{S} - \frac{dF}{dt}$$

The function F can now be chosen in order to comply with the requirement that the function vanishes. The conclusion from this derivation is that the following relation will ensure equivalency of equation (2.26) and (2.27).

$$\lambda \mathcal{S} = \tilde{\mathcal{S}} + \frac{dF}{dt}$$

The final result in equation (2.28) can be found on page 370 in Goldstein et al. (2014), and it can be obtained by substituting the inverse Legendre transforms into the derivation above.

$$\lambda(p_i \dot{q}_i - \mathcal{H}) = P_i \dot{Q}_i - \tilde{\mathcal{H}} + \frac{dF}{dt} \tag{2.28}$$

A canonical transformation performed using equation (2.28) and $\lambda \neq 1$ is referred to as an extended canonical transformation. The constant can, however, be split into two contributions as shown in equation (2.29).

$$Q_i' = \mu q_i \qquad\qquad P_i' = \nu p_i \tag{2.29}$$

Note that the notation Q_i' is simply used to state that it is a scaled version of the transformed coordinate Q_i, not the "Newtonian" derivative notation that it will represent in the rest of this work. Performing a canonical transformation that only scales the coordinates using the Hamiltonian functions $\tilde{\mathcal{H}}(\mathbf{q}', \mathbf{P}') = \mu\nu\mathcal{H}(\mathbf{q}, \mathbf{p})$ is known as a restricted canonical transformation. In this case, equation (2.28) will be reduced to the form shown in equation (2.30).

$$\mu\nu(p_i \dot{q}_i - \mathcal{H}) = P_i' \dot{Q}_i - \tilde{\mathcal{H}}' \tag{2.30}$$

A third alternative is to set the constant $\lambda = 1$. This changes the full transformation in equation (2.28) to the form shown in equation (2.31). This is known as a full canonical transformation.

$$p_i \dot{q}_i - \mathcal{H} = P_i \dot{Q}_i - \tilde{\mathcal{H}} + \frac{dF}{dt} \tag{2.31}$$

This work will only consider full canonical transformations such as those shown in equation (2.31). It will also use the theorem of Pinocaré which states that the result of subsequent canonical transformations is also canonical.

This section will use the form $F = F_1(\mathbf{Q}, \mathbf{P})$ from table (2.1) as an example to introduce the idea behind performing canonical transformations using generating functions. The strategy is to express this function partly in terms of the old and partly in terms of the new variables. The equations (2.24) can be used in order to to express the original coordinates as a function of the new coordinates using half of each set. This will be done by inverting the equation (2.24) which from now on will be referred to as the transformation equations. Using the inverted equations $(q_i(\mathbf{Q}, \mathbf{P}), p_i(\mathbf{Q}, \mathbf{P}))$ the original Hamiltonian can be expressed entirely by a new set of variables. First, the total derivative of the generating function with respect to time must be obtained.

$$F = F_1(\mathbf{q}, \mathbf{Q}, t) \Rightarrow \frac{dF}{dt} = \left(\frac{\partial F_1}{\partial \mathbf{Q}}\right) \dot{\mathbf{Q}} + \left(\frac{\partial F_1}{\partial \mathbf{q}}\right) \dot{\mathbf{q}} + \left(\frac{\partial F_1}{\partial t}\right)$$

The relation in equation (2.31) can now be used in order to generate a canonical transformation using equation (2.24).

$$p_i\dot{q}_i - \mathcal{H} = P_i\dot{Q}_i - \tilde{\mathcal{H}} + \frac{d\mathcal{F}_1}{dt} = P_i\dot{Q}_i - \tilde{\mathcal{H}} + \frac{\partial F_1}{\partial t} + \frac{\partial F_1}{\partial q_i}\dot{q}_i + \frac{\partial F_1}{\partial Q_i}\dot{Q}_i \tag{2.32}$$

The set of variables must be chosen in order to remove all the dependencies on the old and new variables in the expression of the Hamiltonian. This means that the terms $p_i\dot{q}_i$ and $P_i\dot{Q}_i$ in equation (2.32) must be combined in such a way that they vanish. Equation (2.32) can therefore only be independent of the old and new variables if the requirements in equation (2.33) and (2.34) are imposed on the momenta.

$$p_i = \frac{\partial F_1}{\partial q_i} \tag{2.33}$$

$$P_i = -\frac{\partial F_1}{\partial Q_i} \tag{2.34}$$

The requirement in equation (2.33) defines n relations describing the original momentum p_i as a function of $\mathbf{q}, \mathbf{Q}$ and t; in other words $p_i = p_i(\mathbf{q}, \mathbf{Q}, t)$. Half of the relations in equation (2.24) can now be found by inverting the system of equations formed by equation (2.33), thus generating the first half of the transformation equations. Using the same argument on equation (2.34), one can find n relations $P_i(\mathbf{q}, \mathbf{Q})$ and use the functions obtained from equation (2.33) to generate the other half of the transformation equations, $P_i(\mathbf{q}, \mathbf{p})$. Because of the clever choice of coordinates, the relation between the new and the old Hamiltonian is obtained in equation (2.35).

$$\tilde{\mathcal{H}} = \mathcal{H} + \frac{\partial F_1}{\partial t} \tag{2.35}$$

A specific function $F_1(\mathbf{q}, \mathbf{Q}, t)$ is not chosen here since the purpose of this section is to show the methodology. Any continuous twice differentiable function can be chosen as F_1. This will be exploited in section (3.1) where the choice of generating function will become very important. The canonical transformation is now complete and the functions $q_i, p_i(Q, P, t)$ can be inserted into the Hamiltonian and new equations of motion can be found.

Table (2.1) show some fundamental generating functions from Goldstein et al. (2014). The generating function $F_3(\mathbf{p}, \mathbf{Q}, t)$ will be used later in this work.

Table 2.1: Fundamental generating functions from Goldstein et al. (2014)

Generating Function	Generating Function Derivatives	
$F = F_1(\mathbf{q}, \mathbf{Q}, t)$	$p_i = \frac{\partial F_1}{\partial p_i}$	$P_i = -\frac{\partial F_1}{\partial Q_i}$
$F = F_3(\mathbf{p}, \mathbf{Q}, t) - q_i p_i$	$q_i = -\frac{\partial F_3}{\partial p_i}$	$P_i = -\frac{\partial F_3}{\partial Q_i}$

2.2.4 Canonical Transformations from a symplectic perspective

This section considers restricted canonical transformations from a symplectic perspective. It will not become clear until the very end of the section what the term symplectic actually implies and the section methodically performs the derivation which will ultimately lead to the symplectic requirement for a canonical transformation in equation (2.50). Even though the goal of the section is to perform a canonical transformation, it is completely independent from the generating function that was introduced in the previous section. However, the fundamental idea behind the symplectic and generating function approach is the same: to express the new coordinates shown in equation (2.24) in terms of the old coordinates. This means that the goal is to define the transformation equations (2.24) that was introduced in the previous section. Equation (2.36) show the transformation equations using the symplectic notation from section (2.2.2).

$$\boldsymbol{\eta} = \begin{bmatrix} q_1 \\ q_2 \\ p_1 \\ p_2 \end{bmatrix} \qquad \boldsymbol{\zeta} = \begin{bmatrix} Q_1 \\ Q_2 \\ P_1 \\ P_2 \end{bmatrix}$$

$$\dot{\boldsymbol{\zeta}} = \boldsymbol{\zeta}(\boldsymbol{\eta}) \tag{2.36}$$

Now that the symplectic notation has been introduced, the rest of the transformation will first be derived for a single pair of transformed coordinates (Q_i, P_i) before it is generalized using the symplectic matrix notation.

The equations of motion for the pair of transformed coordinates is expressed in terms of the original coordinates as shown in equation (2.37) and (2.38). Remembering that the new coordinate, i, is a function of all the original coordinates as shown in equation (2.24); the summation over i is formally required even though not explicitly written.

$$\dot{Q}_i = \frac{\partial Q_i}{\partial q_j}\dot{q}_j + \frac{\partial Q_i}{\partial p_j}\dot{p}_j = \frac{\partial Q_i}{\partial q_j}\frac{\partial \mathcal{H}}{\partial p_j} - \frac{\partial Q_i}{\partial p_j}\frac{\partial \mathcal{H}}{\partial q_j} \tag{2.37}$$

$$\dot{P}_i = \frac{\partial P_i}{\partial q_j}\dot{q}_j + \frac{\partial P_i}{\partial p_j}\dot{p}_j = \frac{\partial P_i}{\partial q_j}\frac{\partial \mathcal{H}}{\partial p_j} - \frac{\partial P_i}{\partial p_j}\frac{\partial \mathcal{H}}{\partial q_j} \tag{2.38}$$

The transformation equations (2.24) are inverted in equation (2.39) to express the original coordinates as a function of the new.

$$\begin{aligned} q_j &= q_j(\mathbf{Q}, \mathbf{P}) \\ p_j &= p_j(\mathbf{Q}, \mathbf{P}) \end{aligned} \tag{2.39}$$

The idea is now to make sure that the equations of motion for the new coordinates have the same symplectic property as the original. First the Hamiltonian $\mathcal{H}(\mathbf{q}, \mathbf{p})$ is considered as a function of $(\mathbf{Q}, \mathbf{P})$ using the inverted transformation equations and by expanding the partial derivatives.

$$\frac{\partial \mathcal{H}}{\partial P_i} = \frac{\partial \mathcal{H}}{\partial p_j}\frac{\partial p_j}{\partial P_i} + \frac{\partial \mathcal{H}}{\partial q_j}\frac{\partial q_j}{\partial P_i} \tag{2.40}$$

$$-\frac{\partial \mathcal{H}}{\partial Q_i} = -\frac{\partial \mathcal{H}}{\partial p_j}\frac{\partial p_j}{\partial Q_i} - \frac{\partial \mathcal{H}}{\partial q_j}\frac{\partial q_j}{\partial Q_i} \tag{2.41}$$

Now we demand that equation (2.42) and (2.43) must hold for a transformation to be canonical.

$$\dot{Q}_i = \frac{\partial \mathcal{H}}{\partial P_i} \tag{2.42}$$

$$\dot{P}_i = -\frac{\partial \mathcal{H}}{\partial Q_i} \tag{2.43}$$

In order for equation (2.42) to hold we need to study equation (2.37) and (2.40).

$$\Big(\frac{\partial Q_i}{\partial q_j}\Big)_{q,p} = \Big(\frac{\partial p_j}{\partial P_i}\Big)_{Q,P} \qquad \Big(\frac{\partial Q_i}{\partial p_j}\Big)_{q,p} = -\Big(\frac{\partial q_j}{\partial P_i}\Big)_{Q,P} \tag{2.44}$$

The same argument must be made for equation (2.43) and can be found by studying equation (2.38) and (2.41).

$$\Big(\frac{\partial P_i}{\partial q_j}\Big)_{q,p} = -\Big(\frac{\partial p_j}{\partial Q_i}\Big)_{Q,P} \qquad \Big(\frac{\partial P_i}{\partial p_j}\Big)_{q,p} = \Big(\frac{\partial q_j}{\partial Q_i}\Big)_{Q,P} \tag{2.45}$$

The time has now come to generalize this using the symplectic notation from equation (2.36). First recall that in section (2.2.2), concerning the Hamilton equations of motion, the symplectic shorthand was defined as shown below.

$$\dot{\boldsymbol{\eta}} = \mathbf{J}\frac{\partial \mathcal{H}}{\partial \boldsymbol{\eta}}$$

In equation (2.37) and (2.38), the equations of motion for the transformed coordinates are expressed in terms of the original coordinates. The summation over the term j was not written due to notational clarity; however, in matrix notation the summation is easily included as shown in the equation below. This equation is valid for each coordinate, Q_i or P_i.

$$\dot{\zeta}_i = \frac{\partial \zeta_i}{\partial \eta_j}\dot{\eta}_j \qquad ; i,j = 1,\ldots,2n$$

Here $\frac{\partial \zeta_i}{\partial \eta_j}$ is a row vector $\Big[\frac{\partial \zeta_i}{\partial \eta_1},\ldots,\frac{\partial \zeta_i}{\partial \eta_{2n}}\Big]$ and $\dot{\eta}$ is a column vector $\Big[\eta_1,\ldots,\eta_{2n}\Big]^T$. The full matrix notation of all the coordinates is shown in equation (2.46).

$$\begin{aligned} \dot{\boldsymbol{\zeta}} &= \mathbf{M}\dot{\boldsymbol{\eta}} \qquad ; M_{i,j} = \frac{\partial \zeta_i}{\partial \eta_j} \\ &\Updownarrow \\ \dot{\boldsymbol{\zeta}} &= \mathbf{M}\mathbf{J}\frac{\partial \mathcal{H}}{\partial \boldsymbol{\eta}} \end{aligned} \tag{2.46}$$

Now we need to derive an expression for the equations of motion of the original Hamiltonian, $\mathcal{H}(\eta)$, as a function of the transformed variables ζ. Looking back at equation (2.40) and (2.41) this can be achieved as shown below.

$$\frac{\partial \mathcal{H}}{\partial \eta_i} = \frac{\partial \mathcal{H}}{\partial \zeta_j}\frac{\partial \zeta_j}{\partial \eta_i}$$

We define yet a new matrix, $\mathbf{M^T}$, who's elements are $M^T_{i,j} = \frac{\partial \zeta_j}{\partial \eta_i}$. We notice that this is the transpose of the matrix $\mathbf{M}$.

$$\frac{\partial \mathcal{H}}{\partial \boldsymbol{\eta}} = \mathbf{M^T} \frac{\partial \mathcal{H}}{\partial \boldsymbol{\zeta}} \tag{2.47}$$

Finally, substituting equation (2.47) in equation (2.46) we end up with equation (2.48).

$$\dot{\boldsymbol{\zeta}} = \mathbf{M J M^T} \frac{\partial \mathcal{H}}{\partial \boldsymbol{\zeta}} \tag{2.48}$$

From equations (2.42) and (2.43) we formulate the demand that must be met in order for the transformation to be canonical in equation (2.49).

$$\dot{\boldsymbol{\zeta}} = \mathbf{J} \frac{\partial \mathcal{H}}{\partial \boldsymbol{\zeta}} \tag{2.49}$$

Equations (2.48) and (2.49) conclude that the relation equation (2.50) must hold for the transformation to be canonical.

$$\boxed{\mathbf{M J M^T} = \mathbf{J}} \tag{2.50}$$

Equation (2.50) is known as the symplectic condition for a canonical transformation, and any matrix $\mathbf{M}$ satisfying the symplectic condition is by extension a symplectic matrix.

An even $n \times n$ symplectic matrix has determinant equal to one as shown in equation (2.51).

$$\det |\mathbf{M}| = 1 \tag{2.51}$$

The proof is not considered in this work, however it can be seen on page 166 in Weyl (1946) that the relation in equation (2.51) is a requirement for a symplectic transformation.

Chapter 3

Integration of Hamiltonian Systems

The title of this chapter could have been any of the following; *Symplectic Integration*, *Geometric Integration*, *Self Preserving Integration* or *Canonical Integration*. An obvious reason for the abundance of terminology in the literature is that the subject can be studied from different perspectives. This was shown in the sections (2.2.3) and (2.2.4) where both sections produced equal results from two unrelated approaches. Furthermore, the algebraic structure of Hamiltonian systems has been studied for a long time. The term symplectic, on the other hand, was proposed fairly recently by Hermann Weyl in the quote shown below.

> *The name "complex group" formerly advocated by me in allusion to line complexes, as these are defined by the vanishing of antisymetric bilinear forms, has become more and more embarrassing through collision with the word "complex" in the connotation of complex number. I therefore propose to replace it by the corresponding Greek adjective "symplectic". Dickson calls the group the "Abelian linear group" in homage to Abel who first studied it.*
>
> - Hermann Weyl, in Weyl (1946) on page 165.

This chapter is devoted to developing numerical integration algorithms that preserve the structure of the system of equations from Hamiltonian functions of the form shown in equation (3.1). Note that even though all the proposed algorithms have this property, they will be classified into two categories based on how they are derived. The approaches to deriving the algorithms will be related to section (2.2.3) and (2.2.4). Consequently, the categories are respectively referred to as canonical integration and symplectic integration.

3.1 Canonical integration methods

From now on this work will only consider Hamiltonian functions of the form shown in equation (3.1).

$$\mathcal{H} = \frac{1}{2m}\mathbf{p}^2 + U(\mathbf{q}, t) \tag{3.1}$$

Note that the title of the section is canonical integration algorithms. Canonical and symplectic implies exactly the same properties; however, the algorithms that will be derived in this section are solely derived using canonical transformations by generating functions.

The methodology employs the idea of generating functions from section (2.2.3) to create new Hamiltonian functions that are identically equal to zero.

Even though this work does not add any new knowledge to the original paper it is a good way of showing the underlying concepts of some simple and and easy to implement integration algorithms. Furthermore it shows that the idea behind the generating function is very applicable.

3.1.1 Canonical Euler Integration

The goal is to perform a canonical transformation which yields equations of motion of the form shown in equation (3.2), whose solution is simply a constant which is determined by the initial conditions.

$$\begin{aligned} \dot{\mathbf{Q}} &= 0 \\ \dot{\mathbf{P}} &= 0 \end{aligned} \tag{3.2}$$

The corresponding solutions for the equations of motion will be on the form:

$$\mathbf{P} = \mathbf{p}(\mathbf{q}_0, \mathbf{p}_0, t) \quad ; \quad \mathbf{Q} = \mathbf{q}(\mathbf{q}_0, \mathbf{p}_0, t) \tag{3.3}$$

As proposed in Ruth (1983) a generating function of the form $F_3(\mathbf{Q}, \mathbf{p}, t))$ from table (2.1) is used to facilitate the canonical transformation. Following the framework developed in section (2.2.3), the relation in equation (2.31) must hold for the transformation to be canonical. This means that the equivalent of equation (2.32) must be derived for the chosen generating function. This process is shown below with the result shown in equation (3.4).

$$\begin{aligned} p_i\dot{q}_i - \mathcal{H} &= P_iQ_i - \tilde{\mathcal{H}} + \frac{dF}{dt} && ; F = p_iq_i + F_3(\mathbf{Q}, \mathbf{p}, t) \\ p_i\dot{q}_i - \mathcal{H} &= P_i\dot{Q}_i - \tilde{\mathcal{H}} + \frac{d(p_iq_i)}{dt} + \frac{dF_3}{dt} && ; F_3(\mathbf{Q}, \mathbf{p}, t) = -Q_ip_i + G(\mathbf{Q}, \mathbf{p}, t) \\ -q_i\dot{p}_i - \mathcal{H} &= P_i\dot{Q}_i - \tilde{\mathcal{H}} + \frac{\partial F_3}{\partial t} + \frac{\partial F_3}{\partial Q_i}\dot{Q}_i + \frac{\partial F_3}{\partial p_i}\dot{p}_i \end{aligned} \tag{3.4}$$

The function $G(\mathbf{Q}, \mathbf{p}, t)$ will be determined in the end to ensure that the Hamiltonian is identically equal to zero. The only demand on the unknown function is that it must have

continuous second derivatives in order to be able to comply with the Euler-Lagrange equation.

The next step is to ensure that the generating function has no affect on the action. This is done by studying the partial derivatives from equation (3.4) shown below.

$$\frac{\partial F_3}{\partial Q_i} = -p_i + \frac{\partial G}{\partial Q_i}$$
$$\frac{\partial F_3}{\partial p_i} = -Q_i + \frac{\partial G}{\partial p_i}$$

The goal is now to choose the coordinates such that the old and new Hamiltonian are equal. This is done by ensuring that the relation in equation (2.35) is satisfied and takes the form of equation (3.7). In order for this to happen it is necessary that the terms Q_i and p_i vanish. Choosing the relationship between the coordinates as shown in equation (3.5) and (3.6) ensures that this happens.

$$\mathbf{q} = -\frac{\partial F_3}{\partial \mathbf{p}} = \mathbf{Q} - G_p \tag{3.5}$$

$$\mathbf{P} = -\frac{\partial F_3}{\partial \mathbf{Q}} = \mathbf{p} - G_Q \tag{3.6}$$

It can be confirmed that choosing the relations in equation (3.5) and (3.6) results in the equation (3.7) by substituting them into equation (3.4).

$$\tilde{\mathcal{H}} = \mathcal{H} + \frac{\partial F_3}{\partial t} = \mathcal{H} + G_t \tag{3.7}$$

The transformation is now guaranteed to be canonical and the function $G(\mathbf{p}, \mathbf{Q}, t)$ can be chosen in order for the new Hamiltonian to be equal to zero. By looking at equation (3.1) it is clear that choosing the function as shown in equation (3.8) will make this happen.

$$G(\mathbf{p}, \mathbf{Q}, t) = -\Big[\frac{1}{2}\mathbf{p}^2 + U(\mathbf{Q}, 0)\Big]t \tag{3.8}$$

The next step is to determine the relationship between the new and old coordinates. This is done by substituting the function $G(\mathbf{p}, \mathbf{Q}, t)$ from equation (3.8) into equation (3.5) and (3.6). The result was called the transformation equations in section (2.2.3) and is shown in equation (3.9) and (3.10).

$$\mathbf{q} = \mathbf{Q} + \mathbf{p}t \tag{3.9}$$

$$\mathbf{P} = \mathbf{p} - \mathcal{F}(\mathbf{Q}, 0)t \qquad ; \mathcal{F}(\mathbf{Q}, 0) \hat{=} -\frac{\partial U(\mathbf{Q}, 0)}{\partial \mathbf{Q}} \tag{3.10}$$

The transformation equations allows the old coordinates to be expressed as a function of the new. Equation (3.9) and (3.10) is therefore simply a rewritten version of equation (3.9) and (3.10).

$$\mathbf{p} = \mathbf{P} + \mathcal{F}(\mathbf{Q}, 0)t \tag{3.11}$$

$$\mathbf{q} = \mathbf{Q} + t\Big[\mathbf{P} + \mathcal{F}(\mathbf{Q}, 0)t\Big] \tag{3.12}$$

The time has finally come to express the new Hamiltonian function. It was previously shown that the new function must satisfy equation (3.7). Next it was assumed that choosing the function $G(\mathbf{p}, \mathbf{Q}, t)$ in equation (3.8) was useful in order to have the new hamiltonian equal to zero at $t = 0$. It can now be concluded that the new Hamiltonian can be found from the expression below..

$$\tilde{\mathcal{H}} = \frac{1}{2}\mathbf{p}^2 + U(\mathbf{q}, t) - \Big(\frac{1}{2}\mathbf{p}^2 + U(\mathbf{Q}, 0)\Big) \tag{3.13}$$

$$\tag{3.14}$$

In order to express the function solely in terms of the new coordinates the transformation equations from equation (3.9) and (3.10) is used. This results in the final expression for the new Hamiltonian shown in equation (3.15).

$$\tilde{\mathcal{H}} = U\Big(\mathbf{Q} + t\Big[\mathbf{P} + \mathcal{F}(\mathbf{Q}, 0)t\Big], t\Big) - U(\mathbf{Q}, 0) \tag{3.15}$$

Equation (3.15) clearly shows that the value of the new Hamiltonian is equal to zero at $t = 0$. In order to study what happens in the domain around $t = 0$, the Hamiltonian is expanded using a small parameter t. The expansion is shown below and is carried out using a Taylor series which is cut off after the first term.

$$\begin{aligned}
\tilde{\mathcal{H}} &\approx \cancelto{0}{\tilde{\mathcal{H}}\Big|_{t=0}} + \frac{\partial \tilde{\mathcal{H}}}{\partial t}\Big|_{t=0}(t-0) + \mathcal{O}(h^2) \\
&= \frac{\partial}{\partial t}\left\{U\Big(\mathbf{Q} + t\Big[\mathbf{P} + \mathcal{F}(\mathbf{Q}, 0)t\Big], t\Big)\right\}\Bigg|_{t=0} t - \frac{\partial}{\partial t}\Big\{U(\mathbf{Q}, 0)\Big\}t + \mathcal{O}(h^2) \\
&= U_t(\mathbf{Q}, 0)t - t\frac{\partial U}{\partial \mathbf{Q}}\frac{\partial \mathbf{Q}}{\partial t} + \mathcal{O}(h^2) \\
&= U_t(\mathbf{Q}, 0)t - \mathbf{P}\mathcal{F}(\mathbf{Q}, 0)t + \mathcal{O}(h^2) \\
&= 0 + \mathcal{O}(h^2)
\end{aligned} \tag{3.16}$$

Equation (3.16) shows that the Hamiltonian equal to zero plus an error $\mathcal{O}(h^2)$ for any t. This means that the equations of motion must also be equal to zero. The solution is therefore equal to some constant as shown in equation (3.17) and (3.18).

$$\dot{\mathbf{Q}} = \frac{\partial \tilde{\mathcal{H}}}{\partial \mathbf{P}} = 0 + \mathcal{O}(h^2) \qquad \Rightarrow \mathbf{Q} = constant + \mathcal{O}(h^2) \tag{3.17}$$

$$\dot{\mathbf{P}} = -\frac{\partial \tilde{\mathcal{H}}}{\partial \mathbf{Q}} = 0 + \mathcal{O}(h^2) \qquad \Rightarrow \mathbf{P} = constant + \mathcal{O}(h^2) \tag{3.18}$$

Thus the conclusion is that as long as the new coordinates are used as the initial conditions, the method will be of order one and canonical. The numerical algorithm can now be formulated based on equation (3.11) and (3.12).

$$\boxed{\begin{aligned}\mathbf{p}_{(k+1)} &= \mathbf{p}_k + \mathcal{F}(\mathbf{q}_k, 0)h \\ \mathbf{q}_{(k+1)} &= \mathbf{q}_k + \mathbf{p}_{(k+1)}h\end{aligned}} \tag{3.19}$$

The method in equation (3.19) is first order and often referred to as the symplectic Euler method. This derivation was rigorous; however, figure (4.1) shows the advantage of applying the symplectic method to the harmonic oscillator. The following example derives the numerical algorithm for the explicit and implicit Euler method for the harmonic oscillator which is used in the figure.

The explicit, implicit Euler methods will be used to compare the symplectic methods with standard integration methods. This example derives explicit versions of these methods specific for the harmonic oscillator using $\omega_0 = 1$.

Explicit Euler

The explicit Euler algorithm is obtained using a first order Taylor expansion as shown below.

$$\mathbf{y}_{k+1} = \mathbf{y}_k + \frac{\partial \mathbf{y}}{\partial \mathbf{x}}\Big|_k h + \mathcal{O}(h^2) \qquad ;\mathbf{y} = \mathbf{y}(\mathbf{x})$$

Applying this directly to the Hamilton equations of motion yields the following first order approximation of the trajectory.

$$\begin{bmatrix}\mathbf{q}_{k+1}\\ \mathbf{p}_{k+1}\end{bmatrix} = \begin{bmatrix}\mathbf{q}_k\\ \mathbf{p}_k\end{bmatrix} + \frac{\partial \mathcal{H}}{\partial \eta}\Big|_k h + \mathcal{O}(h^2)$$

Using the Hamiltonian for the harmonic oscillator the explicit Euler method can be written as shown below.

$$\boxed{\begin{bmatrix}\mathbf{q}\\ \mathbf{p}\end{bmatrix}_{k+1} = \begin{bmatrix}1 & h\\ -h & 1\end{bmatrix}\begin{bmatrix}\mathbf{q}\\ \mathbf{p}\end{bmatrix}_k}$$

Implicit Euler

Just as the explicit algorithm from the example in section (3.1.1) the implicit Euler algorithm is obtained using a first order taylor expansion as shown below.

$$\mathbf{y}_{k+1} = \mathbf{y}_k + \frac{\partial \mathbf{y}}{\partial \mathbf{x}}\Big|_{k+1} h + \mathcal{O}(h^2)$$

The next step of the algorithm must therefore be found implicitly by solving the equation.

$$\mathbf{y}_{k+1} - \mathbf{y}_k - \frac{\partial \mathbf{y}}{\partial \mathbf{x}}\Big|_{k+1} h = 0$$

In order to obtain an implicit algorithm for the harmonic oscillator the notation is changed to a more familiar representation.

$$\begin{bmatrix}\mathbf{q}_{k+1}\\ \mathbf{p}_{k+1}\end{bmatrix} = \begin{bmatrix}\mathbf{q}_k\\ \mathbf{p}_k\end{bmatrix} + \frac{\partial \mathcal{H}}{\partial \eta}\Big|_{k+1} h + \mathcal{O}(h^2)$$

Now the implicit-euler algorithm can be found. As shown bellow, the implicit method for the harmonic oscillator turns out to have an explicit representation.

$$\boxed{\begin{bmatrix}\mathbf{q}\\ \mathbf{p}\end{bmatrix}_{k+1} = \frac{1}{1+h^2}\begin{bmatrix}1 & h\\ -h & 1\end{bmatrix}\begin{bmatrix}\mathbf{q}\\ \mathbf{p}\end{bmatrix}_k}$$

3.1.2 Leapfrog

The Leapfrog method is a second order canonical method. Even though the symplectic Euler method was tedious to derive, extending the method to second order is not a lot of work. The reason for this is that the method can be built on the results from the previous section which started by using the definition of the canonical transformation from equation (2.31).

In order to obtain a second order method, perform a second canonical transformation based on the first order transformation that was done in the previous section. The assumption that successive canonical transformations can be performed and that the resulting function is still canonical is supported by theorem 2.8 in on page 187 in Hairer et al. (2002).

The first canonical transformation is therefore based on the result from the previous section, however as proposed in Ruth (1983) it will be scaled by the constants a and b. The scaling constants have no effect on the form of the final generating function in the previous section. The function used in equation (3.20) is therefore the same type of generating function that was used earlier.

$$p_i\dot{q}_i - \mathcal{H} = P_iQ_i - \tilde{\mathcal{H}} + \frac{dF}{dt} \qquad F(\mathbf{Q},\mathbf{p},t) = -\mathbf{Qp} - \underbrace{\Big[a\frac{1}{2}\mathbf{p}^2 + U(\mathbf{Q},bt)\Big]t}_{F_3} \tag{3.20}$$

The total derivative of the generating function results in the following partial derivatives with respect to the canonical variables of the function. This is done by following the steps leading to equation (3.4) in the previous section. The corresponding partial derivatives for the generating function in equation (3.20) are shown below.

$$\begin{aligned}\frac{\partial F_3}{\partial Q_i} &= -p_i + t\mathcal{F}(\mathbf{Q},bt) \qquad ;\mathcal{F}\hat{=}-\frac{\partial U}{\partial Q}\\ \frac{\partial F_3}{\partial p_i} &= -Q_i - atp_i\end{aligned}$$

Following the method from the previous section, the relations in equation (3.21) and (3.22) are chosen in order to ensure that the relation between the old and new Hamiltonian function takes the form defined in equation (2.35).

$$\mathbf{q} = -\frac{\partial F_3}{\partial p_i} = \mathbf{Q} + a\mathbf{p}t \tag{3.21}$$

$$\mathbf{P} = -\frac{\partial F_3}{\partial Q_i} = \mathbf{p} - t\mathcal{F}(\mathbf{Q},bt) \tag{3.22}$$

The result from this transformation is a scaled version of the result from the previous section and in order to continue, a second generating function must be chosen for the second transformation. This work will use the second generating function in equation (3.23) based on the suggestion in Ruth (1983). Note that the double ”tilde” superscript

that is used to differentiate the second set of transformed canonical variables from the first.

$$P_i\dot{Q}_i - \tilde{\mathcal{H}} = \tilde{\tilde{P}}_i\dot{\tilde{Q}}_i - \tilde{\tilde{\mathcal{H}}} + \frac{dF}{dt}; \tilde{\tilde{F}}(\tilde{\tilde{\mathbf{Q}}}, \mathbf{P}, t) = -\tilde{\tilde{\mathbf{Q}}}\mathbf{P} - \underbrace{\frac{(1-a)t}{2}\mathbf{P}^2}_{\tilde{\tilde{F}}_3} \tag{3.23}$$

As shown below, the same procedure as before is followed to choose the second set of canonical variables.

$$P_i\dot{\tilde{\tilde{Q}}}_i - \tilde{\mathcal{H}} = \tilde{\tilde{P}}_i\dot{\tilde{Q}}_i - \tilde{\tilde{\mathcal{H}}} + \frac{d(Q_iP_i)}{dt} + \frac{\partial\tilde{\tilde{F}}}{\partial t} + \frac{\partial\tilde{\tilde{F}}}{\partial\tilde{\tilde{Q}}_i}\dot{\tilde{\tilde{Q}}}_i + \frac{\partial\tilde{\tilde{F}}}{\partial P_i}\dot{P}_i$$

$$-Q_i\dot{P}_i - \tilde{\mathcal{H}} = \tilde{\tilde{P}}_i\dot{\tilde{Q}}_i - \tilde{\tilde{\mathcal{H}}} + \frac{\partial\tilde{\tilde{F}}_3}{\partial t} + \frac{\partial\tilde{\tilde{F}}_3}{\partial\tilde{\tilde{Q}}_i}\dot{\tilde{\tilde{Q}}}_i + \frac{\partial\tilde{\tilde{F}}_3}{\partial P_i}\dot{\tilde{\tilde{P}}}_i$$

$$\frac{\partial\tilde{\tilde{F}}_3}{\partial\tilde{\tilde{Q}}_i} = -P_i$$

$$\frac{\partial\tilde{\tilde{F}}_3}{\partial P_i} = -\tilde{\tilde{Q}}_i - (1-a)tP_i$$

The relationship between the coordinates in equation (3.24) and (3.25) is chosen in order to ensure that the transformation is canonical.

$$\mathbf{Q} = \tilde{\tilde{\mathbf{Q}}} + t(1-a)\mathbf{P} \tag{3.24}$$

$$\mathbf{P} = \tilde{\tilde{\mathbf{P}}} \tag{3.25}$$

The choice of coordinates in equations above ensures that the second transformed Hamiltonian can be expressed as shown in equation (3.26).

$$\tilde{\tilde{H}} = \mathcal{H} + \frac{\partial F_3}{\partial t} + \frac{\partial\tilde{\tilde{F}}_3}{\partial t} \tag{3.26}$$

The result from the two transformation is four equations defining the mapping between the three sets of coordinates. The summary below shows the transformation equations between the sets.

$$\mathbf{P} = \tilde{\tilde{\mathbf{P}}}$$

$$\mathbf{Q} = \tilde{\tilde{\mathbf{Q}}} + t(1-a)\tilde{\tilde{\mathbf{P}}}$$

$$\mathbf{p} = \mathbf{P} + t\mathcal{F}(\mathbf{Q}, bt)$$

$$\mathbf{q} = \mathbf{Q} + at\Big[\mathbf{P} + t\mathcal{F}(\mathbf{Q}, bt)\Big]$$

Now that the transformation equations are known, the generating functions are put into equation (3.26) resulting in the expression below.

$$\tilde{\tilde{H}} = \underbrace{\frac{1}{2}\mathbf{p}^2 + \frac{1}{2}U(\mathbf{q}, t)}_{\mathcal{H}} - \frac{\partial}{\partial t}\underbrace{\left\{\Big[a\frac{1}{2}\mathbf{p}^2 + U(\mathbf{Q}, bt)\Big]t\right\}}_{F_3} - \frac{\partial}{\partial t}\underbrace{\left\{\frac{(1-a)t}{2}\mathbf{P}^2\right\}}_{\tilde{\tilde{F}}_3}$$

The final expression for the Hamiltonian as a function of $\tilde{\tilde{Q}}, \tilde{\tilde{P}}$ can be found using the transformation equations. This is a long and messy expression; however, the Taylor expansion around $t = 0$ results in a much simpler form shown in equation (3.27).

$$\tilde{\tilde{H}} = t(1-2a)\tilde{\tilde{\mathbf{P}}}\mathcal{F}(\tilde{\tilde{\mathbf{Q}}}, 0) + t(1-2b)U_t(\tilde{\tilde{\mathbf{Q}}}, 0) + \mathcal{O}(t^2) \tag{3.27}$$

It is clear that choosing the values for a and b shown below will result in the Taylor expansion being equal to zero.

$$a = \frac{1}{2} \qquad b = \frac{1}{2}$$

Following the strategy from the previous section it is now easy to formulate the numerical method using the transformation equations. This reveals the classic two-step method commonly referred to as "Leapfrog".

$$\boxed{\begin{aligned} \mathbf{P}_{k+1} &= \mathbf{p}_k & \mathbf{Q}_{k+1} &= \mathbf{q}_k + \mathbf{P}_{k+1}\frac{h}{2} \\ \mathbf{p}_{k+1} &= \mathbf{P}_k + t\mathcal{F}(\mathbf{Q}_k, t_0 + \frac{h}{2}) & \mathbf{q}_{k+1} &= \mathbf{Q}_k + \mathbf{P}_{k+1}\frac{h}{2} \end{aligned}} \tag{3.28}$$

Even though only the first derivative was included in the Taylor expansion, Leapfrog is a second order numerical method. Ruth (1983) argues that the reason for this is that the order of the method is inherited from the order of the Hamiltonian mapping. Further more, it is explained that because the method is based on a canonical transformation of a first order map, the second Hamiltonian is second order.

3.2 Symplectic integration algorithms

Deriving canonical methods of increasingly higher order becomes significantly more difficult. Instead of using the approach to the canonical transformation using generating functions, this section will use the symplectic approach from the final section of chapter (2).

The section considers Runge-Kutta-Nyström methods specifically intended for equations of motion derived from Hamiltonian functions on the form shown in equation (3.1).

3.2.1 Runge-Kutta-Nyström integration

This section introduces the general Runge-Kutta-Nyström method for second order ODEs without dependence on a first derivative term. By the end of this section it should be clear that it is a good idea to use a method intended for second order ODEs, even though the canonical equations of motion are first order equations.

The general RKN discretization can be found in chapter one in Wu et al. (2013). When the discretization is applied to the ODE in equation (3.29) it becomes significantly simplified and reduces to the form shown in equation (3.30). The connection between the RKN method and the canonical equations of motion will be introduced after the general method along with order conditions has been introduced.

$$\begin{gathered} \ddot{y} = f(y) \\ y(t_0) = y_0 \qquad \dot{y}(t_0) = \dot{y}_0 \end{gathered} \tag{3.29}$$

The result of discretizing the ODE is shown in equation (3.30). The derivation of the discretization will not be considered in this work; however, it can be found applying definition 1.9 in Wu et al. (2013) on equation (3.29).

$$\begin{aligned} y_{k+1} &= y_k + h\dot{y}_k + h^2 \sum_{i=1}^{s} \bar{b}_i k_i \\ \dot{y}_{k+1} &= \dot{y}_k + h \sum_{i=1}^{s} b_i k_i \\ k_i &= f\Big(t_k + c_i h, y_k + c_i h \dot{y}_k + h^2 \sum_{j=1}^{i-1} \bar{a}_{ij} k_j\Big) \qquad ; i = 1 \dots s \end{aligned} \tag{3.30}$$

Equation (3.30) is known as a s-stage RKN method. The coefficients $\bar{b}_i / b_i, \bar{a}_{ij}$ will respectively be referred to as weights and inner weights, and c_i are the nodes of the method. It is conventional to display the coefficients graphically using a Butcher tableau. The tableau shown in (3.31) is valid for any general, explicit s-stage RKN method.

For the purpose of this work however, the inner weights belonging to the first derivative terms (a_{ij}) are redundant. However, since the weights b_i still must be used, the form

$$
\begin{array}{c|ccccc|ccccc}
0 & 0 & & & & & 0 & & & & \\
c_2 & \bar{a}_{21} & & & & & a_{21} & & & & \\
c_3 & \bar{a}_{31} & \bar{a}_{32} & & & & a_{31} & a_{32} & & & \\
\vdots & \vdots & & \ddots & & & \vdots & & \ddots & & \\
c_s & \bar{a}_{s1} & \bar{a}_{s2} & \dots & \bar{a}_{s,s-1} & & a_{s1} & a_{s2} & \dots & a_{s,s-1} & \\
\hline
 & \bar{b}_1 & \bar{b}_2 & \dots & \bar{b}_{s-1} & \bar{b}_s & b_1 & b_1 & \dots & b_{s-1} & b_s
\end{array}
\tag{3.31}
$$

of the Buchner tableau (3.32), which was found on page 285 in Hairer et al. (1993), will be used from now on.

$$
\begin{array}{c|ccccc}
0 & 0 & & & & \\
c_2 & \bar{a}_{21} & & & & \\
c_3 & \bar{a}_{31} & \bar{a}_{32} & & & \\
\vdots & \vdots & & \ddots & & \\
c_s & \bar{a}_{s1} & \bar{a}_{s2} & \dots & \bar{a}_{s,s-1} & \\
\hline
 & \bar{b}_1 & \bar{b}_2 & \dots & \bar{b}_{s-1} & \bar{b}_s \\
\hline
 & b_1 & b_2 & \dots & b_{s-1} & b_s
\end{array}
\tag{3.32}
$$

The coefficients in the tableau are determined by imposing conditions on the method. The conditions are represented by algebraic equations which are derived in order for the method to have the desired properties. It is highly desirable to ensure that the method has a guaranteed accuracy and the order conditions for RKN methods are therefore well known. This work will not consider the derivation of the conditions; however the interested reader is referred to theorem 14.12 on page 291 in Hairer et al. (1993) for a thorough mathematical discussion.

The conditions that are used in this work are shown in table (3.1), however a couple of simplifying assumptions will be introduced first. The first assumption is shown in equation (3.33) and can be found as lemma 14.13 on page 293 in Hairer et al. (1993) and is extensively used in the literature that was considered in this work.

$$
\bar{b}_i = b_i(1 - c_i) \qquad ; i = 1 \dots s \tag{3.33}
$$

The assumption reduces the number of order equations that are needed in order to ensure the accuracy of the method. However, it does not reduce the number of equations that are needed in order to determine the order of a method.

The second assumption is shown in equation (3.34). This assumption is not as frequently used as the assumption in equation (3.33) and will only be used in the example at the end of this section in this work. The assumption can be found as lemma 14.14 in

Hairer et al. (1993).

$$\sum_{j=1}^{s} \bar{a}_{i,j} = \frac{c_i^2}{2} \qquad ; 1 \leq i \leq s \tag{3.34}$$

Just as the previous assumption, this does not change the number of equations. In the example in this section it is used to make the system of equations easier to solve. It becomes apparent that this happens when the order conditions are studied closer.

The conditions needed in this work are listed in table (3.1) and where obtained using tables and equations in (Hairer et al. (1993)). Methods with order higher than four require a significant amount of order equations more than the seven that are listed in the table. According to Table 1 in Sanz-Serna (1992) it is necessary to have 79 conditions to reach order eight compared to the seven conditions required for fourth order.

Table 3.1: Order conditions for the coefficients in the RKN method. The table was made using equations and relations from pages 291-292 in Hairer et al. (1993): equation (14.24), table (14.3) and simplifying assumption in equation (14.26). The order conditions for the lower order must also be used in the higher order methods (e.g. order three require that order conditions 1,2 and 3 are used). Constructing an explicit RKN method will additionally require the following constraint: $a_{ij} = 0 \quad ; i \leq j$. The following assumption must be used in addition to the constraint equations: $\bar{b}_i = b_i(1 - c_i) \quad ; i = 1 \ldots s$.
The following assumption might simplify the system of equations that must be solved: $\frac{c_i^2}{2} = \sum_{j=1}^{s} \bar{a}_{ij} \quad ; i = 1 \ldots s$, using this equation will make some order conditions redundant.

Order	Conditions		
1	$\sum_i b_i = 1$		
2	$\sum_i b_i c_i = \frac{1}{2}$		
3	$\sum_i b_i c_i^2 = \frac{1}{3}$	$\sum_i b_i \sum_j \bar{a}_{ij} = \frac{1}{6}$	
4	$\sum_i b_i c_i^3 = \frac{1}{4}$	$\sum_i b_i c_i \sum_j \bar{a}_{ij} = \frac{1}{8}$	$\sum_i b_i \sum_j c_j \bar{a}_{ij} = \frac{1}{24}$

The example at the end of the section will use the order conditions from table (3.1) to determine the coefficients in a three-stage, fourth order RKN method. The ability to generate high order methods that have few stages for equations of the form shown in equation (3.29) is, according to Hairer et al. (1993), the main attractive property of the RKN method. On page 285 it is stated that a four-stage, fifth order method is possible to construct using the RKN approach and that this would require at least six stages using RK methods. This advantage was the main reason for choosing to consider RKN methods to integrate the equations of motion in this work.

This example considers the fourth order RKN method whose Buchner table is shown on page 285 in Hairer et al. (1993). The derivation of the method is not shown in the textbook; however, from the Buchner table it is clear that it is a three stage method. By using the explicit discretization shown below and order conditions from this section, the values for the coefficients in the textbook will be recreated.

$$
\begin{aligned}
y_{k+1} &= y_k + h\dot{y}_k + h^2\left(\bar{b}_1 k_1 + \bar{b}_2 k_2 + \bar{b}_3 k_3\right) \\
\dot{y}_{k+1} &= \dot{y}_k + h\left(b_1 k_1 + b_2 k_2 + b_3 k_3\right) \\
k_1 &= f\left(t_k + c_1 h, y_k + c_1 h\dot{y}_k\right) \\
k_2 &= f\left(t_k + c_2 h, y_k + c_2 h\dot{y}_k + h^2 \bar{a}_{21} k_1\right) \\
k_3 &= f\left(t_k + c_3 h, y_k + c_3 h\dot{y}_k + h^2 \bar{a}_{31} k_2 + h^2 \bar{a}_{32} k_2\right)
\end{aligned}
$$

Because the method is explicit one can immediately say that $c_1 = 0$.
Next the table is used to set up all the equations for the coefficients. The order requirements are on the left, while the assumptions that are in the caption on the table are on the right.

$$
\begin{aligned}
b_1 + b_2 + b_3 &= 1 \\
b_2 c_2 + b_3 c_3 &= \frac{1}{2} \\
b_2 c_2^2 + b_3 c_3^2 &= \frac{1}{3} \\
b_2 c_2^3 + b_3 c_3^3 &= \frac{1}{4} \\
b_3 c_2 \bar{a}_{32} &= \frac{1}{24}
\end{aligned}
\qquad\qquad
\begin{aligned}
\bar{b}_1 &= b_1 \\
\bar{b}_2 &= b_2(1 - c_2) \\
\bar{b}_3 &= b_3(1 - c_3) \\
\frac{c_2^2}{2} &= \bar{a}_{21} \\
\frac{c_3^2}{2} &= \bar{a}_{31} + \bar{a}_{32}
\end{aligned}
$$

The degree of freedom should be used in a clever place. It is natural to consider the three equations describing b_2, c_2, b_3, c_3. Choosing $c_2 = \frac{1}{2}$ the three equations determine $c_3 = 1, b_3 = \frac{1}{6}$ and $b_2 = \frac{4}{6}$. Determining the rest of the coefficients is trivial and the resulting Buchner tableau is shown below.

0	0		
$\frac{1}{2}$	$\frac{1}{8}$		
1	0	$\frac{1}{2}$	
	$\frac{1}{6}$	$\frac{1}{3}$	0
	$\frac{1}{6}$	$\frac{4}{6}$	$\frac{1}{6}$

$$
\begin{aligned}
y_{k+1} &= y_k + h\dot{y}_k + \frac{h^2}{6}\left(k_1 + 2k_2\right) \\
\dot{y}_{k+1} &= \dot{y}_k + \frac{h}{6}\left(k_1 + 4k_2 + k_3\right) \\
k_1 &= f\left(y_k\right) \\
k_2 &= f\left(y_k + \frac{h}{2}\dot{y}_k + \frac{h^2}{8}k_1\right) \\
k_3 &= f\left(y_k + h\dot{y}_k + \frac{h^2}{2}k_2\right)
\end{aligned}
$$

3.2.2 Symplectic Runge-Kutta-Nyström integration

This section will introduce symplectic RKN methods. A two-stage method will be considered in order to show that the requirement for a symplectic matrix in equation (2.50) can be used. However, the symplectic requirement for the coefficients of RKN methods is well known and can be found in (3.40). The example at the end of the section will therefore use these equations in order to generate a three-stage, third order symplectic method.

An outline of the two-stage method can be found in Simos (2002) and Van de Vyver (2005). Just as in the previous section, the system that is considered is described by the second order ODE from equation (3.29). The previous section has already showed that the canonical equations can be expressed using the RKN framework. However, for the sake of generality the derivation is done by expressing the second order ODE as a system of first order equations as shown in equation (3.35).

$$\ddot{y} = f(y) \Leftrightarrow \begin{bmatrix} \dot{y} \\ \dot{v} \end{bmatrix} = \begin{bmatrix} v \\ f(y) \end{bmatrix} \quad ; f(y) = -\frac{1}{m}\frac{\partial \mathcal{L}}{\partial y} \tag{3.35}$$

Using the relations between the variables in equation (3.35) the RKN discretization equations can be expressed of the form shown in equation (3.36).

$$\begin{aligned} y_{k+1} &= g_1 y_k + h g_2 v_k + h^2 \sum_{i=1}^{s} \bar{b}_i k_i \\ v_{k+1} &= g_3 v_k + h \sum_{i=1}^{s} b_i k_i \\ k_i &= f(y_k + h c_i v_i + h^2 \sum_{j=1}^{i-1} \bar{a}_{ij} k_j) \quad ; i = 1 \dots s \end{aligned} \tag{3.36}$$

Now that the discretization equations have been established, the goal is to scale the numerical flow such that it is symplectic. In order to do this, the strategy will be to introduce scaling coefficients into the discretization. The introduction of the scaling coefficients becomes more clear when the matrix representation of the discretization equations is used.

$$\begin{aligned} \begin{bmatrix} y \\ v \end{bmatrix}_{k+1} &= \mathbf{A} \begin{bmatrix} y \\ v \end{bmatrix}_k + \begin{bmatrix} h^2 \sum_{i=1}^{s} \bar{b}_i k_i \\ h \sum_{i=1}^{s} b_i k_i \end{bmatrix} \\ k_i &= f(y_k + h c_i v_i + h^2 \sum_{j=1}^{i-1} \bar{a}_{ij} k_j) \quad ; i = 1 \dots s \end{aligned}$$

It should now be clear that the matrix $\mathbf{A}$ is the coefficient matrix for the RKN discretization. And that for the standard RKN method it has the form shown below.

$$\mathbf{A} = \begin{bmatrix} 1 & 1 \\ 0 & 1 \end{bmatrix}$$

The RKN method can now be modified by introducing the scaling coefficients in the coefficient matrix of the RKN method.

$$\mathbf{A} = \begin{bmatrix} g_1 & g_2 \\ 0 & g_3 \end{bmatrix} = \mathbf{M}$$

The result of this analysis is the starting point of the symplectic RKN methods in Simos (2002) and Van de Vyver (2005).

The next step is to ensure that the Jacobian of the numerical flow is symplectic. The symplecticity requirement for a matrix was defined in equation (2.51) and stated that the determinant must be equal to one.

$$\Theta_h'(y_k, x_k) = \mathbf{M} \Rightarrow \det \left| \begin{bmatrix} \frac{\partial y_{k+1}}{\partial y_k} & \frac{\partial y_{k+1}}{\partial x_k} \\ \frac{\partial x_{k+1}}{\partial y_k} & \frac{\partial x_{k+1}}{\partial x_k} \end{bmatrix} \right| = 1$$

Following the approach of Simos (2002) and Van de Vyver (2005), the two-stage RKN method in equation (3.37) can now be considered using the symplectic requirement.

$$\begin{aligned} y_{k+1} &= g_1 y_k + g_2 h v_k + h^2 \Big(\bar{b}_1 k_1 + \bar{b}_2 k_2 \Big) \\ v_{k+1} &= g_3 v_k + h \Big(b_1 k_1 + b_2 k_2 \Big) \\ k_1 &= f\Big(y_k \Big) \\ k_2 &= f\Big(y_k + c_2 h v_k + h^2 \bar{a}_{21} k_1 \Big) \end{aligned} \tag{3.37}$$

The determinant of the numerical flow for the two-stage method is shown in equation (3.38).

$$\begin{aligned} \det \left| \Phi_h'(y_k, x_k) \right| =& g_1 g_3 + \Big[(g_3 \bar{b}_1 - g_2 b_1) \frac{\partial f(k_1)}{\partial k_1} + [g_3 \bar{b}_2 + (g_1 c_2 - g_2) b_2] \frac{\partial f(k_2)}{\partial k_2} \Big] h^2 + \\ & \Big[\bar{b}_1 b_2 c_2 + \bar{b}_2 \bar{a}_{21} g_3 - g_2 b_2 \bar{a}_{21} - \bar{b}_2 c_2 b_1 \Big] \frac{\partial f(k_1)}{\partial k_1} \frac{\partial f(k_2)}{\partial k_2} h^4 \\ =& 1 \end{aligned} \tag{3.38}$$

In order for the determinant to be equal to one, it can be concluded that the relations in equation (3.39) must be satisfied. This is equivalent to the symplectic requirements in Simos (2002) and Van de Vyver (2005).

$$\begin{aligned} g_1 g_3 &= 1 \\ g_3 \bar{b}_1 - g_2 b_1 &= 0 \\ g_3 \bar{b}_2 + (g_1 c_2 - g_2) b_2 &= 0 \\ \bar{b}_1 b_2 - \bar{a}_{21} g_1 b_2 - \bar{b}_2 b_1 &= 0 \end{aligned} \tag{3.39}$$

However, it was mentioned in the introduction of the section that the symplectic requirements for explicit RKN methods are well known. Theorem 16.11 on page 330 in Hairer et al. (1993) states that the RKN method for a system that is described by a separable Hamiltonian with square kinetic energy is symplectic if the coefficients satisfy the relations in equation (3.40).

$$\begin{aligned} \bar{b}_i &= b_i (1 - c_i) \\ a_{ij} &= b_i (c_i - c_j) \qquad ; i, j = 1 \dots s \end{aligned} \tag{3.40}$$

The top requirement is recognized as the symmetry assumption from equation (3.33). The second requirement in equation (3.40) has been modified from the original expression in the textbook and can only be applied to explicit methods. The reason it was changed from the original expression is that it allows the symplectic conditions to be nicely summarized in the Butcher tableau for explicit RKN methods shown in (3.41).

$$\begin{array}{c|ccccc} c_1 & 0 & & & & \\ c_2 & b_1(c_2-c_1) & 0 & & & \\ c_3 & b_1(c_3-c_1) & b_2(c_3-c_2) & 0 & & \\ \vdots & \vdots & \vdots & \ddots & & \\ c_s & b_1(c_s-c_1) & b_2(c_s-c_2) & \dots & b_{s-1}(c_s-c_{s-1}) & 0 \\ \hline & b_1(1-c_1) & b_2(1-c_2) & \dots & b_{s-1}(1-c_{s-1}) & b_s(1-c_s) \\ \hline & b_1 & b_2 & \dots & b_{s-1} & b_s \end{array} \tag{3.41}$$

The following example considers the derivation of a third order explicit and symplectic Runge-Kutta-Nyström method using the requirements in equation (3.40). The goal is to reproduce a Buchner tableau found in Zhao and Zhu (1991).

The symplectic conditions are shown below in the Butcher tableau and the order conditions are listed on the right. One coefficient may be chosen at random in order to close the system of equations consisting of seven equations and eight unknown quantities.

$$\begin{array}{c|ccc} 0 & 0 & & \\ c_2 & b_1c_2 & 0 & \\ c_3 & b_1c_3 & b_2(c_3-c_2) & 0 \\ \hline & b_1 & b_2(1-c_2) & b_3(1-c_3) \\ \hline & b_1 & b_2 & b_3 \end{array}$$

$$\begin{aligned} b_1+b_2+b_3 &= 1 \\ b_2c_2+b_3c_3 &= \frac{1}{2} \\ b_2c_2^2+b_3c_3^2 &= \frac{1}{3} \\ b_2a_{21}+b_3a_{31}+b_3a_{32} &= \frac{1}{6} \end{aligned}$$

Choosing $c_3 = 0$ resulted in the Butcher table below, which is equal to the table from the article mentioned in the beginning of the example.

$$\begin{array}{c|ccc} 0 & 0 & & \\ \frac{2}{3} & \frac{7}{36} & 0 & \\ 0 & 0 & -\frac{1}{2} & 0 \\ \hline & \frac{7}{24} & \frac{1}{4} & -\frac{1}{24} \\ \hline & \frac{7}{24} & \frac{3}{4} & -\frac{1}{24} \end{array}$$

$$\begin{aligned} q_{k+1} &= q_k + hv_k + h^2\frac{7}{24}\left(k_1 + 6k_2 - \frac{1}{7}k_3\right) \\ v_{k+1} &= v_k + h\frac{7}{24}\left(k_1 + 28k_2 - \frac{1}{7}k_3\right) \\ k_1 &= f\left(q_k\right) \\ k_2 &= f\left(q_k + h\frac{2}{3}v_k + h^2\frac{7}{36}k_1\right) \\ k_3 &= f\left(q_k + h\frac{2}{3}v_k - \frac{h^2}{2}k_2\right) \end{aligned}$$

3.2.3 Exponentially fitted Runge-Kutta-Nyström integration

This section studies how the Runge Kutta Nyström method can be fitted to the exponential function. The reason why this is desirable in this work is because the systems which are studied have equations of motion which corresponds to oscillatory solutions. It is therefore desirable to use this a priori knowledge to modify the numerical method such that it automatically captures the dynamics of the solution in each iteration. The numerical method will consequently exactly reproduce the analytical solution of a linear problem, whose solution is a linear combination of exponential functions. The underlying mathematical theory is quite rigorous and for this reason the choice was made to consider the subject from a practical perspective. This means that the methods will be derived using definitions and relations from books and papers without a further investigation into the background of these relations. However, references will be made to relevant fundamental sources that can be used in order to study the background more closely.

The starting point of the study of exponential fitting of RKN methods is the discretization in equation (3.42). The notation of the weights and nodes has been changed from the original expression in equation (3.30) to emphasize the dependence of the variable z.

$$\begin{aligned}
y_{k+1} &= y_k + h\dot{y}_k + h^2 \sum_{i=1}^{s} \bar{\beta}_i f(t_k + c_i h, Y_i) && ;\bar{\beta}_i = \bar{b}_i(z) \\
\dot{y}_{k+1} &= \dot{y}_k + h \sum_{i=1}^{s} \beta_i f(t_k + c_i h, Y_i) && ;\beta_i = b_i(z) \\
Y_1 &= y_k + c_1 \gamma_1 h \dot{y}_k && ;\gamma_i = \gamma_i(z) \qquad \alpha_{ij} = a_{ij}(z) \\
Y_i &= y_k + c_i \gamma_i h \dot{y}_k + h^2 \sum_{j=1}^{i-1} \alpha_{ij} f(t_k + c_j h, Y_j) && ;i = 2 \ldots s
\end{aligned} \tag{3.42}$$

The parameter γ is introduced in order to make it possible to fit the RKN method to an exponential function. The first stage Y_1 has the value $\gamma_1 = 1$ for explicit methods because $c_1 = 0$ and the value of y_n does therefore not have to be schooled in order to fit an exponential function. This is thoroughly explained in (Berghe et al. (1999)) and this work continues without further consideration of this parameter. Hoverer, it is clear that in the limit $z \to 0$ the value of γ_i should become one in order to reproduce the classical RKN method. Note that the new variable λ_i is introduced in order to comply with the notation that is used in Franco (2004), Van de Vyver (2005) and Simos (2002). According to Van de Vyver (2005), the exponential method in his article ensures that the method exactly integrates any ODE whose solution is any linear combination of the following basis functions.

$$\left\{1, t, \ldots, t^k, \exp(\pm zt), \ldots, t^p \exp(\pm zt)\right\} \tag{3.43}$$

In this work the particularly interesting case is the set $\{\exp(zt), \exp(-zt)\}$ or equivalently $\{\sin(\omega t), \sin(\omega t)\}$ where $z = i\omega$. The systems in this work are purely oscillatory and the solution will therefore be a linear combination of sine and cosine functions.

The mathematical derivation of the exponential fitting conditions of numerical methods to the above set of functions can be found in Lyche (1972). This article is mathematically dense and the recent publication D'Ambrosio et al. (2014) presents a more practical approach which is restricted to explicit RKN methods. The latter article states that the are associated with the linear functional operators shown in equation (3.44) are associated with the exponential fitting conditions for equation (3.42).

$$\begin{aligned}
\mathcal{J}_i[y(t);h;\boldsymbol{\alpha}] &= y(t+c_ih) - y(t) - c_i\gamma_i h\dot{y} - h^2\sum_{j=1}^{i-1}\alpha_{ij}\ddot{y}(t+c_jh) \qquad ;i=1\dots s \\
\mathcal{J}[y(t);h;\bar{\boldsymbol{\beta}}] &= y(t+h) - y(t) - h\dot{y}(t) - h^2\sum_{i=1}^{s}\bar{b}_i\ddot{y}(t+c_ih) \\
\mathcal{J}[y(t);h;\boldsymbol{\beta}] &= h\dot{y}(t+h) - h\dot{y}(t) - h^2\sum_{i=1}^{s}b_i\ddot{y}(t+c_ih)
\end{aligned} \tag{3.44}$$

The top requirement concerns the internal stages of the method whereas the latter respectively describes the first and final stage. When the operators in equation (3.44) is applied to the set $\{\exp(\nu t), \exp(-\nu t)\}$ the following expressions are found for the coefficients of the RKN discretization.

$$\begin{aligned}
\exp[\pm c_i z] &= 1 \pm z + c_i z\gamma_i + z^2\sum_{j=1}^{i-1}\alpha_{ij}\exp(\pm c_j z) \qquad ;i=2\dots s \\
\exp[\pm z] &= 1 \pm z^2\sum_{i=1}^{s}\bar{\beta}_i\exp[\pm c_i z] \qquad ;z=\nu h \\
\exp[\pm z] &= 1 \pm z\sum_{i=1}^{s}\beta\exp[\pm z]
\end{aligned} \tag{3.45}$$

Note that the variable z has been defined during the derivation as the product $z = \nu h$, which appears when the set of functions is differentiated. In order to obtain the final expression for the coefficients in equation (3.45), the functional was demanded to vanish at $t = 0$ as shown below.

$$\mathcal{J}[e^{\pm\nu t}|_{t=0};h;\bar{\boldsymbol{\beta}}] = 0 \qquad \mathcal{J}[e^{\pm\nu t}|_{t=0};h;\boldsymbol{\beta}] = 0 \qquad \mathcal{J}[e^{\pm\nu t}|_{t=0};h;\boldsymbol{\alpha}] = 0$$

The argument that this is a sufficient requirement for obtaining the coefficients for the method can be found in D'Ambrosio et al. (2014) and (Franco (2004)). The first article focuses on a more specialized method which is not considered in this work and consequently does not show the same conditions which are presented here. However, (Franco (2004)) presents the same conditions for the coefficients in an ERKN method that are shown in equation (3.45). This article also uses the following tableau for the exponentially fitted method in (Franco (2004)) which was also proposed for Runge Kutta methods in (Berghe et al. (1999)).

$$
\begin{array}{c|c|ccccc}
0 & 1 & 0 & & & & \\
c_2 & \gamma_2 & \alpha_{21} & & & & \\
c_3 & \gamma_3 & \alpha_{31} & a_{32} & & & \\
\vdots & \vdots & \vdots & \vdots & \ddots & & \\
c_s & \gamma_s & \alpha_{s1} & \alpha_{s2} & \dots & \alpha_{s,s-1} & \\
\hline
 & & \bar{\beta}_1 & \bar{\beta}_2 & \dots & \bar{\beta}_{s-1} & \bar{\beta}_s \\
\hline
 & & \beta_1 & \beta_2 & \dots & \beta_{s-1} & \beta_s
\end{array}
\tag{3.46}
$$

The expressions in equation (3.45) can be rewritten using the trigonometric relations for hyperbolic functions.

$$\cosh(z) = \frac{1}{2}\Big(e^z + e^{-z}\Big) \qquad ; \sinh(z) = \frac{1}{2}\Big(e^z - e^{-z}\Big)$$

This leads to the system shown in equation (3.47) which can also be found in Franco (2004).

$$
\begin{aligned}
\sum_{j=1}^{i-1} \alpha_{ij} \cosh(c_j z) &= \frac{1}{z^2}\Big(\cosh(c_i z) - 1\Big) && ; i = 2 \dots s \\
\sum_{j=1}^{i-1} \alpha_{ij} \sinh(c_j z) &= \frac{1}{z^2}\Big(\sinh(c_i z) - c_i z \gamma_i\Big) && ; i = 2 \dots s \\
\sum_{i=1}^{s} \bar{\beta}_i \cosh(c_i z) &= \frac{1}{z^2}\Big(\cosh(z) - 1\Big) \\
\sum_{i=1}^{s} \bar{\beta}_i \sinh(c_i z) &= \frac{1}{z^2}\Big(\sinh(z) - z\Big) \\
\sum_{i=1}^{s} \beta_i \sinh(c_i z) &= \frac{1}{z}\Big(\cosh(z) - 1\Big) \\
\sum_{i=1}^{s} \beta_i \cosh(c_i z) &= \frac{1}{z}\sinh(z)
\end{aligned}
\tag{3.47}
$$

The specific expressions for the exponential fitting conditions that are used in Simos (2002), Van de Vyver (2005) and Franco (2004) can now be obtained using the system in equation (3.47). The methods in the articles are two-stage methods, which reduces the system in equation (3.47) to the form shown in equation (3.48).

$$
\begin{aligned}
\alpha_{21} &= \frac{1}{z^2}\Big(\cosh(c_2 z) - 1\Big) & \gamma_2 &= \frac{1}{c_2 z}\sinh(c_2 z) \\
\bar{\beta}_1 &= \frac{1}{z^2}\Big(\cosh(z) - 1\Big) - \bar{\beta}_2 \cosh(c_2 z) & \bar{\beta}_2 &= \frac{\sinh(z) - z}{z^2 \sinh(c_2 z)} \\
\beta_2 &= \frac{\cosh(z) - 1}{z \sinh(c_2 z)} & \beta_1 &= \frac{1}{z}\sinh(z) - \beta_2 \cosh(c_2 z)
\end{aligned}
$$

Note that there is still one degree of freedom (c_2) left in this system of equations before any other constraints are added. Simos (2002) and Van de Vyver (2005) both derive symplectic methods that require the degree of freedom in order to ensure symplecticness of the methods. Franco (2004) on the other hand solves the system along with the conditions for third order RKN methods shown below.

0	1	0	
c_2	γ_2	α_{21}	0
		$\bar{\beta}_1$	$\bar{\beta}_2$
		β_1	β_2

$$\begin{aligned} \beta_1 + \beta_2 &= 1 \\ \beta_2 c_2 &= \frac{1}{2} \\ \beta_2 c_2^2 &= \frac{1}{3} \\ \bar{\beta}_1 &= \beta_1 \\ \bar{\beta}_2 &= \beta_2 + \beta_2 c_2 \end{aligned} \tag{3.48}$$

The system of equations was solved in this work as well, arriving at the conclusion that $c_2 = \frac{2}{3}$ will produce a third order method that is exponentially fitted when the equations shown below are used for the remaining coefficients.

$$\alpha_{21} = \frac{1}{z^2}\Big(\cosh\left(\frac{2}{3}z\right) - 1\Big) \qquad \gamma_2 = \frac{1}{\frac{2}{3}z}\sinh\left(\frac{2}{3}z\right)$$

$$\bar{\beta}_1 = \frac{1}{z^2}\Big(\cosh\left(z\right) - 1\Big) - \frac{\left(\sinh\left(z\right) - z\right)\cosh\left(\frac{2}{3}z\right)}{z^2\sinh\left(\frac{2}{3}z\right)} \qquad \bar{\beta}_2 = \frac{\sinh\left(z\right) - z}{z^2\sinh\left(\frac{2}{3}z\right)}$$

$$\beta_1 = \frac{1}{z}\sinh\left(z\right) - \frac{\left(\cosh\left(z\right) - 1\right)\cosh\left(\frac{2}{3}z\right)}{z\sinh\left(\frac{2}{3}z\right)} \qquad \beta_2 = \frac{\cosh\left(z\right) - 1}{z\sinh\left(\frac{2}{3}z\right)}$$

The value of ν, which determines $z = \nu h$, is proposed in Van de Vyver (2005) to be set equal to the step size h. All of the articles also states that for "small" values of z the expressions for the coefficients must be obtained using a Taylor expansion around $t = 0$. Van de Vyver (2005) goes on to propose that the parameter can be assumed "small" when $z \leq 0.1$. The following coefficients was found when the third order method was expanded around $t = 0$.

The coefficients are shown on the next page and are equivalent to the set proposed in (Franco (2004)). The final result is the third order explicit RKN method (ERKN) that can be using the scheme shown in equation (3.49).

$$\boxed{\begin{aligned} q_{k+1} &= q_k + hv_k + h^2\left(\bar{\beta}_1 k_1 + \bar{\beta}_2 k_2 + \bar{\beta}_3 k_3\right) \\ v_{k+1} &= v_k + h\left(k_1\beta_1 + k_2\beta_2 + k_3\beta_3\right) \\ k_1 &= f\left(q_k\right) \qquad ; f(y) = -\frac{1}{m}\frac{\partial \mathcal{L}}{\partial y} \\ k_2 &= f\left(q_k + \gamma_2 h\frac{2}{3}v_k + h^2\alpha_{21}k_1\right) \end{aligned}} \tag{3.49}$$

The following equations show the coefficients for the ERKN method that where found based on a Taylor expansion of the trigonometric-hyperbolic constraint equations around t=0.

$$\begin{aligned}
\alpha_{21} &= \frac{2}{9} + \frac{2}{243}z^2 + \frac{4}{32805}z^4 + \frac{2}{2066715}z^6 + \frac{4}{837019575}z^8 + \frac{4}{248594813775}z^{10} \\
&\quad + \frac{8}{203599152481725}z^{12} + \frac{2}{27485885585032875}z^{14} + \mathcal{O}\left(z^{16}\right) \\
\gamma_2 &= 1 + \frac{2}{27}z^2 + \frac{2}{1215}z^4 + \frac{4}{229635}z^6 + \frac{2}{18600435}z^8 + \frac{4}{9207215325}z^{10} \\
&\quad + \frac{4}{3231732579075}z^{12} + \frac{8}{3053987287225875}z^{14} + \mathcal{O}\left(z^{16}\right) \\
\bar{\beta_1} &= \frac{1}{4} - \frac{17}{2160}z^2 + \frac{55}{163296}z^4 - \frac{13231}{881798400}z^6 + \frac{117673}{174596083200}z^8 - \frac{780698467}{25738954585344000}z^{10} \\
&\quad + \frac{34511669}{25270973592883200}z^{12} - \frac{1046191876349}{17012419422728970240000}z^{14} + \mathcal{O}\left(z^{16}\right) \\
\bar{\beta_2} &= \frac{1}{4} - \frac{13}{2160}z^2 + \frac{271}{816480}z^4 - \frac{1877}{125971200}z^6 + \frac{23497}{34919216640}z^8 - \frac{780383783}{25738954585344000}z^{10} \\
&\quad + \frac{379590131}{277980709521715200}z^{12} - \frac{95105958011}{1546583583884451840000}z^{14} + \mathcal{O}\left(z^{16}\right) \\
\beta_1 &= \frac{1}{4} - \frac{1}{144}z^2 + \frac{11}{38880}z^4 - \frac{731}{58786560}z^6 + \frac{589}{1058158080}z^8 - \frac{471953}{18856376985600}z^{10} \\
&\quad + \frac{14913991}{13237176643891200}z^{12} - \frac{307687339}{6065033662291968000}z^{14} + \mathcal{O}\left(z^{16}\right) \\
\beta_2 &= \frac{3}{4} + \frac{1}{144}z^2 + \frac{13}{38880}z^4 - \frac{709}{58786560}z^6 + \frac{587}{1058158080}z^8 - \frac{471487}{18856376985600}z^{10} \\
&\quad + \frac{14910353}{13237176643891200}z^{12} - \frac{3384354151}{66715370285211648000}z^{14} + \mathcal{O}\left(z^{16}\right)
\end{aligned}$$

3.2.4 Symplectic, Exponentially fitted Runge-Kutta-Nyström integration

Symplectic and exponentially fitted integrators require the merging of the methods from section (3.2.3) and (3.2.2). The main section considers the derivation of the symplectic and exponentially fitted (SERKN) method from Van de Vyver (2005). The example at the end of the section considers a symplectic and trigonometric fitted (STRKN) method from Monovasilis et al. (2013).

The form of the RKN discretization shown in equation (3.50) uses notation from the discretization in equation (3.42) and (**??**) which was respectively used for the exponential and symplectic methods.

$$\begin{aligned} q_{k+1} &= g_1 q_k + g_2 h v_k + h^2 \sum_{i=1}^{s} \bar{\beta}_i f(Y_i) && ;\bar{\beta}_i = \bar{b}_i(z) \\ v_{k+1} &= g_3 v_k + h \sum_{i=1}^{s} \beta_i f(Y_i) && ;\beta_i = b_i(z) \qquad \alpha_{ij} = a_{ij}(z) \\ Y_1 &= q_k + c_1 \gamma_1 h v_k \\ Y_i &= q_k + c_i \gamma_i h v_k + h^2 \sum_{j=1}^{i-1} \alpha_{ij} f(Y_j) && ;i = 2 \dots s \end{aligned} \tag{3.50}$$

It is clear that this section requires the combined knowledge of chapter (2) and the previous sections in this chapter in order to construct the method. The introduction mentioned that the goal of this section is to reproduce the SERKN method which can be found in Van de Vyver (2005). This article is based on the work presented in Simos and Aguiar (2003); however, uses a more methodical approach. Because both methods are two-stage explicit RKN methods the discretization equation (3.50) can be expressed as shown below.

$$\begin{aligned} q_{k+1} &= g_1 q_k + g_2 h v_k + h^2 \left(\bar{\beta}_1 k_1 + \bar{\beta}_2 k_2\right) \\ v_{k+1} &= g_3 v_k + h \left(\beta_1 k_1 + \beta_2 k_2\right) \\ k_1 &= f(q_k) \\ k_2 &= f(q_k + c_2 \gamma_2 h v_k + h^2 \alpha_{21}) \end{aligned}$$

The symplectic conditions will first be considered using the equivalent approach discussed in section (3.2.2) by using the symplectic condition for a two stage method equivalent to the expression in equation (3.38).

$$\begin{aligned} \det \left| \Phi_h'(q_k, p_k) \right| =& g_1 g_3 + \left[(g_3 \bar{b}_1 - g_2 b_1) \frac{\partial k_1}{\partial q} + [g_3 \bar{b}_2 + (g_1 c_2 - g_2) b_2] \frac{\partial k_2}{\partial q} \right] h^2 + \\ & \left[\bar{b}_1 b_2 c_2 \gamma_2 + \bar{b}_2 \alpha_{21} g_3 - g_2 b_2 \alpha_{21} - \gamma_2 \bar{b}_2 c_2 b_1 \right] \frac{\partial k_1}{\partial y} \frac{\partial k_2}{\partial y} h^4 \\ =& 1 \end{aligned} \tag{3.51}$$

The expression above leads to the following symplectic conditions for the coefficients of the method.

$$\begin{aligned} g_1 g_3 &= 1 \\ g_3\bar{\beta}_1 - g_2\beta_1 &= 0 \\ g_3\bar{\beta}_2 + (g_1\gamma_2 c_2 - g_2)\beta_2 &= 0 \\ \bar{\beta}_1\beta_2 - \alpha_{21} g_1\beta_2 - \bar{\beta}_2\beta_1 &= 0 \end{aligned} \tag{3.52}$$

Exponential fitting was discussed in section (3.2.3), however for this method it is important to include the new coefficients g_1, g_2, g_3 in the requirement. This does not change the general derivation that lead to the hyperbolic expressions in equation (3.47), however the expressions themselves as shown in equation (3.53).

$$\begin{aligned} \sum_{j=1}^{i-1} \alpha_{ij} \cosh(c_j z) &= \frac{1}{z^2}\Big(\cosh(c_i z) - 1\Big) \\ \sum_{j=1}^{i-1} \alpha_{ij} \sinh(c_j z) &= \frac{1}{z^2}\Big(\sinh(c_i z) - c_i z\gamma_i\Big) \\ \sum_{i=1}^{s} \bar{\beta}_i \cosh(c_i z) &= \frac{1}{z^2}\Big(\cosh(z) - g_1\Big) \\ \sum_{i=1}^{s} \bar{\beta}_i \sinh(c_i z) &= \frac{1}{z^2}\Big(\sinh(z) - z g_2\Big) \\ \sum_{i=1}^{s} \beta_i \sinh(c_i z) &= \frac{1}{z}\Big(\cosh(z) - g_3\Big) \\ \sum_{i=1}^{s} \beta_i \cosh(c_i z) &= \frac{1}{z}\sinh(z) \end{aligned} \tag{3.53}$$

When the system of equations was expressed for a two-stage method the exponential fitting conditions for the coefficients in equation (3.54) was obtained.

$$\begin{aligned} \alpha_{21} &= \frac{1}{z^2}\Big(\cosh(c_2 z) - 1\Big) & \gamma_2 &= \frac{1}{c_2 z}\sinh(c_2 z) \\ \bar{\beta}_1 &= \frac{1}{z^2}\Big(\cosh(z) - g_1\Big) - \bar{\beta}_2\cosh(c_2 z) & \bar{\beta}_2 &= \frac{\sinh(z) - z g_2}{z^2\sinh(c_2 z)} \\ \beta_2 &= \frac{\cosh(z) - g_3}{z\sinh(c_2 z)} & \beta_1 &= \frac{1}{z}\sinh(z) - \beta_2\cosh(c_2 z) \end{aligned} \tag{3.54}$$

The article Van de Vyver (2005) suggests using the value $c_2 = 1$ to solve the system of equations defined by equations in (3.52) and (3.54). However, this means that there are no degrees of freedom left to guarantee the order of the method. This can be avoided by using theorem 2.2 in Franco (2004). The theorem states that an explicit ERKN method

with $2 \leq s$ that satisfies equation 3.55 has algebraic order $2 \leq \mathcal{O}$.

$$\begin{aligned}
\bar{\beta} &\approx \bar{\beta} + \bar{\beta}'' h^2 + \bar{\beta}'''' h^4 + \dots \\
\beta &\approx \beta + \beta'' h^2 + \beta'''' h^4 + \dots \\
\gamma &\approx 1 + \gamma'' h^2 + \gamma'''' h^4 + \dots \\
\alpha_{ij} &\approx \alpha_{ij} + \alpha_{ij}'' h^2 + \alpha_{ij}'''' h^4 + \dots
\end{aligned} \tag{3.55}$$

Simultaneously solving the order conditions in (3.52) and exponential conditions in equation (3.54) using $c_2 = 1$ result in the following expression for the coefficients of the method:

$$\begin{gathered}
\bar{\beta}_2 = 0 \qquad g_1 = g_3 = 1 \qquad g_2 = \gamma_2 \qquad \beta_1 = \beta_2 \qquad \bar{\beta}_1 = \alpha_{21} \\
\gamma_2 = \frac{\sinh(z)}{z} \qquad \alpha_{21} = \frac{\cosh z - 1}{z^2} \qquad \beta_2 = \frac{\cosh z - 1}{z \sinh(z)}
\end{gathered} \tag{3.56}$$

It can now be assumed that $z \leq 0.1$ and the coefficients are expanded using a Taylor series around $t = 0$. This means that the method satisfies equation (3.54) and ensures the order of the method is more than one.

$$\begin{aligned}
\beta_2 &= \frac{1}{2} - \frac{1}{24} z^2 + \frac{1}{240} z^4 - \frac{17}{40320} z^6 + \frac{31}{725760} z^8 - \frac{691}{159667200} z^{10} \\
&\quad + \frac{5461}{12454041600} z^{12} - \frac{929569}{20922789888000} z^{14} + \mathcal{O}\left(z^{16}\right) \\
\gamma_2 &= 1 + \frac{1}{6} z^2 + \frac{1}{120} z^4 + \frac{1}{5040} z^6 + \frac{1}{362880} z^8 + \frac{1}{39916800} z^{10} \\
&\quad + \frac{1}{6227020800} z^{12} + \frac{1}{1307674368000} z^{14} + \mathcal{O}\left(z^{16}\right) \\
\alpha_{21} &= \frac{1}{2} + \frac{1}{24} z^2 + \frac{1}{720} z^4 + \frac{1}{40320} z^6 + \frac{1}{3628800} z^8 + \frac{1}{479001600} z^{10} \\
&\quad + \frac{1}{87178291200} z^{12} + \frac{1}{20922789888000} z^{14} + \mathcal{O}\left(z^{16}\right)
\end{aligned} \tag{3.57}$$

The Taylor expansion coincides exactly with the values that are given in Van de Vyver (2005). This means that the coefficients can now be used in the discretization to form the final expression for the symplectic and exponentially fitted RKN method as shown in equation (3.58).

$$\boxed{\begin{aligned}
q_{k+1} &= q_k + g_2 h v_k + h^2 \left(\bar{\beta}_1 k_1\right) \\
v_{k+1} &= v_k + h\beta_2 \left(k_1 + k_2\right) \\
k_1 &= f\left(q_k\right) \qquad ; f(y) = -\frac{1}{m}\frac{\partial \mathcal{L}}{\partial y} \\
k_2 &= f\left(q_k + \gamma_2 h v_k + h^2 \alpha_{21} k_1\right)
\end{aligned}} \tag{3.58}$$

The main section rigorously derived the symplectic and exponential fitting conditions. This example considers the derivation of a third order RKN method that is symplectic and fitted to trigonometric functions (STRKN). The derivation does not rigorously derive the method, however uses well established symplectic requirements along with the trigonometric fitting retains in the derivation. The method was presented in in Monovasilis et al. (2013).

The starting point is the three stage, symplectic method from the example in section (3.2.2). This example used the tableau from equation (3.40) to define the symplectic conditions method. The conditions from table (3.1) that are necessary to ensure that the method is third order is shown below in addition to the tableau.

0	0		
c_2	$\beta_1 c_2$	0	
c_3	$\beta_1 c_3$	$\beta_2(c_3 - c_2)$	0
	β_1	$\beta_2(1 - c_2)$	$\beta_3(1 - c_3)$
	β_1	β_2	β_3

$$\beta_1 + \beta_2 + \beta_3 = 1$$
$$\beta_2 c_2 + \beta_3 c_3 = \frac{1}{2}$$
$$\beta_2 c_2^2 + \beta_3 c_3^2 = \frac{1}{3}$$
$$\beta_2 \alpha_{21} + \beta_3 \alpha_{31} + \beta_3 \alpha_{32} = \frac{1}{6}$$

The strategy for the trigonometric fitting is to use the same procedure as in section (3.2.3), however using the set $\{\exp(\imath\nu t), \exp(-\imath\nu t)\}$. This correspond to changing the variable of the exponential fitting to $z = \imath\omega$. The general conditions from equation (3.47) can now be rewritten using:

$$\cosh(\imath x) = \cos(x) \quad \text{and} \quad \sinh(\imath x) = \imath \sin(x)$$

This lead to the conditions for the trigonometric fitting conditions for explicit RKN methods shown bellow. The conditions an equivalent form of the conditions was found in Paternoster (1998).

$$\sum_{j=1}^{i-1} \alpha_{ij} \cos(c_j\omega) = \frac{1}{\omega^2}\Big(1 - \cos(c_i\omega)\Big) \qquad i = 2 \ldots n$$
$$\sum_{j=1}^{i-1} \alpha_{ij} \sin(c_j\omega) = \frac{1}{\omega^2}\Big(c_i\omega - \sin(c_i\omega)\Big) \qquad i = 2 \ldots n$$
$$\sum_{i=1}^{s} \bar{\beta}_i \cos(c_i\omega) = \frac{1}{\omega^2}\Big(1 - \cos(\omega)\Big)$$
$$\sum_{i=1}^{s} \beta_i \sin(c_i\omega) = \frac{1}{\omega}\Big(1 - \cos(\omega)\Big)$$
$$\sum_{i=1}^{s} \bar{\beta}_i \sin(c_i\omega) = \frac{1}{\omega^2}\Big(\omega - \sin(\omega)\Big)$$
$$\sum_{i=1}^{s} \beta_i \cos(c_i\omega) = \frac{1}{\omega}\sin(\omega)$$

The approach in Monovasilis et al. (2013) is different however, and solving the system of equations above does not lead to the coefficients presented in the mentioned article. However, the equations for the coefficients are related to the trigonometric fitting conditions in this work and they can be expressed as follows:

$$\begin{aligned}
\cos\omega - 1 &= -\omega^2\bar{\boldsymbol{\beta}}^T\mathbf{e} + \omega^4\bar{\boldsymbol{\beta}}^T\mathbf{A}\mathbf{e} - \omega^6\bar{\boldsymbol{\beta}}^T\mathbf{A}\mathbf{A}\mathbf{e} \\
\frac{\sin\omega}{\omega} &= 1 - \omega^2\bar{\boldsymbol{\beta}}^T\mathbf{C}\mathbf{e} + \omega^4\bar{\boldsymbol{\beta}}^T\mathbf{A}\mathbf{C}\mathbf{e} \\
\cos\omega - 1 &= -\omega^2\boldsymbol{\beta}^T\mathbf{C}\mathbf{e} + \omega^4\boldsymbol{\beta}^T\mathbf{A}\mathbf{C}\mathbf{e} \\
\frac{\sin\omega}{\omega} &= \boldsymbol{\beta}^T\mathbf{e} - \omega^2\boldsymbol{\beta}^T\mathbf{A}\mathbf{e} + \omega^4\boldsymbol{\beta}^T\mathbf{A}\mathbf{A}\mathbf{e}
\end{aligned}$$

The derivation of these conditions is related to the trigonometric conditions that was presented earlier and can be found in Kalogiratou and Simos (2002). The notation was not presented in the article, however in order for the matrix notation to follow standard multiplication rules, the following vectors and matrices must be used:

$$\bar{\boldsymbol{\beta}} = \begin{bmatrix}\bar{\beta}_1 & \dots & \bar{\beta}_s\end{bmatrix}^T \qquad \boldsymbol{\beta} = \begin{bmatrix}\beta_1 & \dots & \beta_s\end{bmatrix}^T \qquad \mathbf{e} = \begin{bmatrix}1 & \dots & 1\end{bmatrix}^T$$

$$\mathbf{A} = \begin{bmatrix} 0 & & & & \\ \alpha_{21} & \ddots & & & \\ \alpha_{31} & \alpha_{32} & \ddots & & \\ \vdots & \vdots & \ddots & \ddots & \\ \alpha s1 & \alpha s2 & \dots & \alpha_{s(s-1)} & 0 \end{bmatrix} \qquad \mathbf{C} = \begin{bmatrix} 0 & & & \\ & c_2 & & \\ & & \ddots & \\ & & & c_s \end{bmatrix}$$

When the equations are expanded and solved using the symplectic conditions from the Butcher tableau in the beginning of the example the following expressions for the coefficients are obtained.

$$\begin{aligned}
\beta_2 &= \frac{-2 + 2\cos(\omega) - \beta_1\cos(\omega)\omega^2 + (1+\beta_1)\omega\sin(\omega)}{pol} \\
\beta_3 &= -\frac{\left[1 - \cos(\omega) + \beta_1 c_2\cos(\omega)\omega^2 - c_2\omega\sin(\omega)\right]^2}{pol} \\
c_3 &= \frac{c_2\omega - \left[1 - c_2 + c_2\beta_1\omega^2\right]\left[\omega\cos(\omega) - \sin(\omega)\right]}{\omega\left[1 - \cos(\omega) + c_2\beta_1\cos(\omega)\omega^2 - c_2\omega\sin(\omega)\right]} \\
pol &= \left[\omega - \beta_1(1-c_2)c_2\omega^3\right]\omega^2\cos(\omega) - \left[1 - (1+\beta_1)c_2\omega^2 + c_2^2\omega^2\right]\omega\sin(\omega)
\end{aligned}$$

There are two degrees of freedom in the system β_1, c_2 and these can be used to ensure that the method is third order. The following values where also found in Monovasilis et al. (2013) where it is pointed out that they satisfy several of the fourth order conditions as well.

$$\begin{aligned}
\beta_1 &= 0.55924973878536667 \\
c_2 &= -0.18799161879915978201
\end{aligned}$$

$$
\begin{aligned}
\beta_2 = & -0.18799161879915978201 + 0.014823031830119705447\omega^2 \\
& - 0.00065676356989888196 74\omega^4 + 0.000050089992619037566 59\omega^6 \\
& - 2.2837596032644413 \cdot 10^{-6}\omega^8 + 1.6950437269127458 \cdot 10^{-7}\omega^{10} \\
\beta_3 = & \, 0.635066644920623115 - 0.014823031830119705 45\omega^2 \\
& - 0.0014383992816085817 91\omega^4 + 0.000082794662707730077 7\omega^6 \\
& - 1.4655145815655087 \cdot 10^{-6}\omega^8 + 2.9118114430067654 \cdot 10^{-8}\omega^{10} \\
c_3 = & \, 0.73166990421824007504 - 0.011642558630267127 75\omega^2 \\
& - 0.0003547727955728088 74\omega^4 - 0.000025007793862487023 2\omega^6 \\
& - 5.568816130391094 \cdot 10^{-7}\omega^8 - 5.801982609741059 \cdot 10^{-8}\omega^{10}
\end{aligned}
$$

The final version of the STRKN method can now be expressed as follows:

$$
\boxed{
\begin{aligned}
q_{k+1} &= q_k + hv_k + h^2\left(k_1\bar{\beta}_1 + k_2\bar{\beta}_2 + k_3\bar{\beta}_3\right) \\
v_{k+1} &= v_k + h\left(k_1\beta_1 + k_2\beta_2 + k_3\beta_3\right) \\
k_1 &= f\left(q_k\right) \qquad ; f(y) = -\frac{1}{m}\frac{\partial \mathcal{L}}{\partial y} \\
k_2 &= f\left(q_k + c_2 h v_k + h^2\alpha_{21}\right) \\
k_3 &= f\left(q_k + c_3 h v_k + h^2[\alpha_{31} + \alpha_{32}]\right)
\end{aligned}
}
$$

Note that the coefficients $\bar{\beta}$ and α must be calculated using the relations in the Butcher tableau.

Chapter 4

Numerical experiments

This chapter presents numerical experiments performed using the algorithms that were developed in chapter (3). The systems of ODEs that will be used for the experiments have been derived in the examples throughout chapter (2). The ultimate goal of this chapter will be to perform numerical experiments with the interest of choosing a numerical method that is well suited for long time integration of Hamiltonian systems.

The MatLab implementation of the integration methods from chapter (3) can be seen in appendix (E). Note that the introduction of the code clearly states how it can be used for any system using a single function that defines the ODE in equation (4.1).

$$f(y) = \dot{v}(y) = -\frac{\partial \mathcal{L}}{\partial q} \tag{4.1}$$

The implementation in the appendix is specific to the chain of harmonic oscillators, all plotting functionality has been left out for the sake of space and the script has also been written with respect to esthetics rather than speed. Consequently, it can not be used directly in order to reproduce the results in this section. However, the entire simulation library can be found in Karolius (2014).

4.1 Characteristics of symplectic algorithms

The symplectic methods in this work all aim at conserving the geometry of Hamiltonian ODE systems. This section aims at investigating the basic properties of the symplectic integration interval by comparing the first order algorithms (symplectic, implicit and explicit Euler) from section (3.1). The algorithms are applied to the simple harmonic oscillator using $\omega_0 = 1$, which results in the following Hamiltonian system of equations:

$$\ddot{y} = -y \Leftrightarrow \begin{bmatrix} \dot{y} \\ \dot{v} \end{bmatrix} = \begin{bmatrix} 0 & -1 \\ 1 & 0 \end{bmatrix} \begin{bmatrix} y \\ v \end{bmatrix}$$

The results from the numerical simulation can be seen in figure (4.1), where the red circle is the analytical solution from section (D.2).

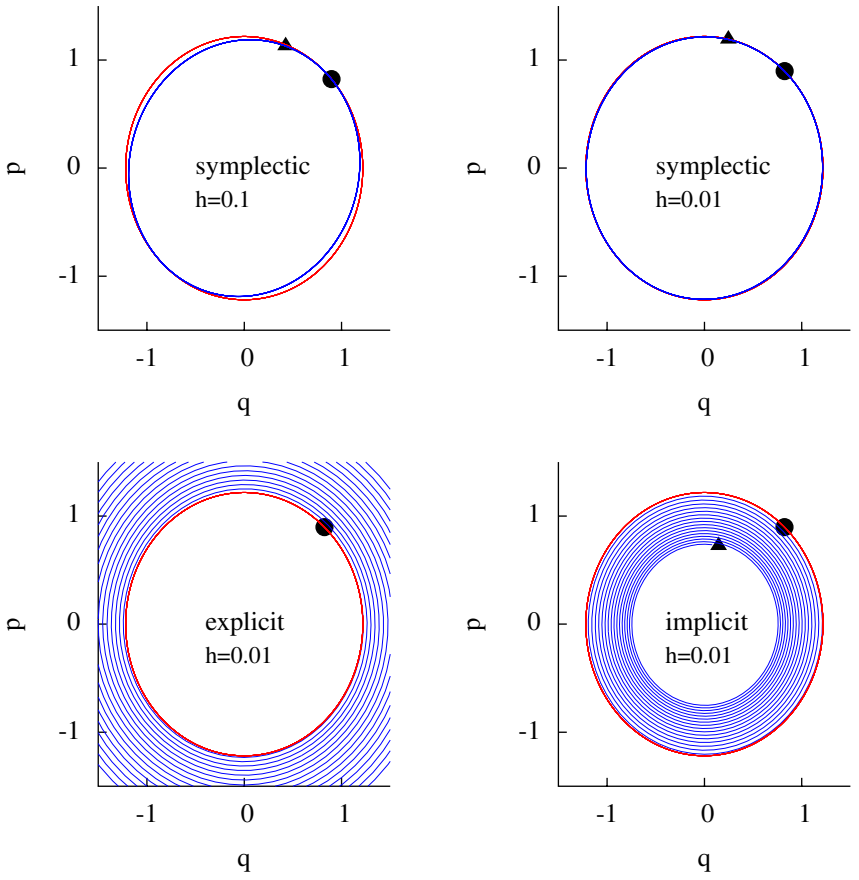

Figure 4.1: The figure compares first order explicit, implicit and symplectic integration algorithms with the analytical solution of the harmonic oscillator. The figures where created by integrating a simple harmonic oscillator using $\omega_0 = 1$ and initial conditions $q_0 = 0.8, p_0 = 0.9$. This corresponds to the total energy $\mathcal{H}_0 = 0.7421168$

From the figure it is clear that the explicit method is unstable and spirals outwards to infinity from the initial conditions. The implicit method, on the other hand, spirals inward from the initial conditions. If the integration interval is increased, it will eventually settle at the centre of the circle; therefore, the method is numerically stable even though the solution is obviously wrong. The symplectic algorithm follows the analytical solution quite well when the smallest step size is used. However, when the figure is studied closely it is possible to see the red line representing the analytical solution around the entire circumference of the phase space trajectory. The figure also shows that the symplectic method will break down when the step size is increased, but the phase space trajectory is still close.

In order to understand what happens with the explicit and implicit methods, it is useful to study figure (4.2) which shows that the energy surface is a potential well. The implicit method consequently overestimates the curvature of the manifold and creeps down before it settles in the bottom of the well. The explicit method, on the other hand, underestimates the curvature and diverges up the manifold to infinity.

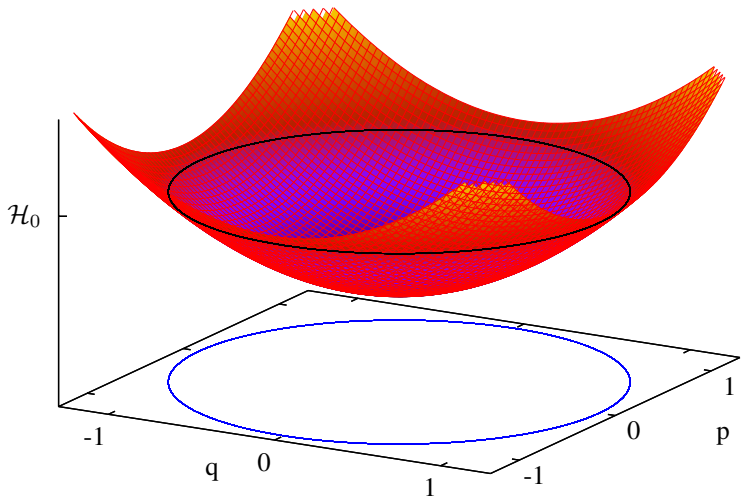

Figure 4.2: Illustration of how the phase space trajectory correlates with the Hamiltonian manifold for the simple harmonic oscillator.

If the results from figure (4.1) alone were considered, it would be tempting to conclude that the symplectic method is identical to the analytical solution. However, it was illustrated in figure (4.2) that the solution must also remain on the energy manifold throughout the integration. This is a useful property to check in order to ensure that the implementation of the equations of motion and the symplectic method is correct. However, when the value of the Hamiltonian is plotted throughout the integration interval, it becomes clear that using the degrees of freedom to ensure that the method is symplectic has an effect on the Hamiltonian. Figure (4.3) show that the Hamiltonian oscillates around a value close to the initial value and that the amplitude of the oscillations is dependent on the step size of the method. The results for the first order methods shows that symplectic methods are useful for integration Hamiltonian systems. However, the first order method is not accurate enough for integration of the systems of harmonic chains.

Figure (4.4) shows the result when second order methods are applied to the same problem that was considered in figure (4.1). The figure shows that the phase space trajectories

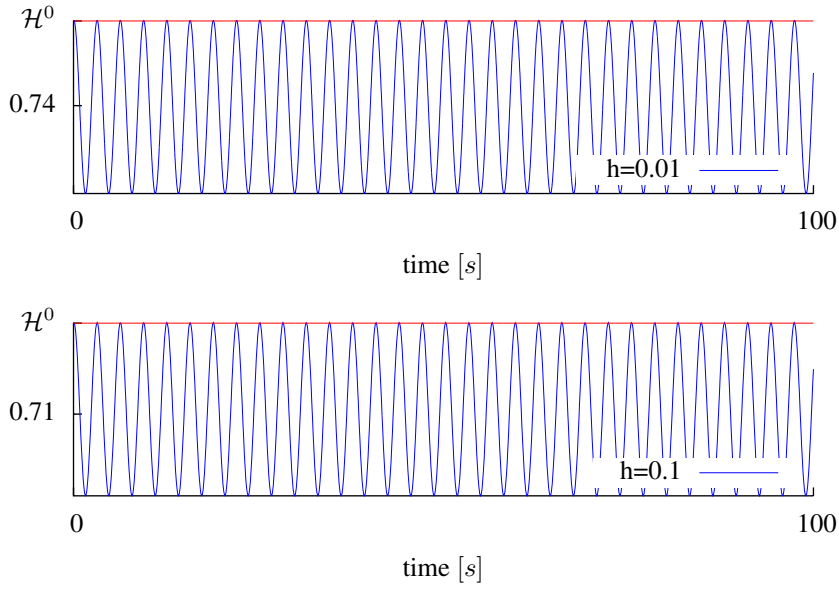

Figure 4.3: Plot of the Hamiltonian agains time for the symplectic Euler methods from figure (4.1). The blue line is the value calculated using the numerical states, whereas the red line is the Hamiltonian value of the analytical state.

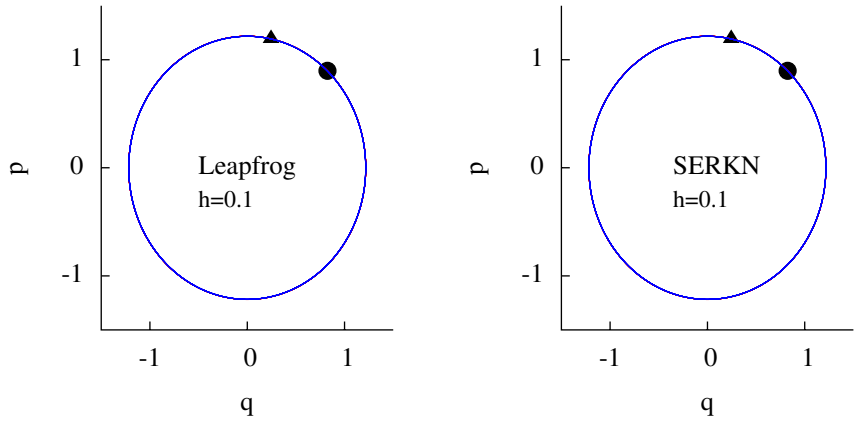

Figure 4.4: The figure compares the Leapfrog and SERKN integration methods from section (3.1.2) and (3.2.2) respectively with the analytical solution of the harmonic oscillator. The parameters for the integration are the same as presented in figure (4.1).

from the second order methods are indistinguishable from the analytical solution. Even though it looks like the solutions are equal, the plot of the Hamiltonian for the time inter-

val in figure (4.5) shows that this is not the case. Figure (4.5) shows that both the second

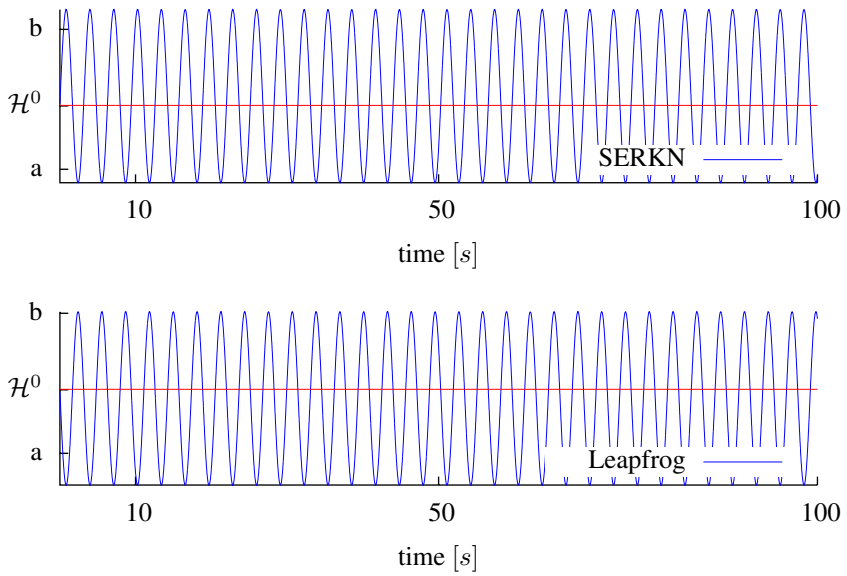

Figure 4.5: Plot of the Hamiltonian agains time for the Leapfrog and SERKN methods from figure (4.4). The blue line is the value calculated using the numerical states, whereas the red line is the Hamiltonian value of the analytical state. $a = \mathcal{H}_0 - \mathcal{O}(10^{-5}), b = \mathcal{H}_0 + \mathcal{O}(10^{-5})$

order methods oscillates around the true hamiltonian value with an aptlitude in the order of $\mathcal{O}(10^{-5})$. The phase of the oscillations is shifted π with respect to each other and the point around which the solutions oscillate is clearly different. The SERKN method seems to be centered around the analytical value, whereas the Leapfrog oscillates around a value close to the true Hamiltonian value. This suggests that even though the exponential fitting was not able to exactly reproduce the analytical solution, it has centered the oscillation of the Hamiltonian around the true value.

4.2 Long-time integration of linear oscillatory systems

The previous section showed the characteristics of symplectic integration methods. For systems where the particles interact, the state space trajectory will not have the nice property of the harmonic oscillator and close in each period. For this reason, and because the integration interval is much longer, it is not practical to study the phase plot of the individual mass points in the system in order to assess the quality of the integration.

This section will study the horizontal harmonic chain using the methods of order higher than one that was derived in chapter (3). The properties of the methods along with the section were the derivation can be found is shown in table (4.1). The goal of the section is

Table 4.1: This table summarizes the properties of the methods that was derived in chapter (3). It also includes the number of the section where more information about the specific methods can be found. $\mathcal{O}$ is the order of the method, Sym and Exp denotes wether the meted is symplectic or exponentially fitted. nf_{eval} is the number of function evaluations, i.e. number of times equation (4.1) is evaluated in each numerical step as implemented in appendix (E).

Method	Section	Source	$\mathcal{O}$	Sym	Exp	nf_{eval}
Leapfrog	(3.1.2)	Ruth (1983)	2	✓		2
RKN	(3.2.1)	Hairer et al. (1993)	4			3
SRKN	(3.2.2)	Zhao and Zhu (1991)	3	✓		3
ERKN	(3.2.3)	Franco (2004)	3		✓	2
SERKN	(3.2.4)	Van de Vyver (2005)	2	✓	✓	1
STRKN	(3.2.4)	Monovasilis et al. (2013)	3	✓	✓	3

to perform numerical simulations using the chain of interacting harmonic oscillators using the methods in table (4.1). In order to assess the quality of the integration the numerical integration will be combated with the analytical solution of the systems of first order ODEs. The solution is in both cases described by the linear system of second order ODEs shown in equation (4.2).

$$\ddot{\mathbf{q}} = -\omega_0^2 \mathbf{T}\mathbf{q} \quad ; \omega_0 = \sqrt{\frac{k}{m}} \tag{4.2}$$

The derivation of the equation of motion can be found in section (2.1.3). It involves rewriting the original equations of motion in deviation variables using the static distribution ($\mathbf{x}^0$) from the recursive relation in equation (2.10). When the deviation from the static positions ($\mathbf{q} \hat{=} \mathbf{x} - \mathbf{x}^0$) are introduced into the equations of motion, the inhomogeneous terms cancel and the system can be expressed as a homogeneous using the tridiagonal matrix ($\mathbf{T}$) shown below.

$$\mathbf{T} = \begin{bmatrix} 2 & -1 & & & \\ -1 & 2 & -1 & & \\ & -1 & 2 & -1 & \\ & & \ddots & \ddots & \ddots \\ & & & -1 & 2 \end{bmatrix}$$

The linear system of second order ODEs can be expressed as a system of first order ODEs as shown in section (3.2.2).

$$\begin{bmatrix}\dot{\mathbf{q}}\\ \dot{\mathbf{v}}\end{bmatrix} = \mathbf{A}\begin{bmatrix}\mathbf{q}\\ \mathbf{v}\end{bmatrix} \quad ;\mathbf{A} = \begin{bmatrix}0 & \mathbf{I}\\ -\omega_0^2\mathbf{T} & 0\end{bmatrix} \quad \omega_0^2 = \sqrt{\frac{k}{m}} \tag{4.3}$$

The next step is to use the analytical solution in order to estimate the error of the numerical method. An obvious way to estimate the error is to compare the numerical method with the analytical solution. The section (D.1) shows how a linear system such as the one shown in equation (4.3) can be solved analytically. However, instead of directly comparing the analytical and numerical solutions, the analytical expression can be rewritten as shown in equation (4.4).

$$\mathbf{y}^0\Big|_{t=t} = \mathbf{S}^{-1}e^{-\Lambda t}\mathbf{S}\mathbf{y}(t) \tag{4.4}$$

This equation estimates the initial conditions that were used to start the simulation based on the numerical solution at a given time. The numerical error (τ) can now be defined as the deviation between the actual initial conditions and the estimation based on equation (4.4). This work considers the absolute value of the error as shown in equation (4.5).

$$\tau = \left|\mathbf{y}^0|_{t=0} - \mathbf{y}^0|_{t=t}\right| \tag{4.5}$$

Each iteration will necessarily have $2n$ error terms and it is assumed that the highest number can be used in order to describe the accuracy of the numerical method.

The analytical solution can also be used to ensure that the step size is sufficiently small in order to describe the dynamics of the largest normal mode of the system. The normal modes correspond to the eigenvalues of the coefficient matrix ($\mathbf{A}$) in equation (4.3), which are purely imaginary in the case of pure oscillations without damping. Equation (4.6) shows how the maximum value of the numerical step size can be chosen with respect to the dominating mode in the system.

$$h \leq \frac{K}{|\lambda_{max}|} \tag{4.6}$$

This work will use the parameter K in equation (4.6) in order to determine the step sizes of the numerical method.

A similar approach can be used in order to determine when the sampling of data should begin. When the simulation is started, it takes time before the dynamics of the system is no longer affected by the initial perturbation. The slowest dynamic in the system is represented by the smallest eigenvalue in the system. As shown in equation (4.7) this work assumes that five times the slowest time constant of the system is sufficient in order to avoid the initial transient period when the initial perturbation affects the system.

$$\tau_s = \frac{5}{|\lambda_{min}|} \tag{4.7}$$

Another important factor in the simulations is to choose initial conditions that represents as many cases as possible. This is important in order to validate the comparison of the numerical methods for as many cases as practically possible. The strategy in this work was to use different initial conditions for all of the simulations but scale them in order to have the same initial value of the Hamiltonian.

The static equilibrium distribution will be used as the reference state for the Hamiltonian function as shown below.

$$\mathcal{H} = \mathcal{H}\Big|_t - \mathcal{H}^0 \quad ; \mathcal{H}^0 \hat{=} \mathcal{H}(\mathbf{x}^0, 0)$$

Note that when the system is started in the static equilibrium position the value of the relative hamiltonian is identically equal to zero.

The simulations considers two systems of different sizes. The system in table (4.2) contains five mass points and the initial total energy was set to $\mathcal{H} = 3[J]$ in all the simulations. However, the simulations use different types of initial conditions, i.e. the initial state of the system is changed but scaled such that the total energy is the same in all the simulations. The same strategy is applied to the system in table (4.3) which consists of 13 mass points and a total energy of $\mathcal{H} = 90[J]$. Moreover, the mass ($m = 0.12\ [kg]$) and spring constant ($k = 16.12\ [kgs^{-2}]$) are constant in all the simulations.

An example of the implementation can be seen in appendix (E); however, as mentioned in the introduction the script will not automatically reproduce the results in the tables. The full framework is available in Karolius (2014).

The simulations in table (4.2) are considered to be "low-energy" simulations.

Table 4.2: The value of the step size is found form equation (4.6) using the eigenvalue $\lambda_{max} 0.0045$ and the parameter (K) listed in the table. The table has two rows for each step size, the top row is the error τ_k from equation (4.5) and the bottom is the difference between the largest and smallest value of the Hamiltonian $\mathcal{H}$. All the step sizes was integrated using $2 \cdot 10^7$ steps and the initial conditions where changed for all the methods but scaled such that the initial value of the Hamiltonian was $\mathcal{H}^0 = 3[J]$. *Note that a value of* 0 *implies that the value is less than* 10^{-6} *and an empty row means that the error of the method is greater than one.*

K	STRKN	SERKN	ERKN	SRKN	RKN	Leapfrog	ode45
0.001	0	0	$2 \cdot 10^{-4}$	0	0	$2 \cdot 10^{-3}$	$2 \cdot 10^{-3}$
	0	0	$1 \cdot 10^{-4}$	0	0	$1 \cdot 10^{-4}$	$3 \cdot 10^{-3}$
0.01	0	0.1	$2 \cdot 10^{-4}$	0	$1 \cdot 10^{-5}$	0.1	$2 \cdot 10^{-3}$
	0	$1 \cdot 10^{-4}$	$2 \cdot 10^{-3}$	0	$1 \cdot 10^{-5}$	$1 \cdot 10^{-4}$	$3 \cdot 10^{-3}$
0.1	$4 \cdot 10^{-3}$		0.1	0.01	$8 \cdot 10^{-3}$		$2 \cdot 10^{-3}$
	$1 \cdot 10^{-4}$		0.1	$1 \cdot 10^{-4}$	$1 \cdot 10^{-3}$		$3 \cdot 10^{-3}$

The trend in the table clearly shows that the second order methods (SERKN and Leapfrog) have problems with the coupled system. By comparing the results of the symplectic and the symplectic-exponentially fitted methods of the same order, i.e. comparing the SERKN with the Leapfrog and the STRKN with the SRKN, it is clear that the exponential fitting is effective. The exponentially fitted methods consistently have lower error for the total energy. Furthermore, the STRKN method is also superior compared with the fourth order RKN method.

The results from $ode45$ are not sufficiently accurate and the accuracy of the integrator was set to the maximum practical values using the $odeset$ function and the following absolute and relative error tolerances:$AbsTol, RelTol = 10^{-10}$.

The "high energy" simulations in table (4.3) shows the same trend as table (4.2). However, the increased energy has made all the methods consistently less accurate.

Table 4.3: The value of the step size is found form equation (4.6) using the eigenvalue $\lambda_{max}0.0045$ and the parameter (K) listed in the table. The table has two rows for each step size, the top row is the error τ_k from equation (4.5) and the bottom is the difference between the largest and smallest value of the Hamiltonian $\mathcal{H}$. All the step sizes was integrated using $2 \cdot 10^7$ steps and the initial conditions where changed for all the methods but scaled such that the initial value of the Hamiltonian was $\mathcal{H}^0 = 90[J]$. *Note that a value of* 0 *implies that the value is less than* 10^{-6} *and an empty row means that the error of the method is greater than one*

K	STRKN	SERKN	ERKN	SRKN	RKN	Leapfrog	ode45
0.001	0	$1 \cdot 10^{-5}$	$1 \cdot 10^{-4}$	0	0	$1 \cdot 10^{-4}$	$2 \cdot 10^{-3}$
	0	0	$1 \cdot 10^{-3}$	0	0	0	0.3
0.01	0	0.03	$2 \cdot 10^{-3}$	0	$1 \cdot 10^{-5}$	0.03	$2 \cdot 10^{-3}$
	$1 \cdot 10^{-5}$	0.01	0.01	$1 \cdot 10^{-5}$	$1 \cdot 10^{-5}$	0.01	0.3
0.1	$1 \cdot 10^{-3}$			$4 \cdot 10^{-3}$	$2 \cdot 10^{-3}$		$2 \cdot 10^{-3}$
	0.01			0.1	0.1		0.3

Based on the results from the numerical experiments it is concluded that the STRKN method is favorable. However, this method requires three function evaluations for each step, whereas the SERKN can be implemented using only one. This work will use the STRKN methods due to its increased accuracy for coupled systems, but for integrating a simple system the SERKN will be much faster even though it requires a smaller step size.

Chapter 5

Model of a one-dimensional system of magnets in a gravitational field

The system consists of $n + 2$ magnets where the boundary conditions on the top and bottom magnets prevents them from moving relative to the static equilibrium position. A system of n magnets therefore refers to a system of n freely floating magnets with the top and bottom magnets remaining stationary. The top magnet will simply ”float” on top of the stack and it is expected that the distance between the magnets will decrease towards the bottom of the stack due to the increasing number of magnets whose weight must be supported. The repulsive force between the magnets that supports the weight of the stack is assumed to be described by a force law, which is inversely proportional with the distance squared.

The chapter will introduce a mathematical model for the stack of magnets based on the assumption that the only forces in the system are the magnetic forces and gravity. The model will subsequently be validated by performing numerical simulations using the STRKN integration method. However, the ultimate goal of the chapter is to study whether the system can be used as a mechanical analogue to an atmosphere of an ideal gas.

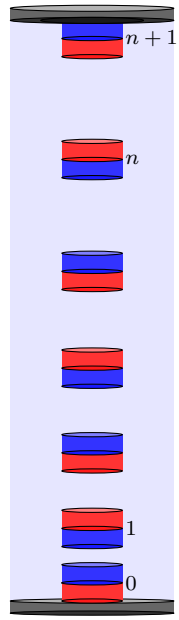

Figure 5.1: Illustration of a vertically stacked system of n magnets.

5.1 Equations of motion

The equations of motion for the system are derived using the basic mechanical theory from chapter (2). The rigorous derivation follows the same lines as the examples from the chapter and will therefore not be presented here. However, anything that is beyond the scope of the examples of the harmonic chain is considered in appendix (A) and will be referenced appropriately.

The difference between the system of magnets and the harmonic oscillators lies in the nonlinearity of the force model that will be used to describe the magnets. This section will introduce the complete (nonlinear) model for the system along with a linearized version.

5.1.1 Complete model

The introduction of the chapter stated that the force law that is assumed to apply for the magnets is inversely proportional to the distance between the magnets squared. The mathematical formulation of this assumption is shown in equation (5.1), where k_m is the magnetic force constant.

$$\mathcal{F}_{i+1,i} = \frac{k_m}{(y_{i+1} - y_i)^2} \tag{5.1}$$

The following expression is found for the potential energy due to the magnetic force. It can be described by integrating the force model and yields the following result:

$$U^{(m)} = \sum_{i=0}^{n} \frac{k_m}{(y_{i+1} - y_i)}$$

The Lagrangian function can now be expressed using the definition in equation (2.2).

$$\mathcal{L} = \frac{1}{2} m \dot{\mathbf{y}}^T \dot{\mathbf{y}} - mg\mathbf{e}^T\mathbf{y} - \sum_{i=0}^{n} \frac{k_m}{(y_{i+1} - y_i)} \tag{5.2}$$
$$\mathbf{e} = [1 \dots 1]^T \qquad \mathbf{y} = [y_1 \dots y_n]^T$$

The Lagrange equations of motion for the system is obtained using the Euler-Lagrange equation from section (2.1.2). This results in a system of equations, one for each magnet, each of the form shown in equation (5.3).

$$m\ddot{y}_i + mg + \frac{k_m}{(y_{i+1} - y_i)^2} - \frac{k_m}{(y_i - y_{i-1})^2} = 0 \tag{5.3}$$

As expected, the nonlinearity of the Lagrangian is also present in the equations of motion; in addition, the force terms from equation (5.1) are also retrieved.

Section (2.2.1) showed that the canonical momentum for a Lagrangian of the form of equation (5.3) becomes $p_i = \frac{\partial \mathcal{L}}{\partial \dot{q}_i} = m\dot{q}$. The Hamiltonian is generated by inverting the

expression for the momentum and using it in the Legendre transform $\mathcal{H} = \dot{\mathbf{q}}\mathbf{p} - \mathcal{L}$. This results in the expression in equation (5.4) for the system of magnets.

$$\mathcal{H} = \frac{1}{2m}\mathbf{p}^T\mathbf{p} + mg\mathbf{e}^T\mathbf{y} + \sum_{i=0}^{n} \frac{k_m}{(y_{i+1} - y_i)} \tag{5.4}$$

The canonical equations of motion consists of a system of $2n$ first order ODEs shown below.

$$\begin{aligned}
\dot{q}_i &= \frac{\partial \mathcal{H}}{\partial p_i} = \frac{1}{m} p_i \\
\dot{p}_i &= -\frac{\partial \mathcal{H}}{\partial q_i} = k_m \left[\frac{1}{(y_i - y_{i-1})^2} - \frac{1}{(y_{i+1} - y_i)^2} \right] - mg
\end{aligned}$$

However, it was shown in section (2.2.2) that the Lagrange equations of motion for the systems in this work can also be expressed as a Hamiltonian set of ODEs. In order to use the RKN methods from section (3), the Lagrange equations of motion are rewritten to the following form:

$$\begin{aligned}
\dot{q}_i &= v_i \\
\dot{v}_i &= \omega_0^2 \left[\frac{1}{(y_i - y_{i-1})^2} - \frac{1}{(y_{i+1} - y_i)^2} \right] - g \qquad ; \omega_0 = \sqrt{\frac{k_m}{m}}
\end{aligned} \tag{5.5}$$

The reason that the equations of motion can be written in the form of equation (5.5) can be understood by expressing the second order Lagrange equations of motion as a system of first order equation. Alternatively they can be derived by using the result from appendix (C) which proves the Hamiltonian is equal to the total energy, i.e. it can be expressed as follows:

$$\mathcal{H} = \frac{1}{2}m\mathbf{v}^T\mathbf{v} + mg\mathbf{e}^T\mathbf{y} + \sum_{i=0}^{n} \frac{k_m}{(y_{i+1} - y_i)}$$

The implementation of the model in Karolius (2014) uses the latter form of the Hamiltonian function.

5.1.2 Linearized model

The nonlinearity of the model is due to the force power law of the magnetic dipoles in equation (5.1). The model can therefore be linearized by approximating the force field by a linear relation that still bares relevance to the original model. This work considers the linearization around the relaxed equilibrium state from section (5.2.1). The term "relaxed" implies that magnet $n+1$ only exerts a force equivalent to its own force of gravity on the stack below.

The recursion relation in equation (5.9) describes the equilibrium distribution of the magnets by choosing the position of the first magnet when the system is in the relaxed state. When the relation is rewritten to the form shown below, it is clear that it represents the denominator of the magnetic force in equation (5.1).

$$y_{i+1}^0 - y_i^0 = \frac{L}{2n+1}\sqrt{\frac{1}{1-\alpha i}} \quad ;\alpha = \frac{1}{n+1}$$

This relation can now be used in the definition of the force from equation (5.1) to formulate an explicit expression for the force which in turn can be linearized. The full derivation of the linearized model is performed in section (A.4) of appendix (A).

The result of the linearization process is equation (5.6).

$$\ddot{\mathbf{q}} = -m^{-1}\mathbf{T}\mathbf{q} \quad ;\mathbf{q}\hat{=}\mathbf{y} - \mathbf{y}^0 \tag{5.6}$$

Just as for the harmonic chain in the section (2.1.3) the coordinate $\mathbf{q}$ in equation (5.6) is the deviation from the static equilibrium position. In contrast to the harmonic chain, the elements of the tridiagonal matrix are no longer constant, but a function of the magnet index. The resulting elements of the tridiagonal matrix are described by the following relations:

$$\begin{aligned} t_{i,i} &= k_{i,i-1} + k_{i+1,i} \\ t_{i,i+1} &= t_{i+1,i} = -k_{i+1,i} \end{aligned}$$

The elements are placed in the following tridiagonal matrix:

$$\mathbf{T} = \begin{bmatrix} t_{1,1} & t_{1,2} & & & & & \\ t_{2,1} & t_{2,2} & t_{2,3} & & & & \\ & \ddots & \ddots & \ddots & & & \\ & & t_{i,i-1} & t_{i,i} & t_{i,i+1} & & \\ & & & \ddots & \ddots & \ddots & \\ & & & & t_{n,n-1} & t_{n,n} & t_{i,n+1} \end{bmatrix}$$

Finally the elements are calculated using the following expressions:

$$\begin{aligned} c_{i+1,i} &= \frac{3k_m}{y_{i+1}^0 - y_i^0} \\ k_{i+1,i} &= \left(\frac{2k_m}{y_{i+1}^0 - y_i^0}\right)^{\frac{3}{2}} \end{aligned} \tag{5.7}$$

5.2 Static equilibrium distribution

The strategy of solving the static Lagrangian equations of motion in order to obtain the equilibrium distribution was introduced in section (2.1.3). However, the nonlinear equations of motion of the system of magnets makes the static equilibrium difficult to obtain analytically. The strategy presented in this section was originally performed in Warberg (2013) and is based on performing an analysis of the static state and obtaining an approximate solution by imposing a-priori knowledge on the system.

The state of the system is characterized by the force exerted by the top $(n+1)$ magnet on the stack below. This work will consider two different initial states for the system. One in which the top magnet is simply floating on top of the stack, only exerting the force of gravity on the magnets below. This state will be referred to as the "relaxed" state of the system and the distribution for some systems is shown in figure (5.2). In the second state the top magnet is compressing the system, e.g. by adding mass to the top of the column. Consequently it will be referred to as a "compressed" state.

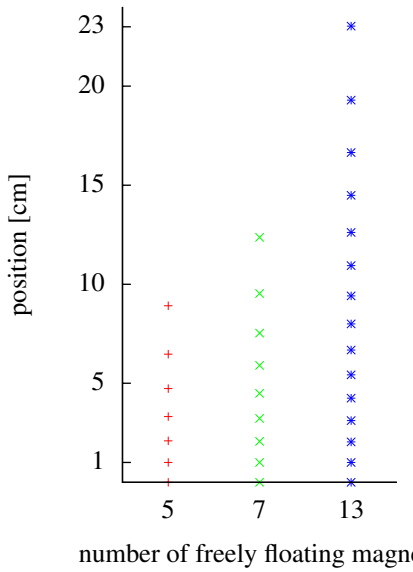

Figure 5.2: Static equilibrium distribution for a system of 5, 7 and 13 freely floating magnets. Note that the total number of magnets in the systems are $n + 2$, even though the system is referred to as having n magnets

5.2.1 Relaxed state

The derivation of the relaxed state equilibrium distribution can be found in its entirety in appendix (A.2). From the derivation it was found that the height of the column can no longer be chosen, but will be determined by the position of the first magnet in the stack.

$$L = y_1^0 \left[1 + \sum_{i=0}^{n} \sqrt{\frac{1}{1-\alpha i}} \right] \quad ; \alpha = \frac{1}{n+1} \tag{5.8}$$

The position of the first magnet can now be chosen to determine the height of the stack using equation (5.8). The distribution of the rest of the magnets can thereafter be determined using the recursive relation in equation (5.9).

$$y_{i+1}^0 = y_i^0 + \frac{L}{2(n+1)} \sqrt{\frac{1}{1-\alpha i}} \quad ; i = 1 \ldots n-1 \tag{5.9}$$

The equilibrium distribution from equation (5.9) is increasing with the height of the stack due to the constant α. This is clearly seen in figure (5.2) which shows the equilibrium

distribution for systems with a different number of magnets.

The parameter (α) in these equations was chosen such that it represents the maximum value of $\alpha \hat{=} \left(\frac{y_1^0}{y_{eq}^0}\right)^2$. This is a measure of the ratio between the force of one magnet floating on top of another and the force necessary in order to have the bottom magnet at the chosen position y_1^0 while supporting the weight of the stack. The parameter can therefore be used to determine the magnetic force constant using equation (5.10).

$$k_m = \frac{mg(y_1^0)^2}{\alpha} \tag{5.10}$$

5.2.2 Compressed state

The compressed state of the system is based in the assumption that the value of α is very small, but that the value of $n\alpha$ is still large. The first assumption can be understood physically by imagining that the first magnet is compressed significantly, which in turns makes the ratio $\left(\frac{y_1^0}{y_{eq}^0}\right)$ small. The second assumption is a mathematical assumption that ensures the expression in the square root of the recursive relation in equation (5.8) still exists. The result form the derivation in appendix (A.3) shows that the recursive relation can be approximated directly as follows:

$$L = y_1^0 \left[1 + \sum_{i=0}^{n} \sqrt{\frac{1}{1-\alpha i}}\right] \approx y_1^0 \left(n + 1 + \frac{\alpha n(n+1)}{4}\right)$$

This leads to the following expression for the equilibrium position of the first magnet:

$$y_1^0 = \frac{L}{n+1}$$

The assumptions along with the position of the first magnet in the stack leads to the following distribution for all of the magnets in the system.

$$y_{i+1}^0 = y_i^0 + \frac{L}{n+1} \qquad ; i = 0 \ldots n-1$$

5.3 Simulation parameters and model validation

This section will introduce model parameters and conventions that will be used in all the simulations in this work. The simulations in the rest of this work will be performed using the same parameters that are presented in this section, but changing the initial conditions and consequently the total energy of the system. The validation of the model aims at demonstrating that the canonical equations of motion and the static initial conditions behaves physically reasonable.

5.3.1 Model and integrator parameters

In order to ensure that the value of the Hamiltonian in the simulations is more intuitive it will be defined as the deviation from the value from the static case in section (5.2). This means that the value of the Hamiltonian for the static case will become zero using the following definition:

$$\mathcal{H} \hat{=} \mathcal{H}_{tot} - \mathcal{H}_{static}$$

Where $\mathcal{H}_{tot}$ refers to the actual value of the Hamiltonian obtained from equation (5.4). The size of the Hamiltonian can be viewed in relationship to the values in figure (5.3) which exemplifies large values. The values are regarded to be large because they were calculated by assuming that all of the freely floating magnets in the system were at their respective terminal velocity using:

$$\frac{1}{2}mv^2 = mgy_i^0$$

The constants that were used in the calculation of the maximum Hamiltonian as well as parameters specific to the canonical equations of motion for all the simulations in this work are:

$$\begin{aligned} m &= 0.12\ [kg] \\ g &= 980.65\ [cm\ s^{-2}] \\ n &= 7 \\ y_1^0 &= 1\ [cm] \\ \Rightarrow \alpha &= 0.125 \\ \Rightarrow k_m &= 941.4\ [kg\ cm^3\ s^{-2}] \\ \Rightarrow L &= 12.4\ [cm] \end{aligned}$$

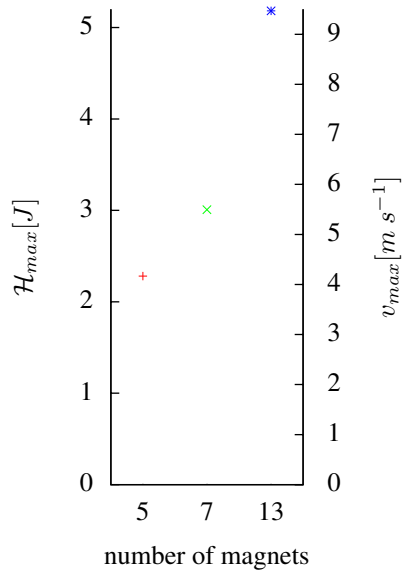

Figure 5.3: Illustration of large values of the Hamiltonian for systems with a different number of magnets. v_{max} corresponds to the speed that corresponds to the speed which one magnet must possess in order to have pure kinetic energy equal to the value of the Hamiltonian.

Where the arrow implies that the value of the parameters has been calculated based on the relaxed static equilibrium distribution in section (5.2.1).

Even though the integration method is chosen specifically to mirror the dynamics of the system it is necessary to choose the step size with care. As described in section (4.2), one way of determining the appropriate step size is to use the eigenvalues of the system. However, the nonlinear model is not described by a finite set of eigenfrequencies that can be pre-calculated. The harmonic eigenvalues from the linearized model in section (5.1.2) was therefore used instead. This leads to the following system of equations:

$$\det|\mathbf{A} - \lambda\mathbf{I}| = 0 \quad ; \mathbf{A} = \begin{bmatrix} 0 & \mathbf{I} \\ -\mathbf{T} & 0 \end{bmatrix}$$

The oscillatory nature of the equations of motion leads to purely imaginary eigenvalues. By taking the absolute value the following minimum and maximum values were found:

$$|\lambda_{max}| = 2.5$$
$$|\lambda_{min}| = 0.3$$

Note that the minimum and maximum eigenvalues correspond to a linearized model of seven magnets. There is therefore no guarantee that these will be the same if the size of the system is changed. Moreover, the nonlinearity of the system will make the step size highly dependent on the total energy of the system. The value shown below is consequently a rough estimate and the actual value that was used for the simulations was chosen using trial and error.

$$h \leq \frac{1}{|\lambda_{max}|} = 0.4\ [s]$$

The criteria for choosing the step size in this work was based on the oscillation of the value of the Hamiltonian, that as shown in section (4.1), characterizes symplectic integration methods. The requirement was therefore that the value was to remain constant throughout the integration interval to the fourth decimal place. It was found that for low values of the total energy the step size can be in the order of 10^{-3}. However, for Hamiltonian values of the order of magnitude shown in figure (5.3) it must be lowered to 10^{-4}.

The time to start the sampling of the results on the other hand was chosen directly according to equation (4.7). The assumption is that the nonlinearity will ensure that the dynamics of the system will settle faster than in the linear case and the time shown below will be used for all initial conditions:

$$\tau_s = \frac{5}{|\lambda_{min}|} = 16\ [s]$$

Even though the method waits 16 seconds before starting to sample the results, the long integration intervals will lead to large amounts of data. The results in this work were therefore sampled at $10,000$ randomly selected points in the integration interval.

5.3.2 Validation of static initial conditions

A minimal requirement for the model is that the static equilibrium distribution from section (5.2.1) leads to static trajectories. The initial conditions in table (5.1) were used for the static equilibrium simulation and the result from the simulation is shown in figure (5.4).

Table 5.1: Initial conditions for the static equilibrium simulation used to create figure (5.4). "Static" refers to the position calculated using equation (5.9).
The units of the table are: $y[cm] \quad v[cm\ s^{-1}] \quad \mathcal{H}\ [J]$.

Magnets	y_1	$y_{2\to n}$	$v_{1\to n}$	$\mathcal{H}$	step size
7	1	$static$	0	0	$4 \cdot 10^{-3}$

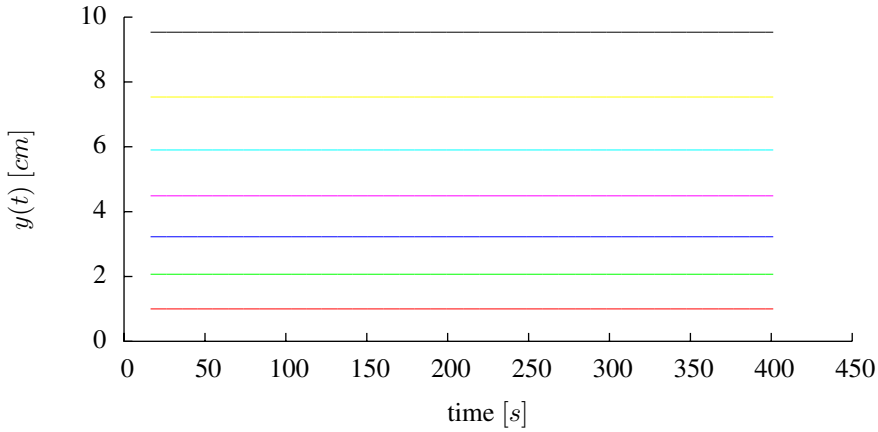

Figure 5.4: The simulations shows the trajectory for a system of seven magnets when initiated at the static equilibrium condition from section (5.2.1). The initial conditions for the simulation can be found in table (5.1)

The figure shows the trajectory of the system throughout the integration interval and confirms that the static distribution from section (5.2.1) leads to stationary trajectories.

A more rigorous requirement is that the canonical equations of motion conserve the static distribution when the system is initiated away from the static equilibrium. This was checked by performing a simulation where all the positions where perturbed and the momentum was set to zero as shown in table (5.2). The trajectory of the system now becomes difficult to interpret due to the long time interval combined with the highly oscillatory solutions. The results from the simulation in figure (5.5) shows the probability density for the position of each magnet.

Table 5.2: Initial conditions for the static equilibrium simulation used to generate the figures in this section figure (5.5). The random initial conditions where chosen in the following way: $y_i^0 = y_i^{eq} + (rand(seed) - 0.5)$. Using the 'twister' random number generator in MatLab. The units in the table are as follows: $y[cm]$ $v[cm\ s^{-1}]$ $\mathcal{H}[J]$ $time\ [s]$.

Magnets	$y_{1\to n}$	$v_{1\to n}$	$\mathcal{H}$	seed	time	step size
7	$rand$	0	1	39187	4012	$4 \cdot 10^{-4}$

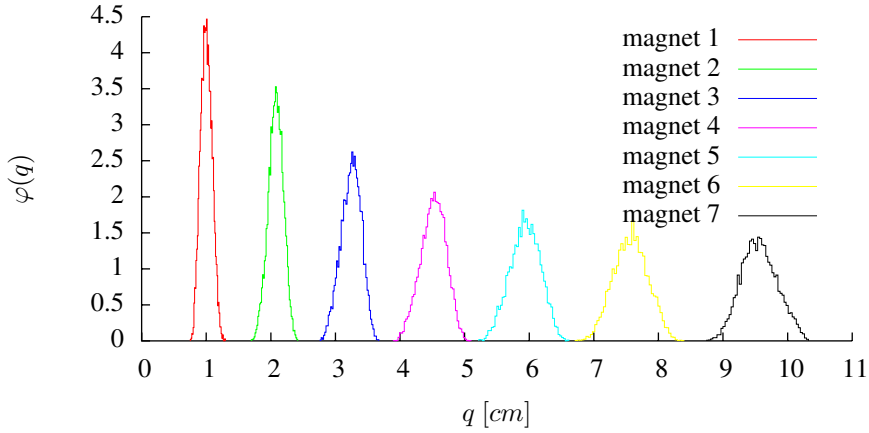

Figure 5.5: The figure shows the weighted probability density for each magnet occupying a given position when initiated at a random perturbation from the static equilibrium. The probability curve was obtained by sampling the results from the integrator and dividing the position for each magnet into 53 bins. The initial conditions can be found in table (5.2).

The figure clearly shows that the position with the highest probability lies somewhere around the static equilibrium position. The width of the density functions also suggests that the amplitude of the top magnet (7) is much larger than the bottom magnet (1). This is also a reasonable result since the space between the neighboring magnets will be much smaller towards the bottom of the stack. The thermodynamic analogue can be thought of as the density of an ensemble, which consequently decreases along the height of the stack.

It can also be seen that the density functions does not overlap, this is important since the model do not account for collisions between magnets. By looking at equation (5.1), this is also a reasonable result because the magnetic force model ensures that as the distance between two magnets approaches zero, the force becomes infinity.

5.3.3 Validating diffusion of kinetic energy

The kinetic energy must disperse correctly throughout the system. This means that an initial perturbation of the top magnet should not be visible in the bottom magnet before it has also been registered in the rest of the system. This was tested by initiating top magnet using a small velocity as shown in table (5.3). The result from the simulation is shown in figure (5.6) as the cumulative distribution of the momentum.

Table 5.3: Initial conditions for the static equilibrium simulation used to generate the figures in this section figure (5.6). The term "static" refers to the values that are calculated using equation (5.9). The units of the table are: $y[cm]$ $v[cm\ s^{-1}]$ $\mathcal{H}[J]$ $time[s]$.

Magnets	y_1	$y_{2\to n}$	$v_{1\to n-1}$	v_n	$\mathcal{H}$	time	step size
7	1	$static$	0	1	$6 \cdot 10^{-4}$	4012	$4 \cdot 10^{-3}$

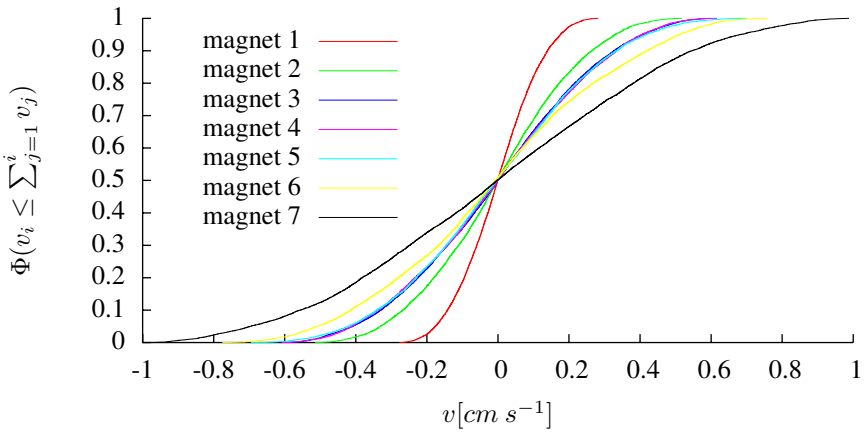

Figure 5.6: The figure shows the cumulative density curve of the system when initiated with the magnets in their static equilibrium positions and giving the top magnet a small initial momentum. More information about the initial conditions and simulation parameters can be found in table (5.3).

Figure (5.6) demonstrates that the probability of occupying the state with the highest momentum increases towards the top of the stack. This result was expected as the initial condition only affected the top magnet. However, the simulation also shows that the magnets have significantly different probabilities of occupying the same momentum. This suggests that even if the velocity of the magnets follows the same probability distribution, the shape of the function is dependent on the position of the magnet. The long integration interval combined with the widely different cumulative probabilities for the magnets suggests that something special is happening in the system. One possibility is that the single source of the initial condition sends a wave through the system which when reflected at the bottom of the stack results in sustained harmonic oscillations.

This result motivated the simulation using the initial conditions in table (5.4). The intention was to consider if changing the initial conditions without significantly increasing the total energy of the system will change the results compared with the results in figure (5.6). As shown in figure (5.7) the result using the initial conditions becomes significantly different.

Table 5.4: Initial conditions for the static equilibrium simulation used to generate the figures in this section figure (5.7). The static equilibrium positions for the rest of the magnets was calculated using equation (5.9).
The units of the table are: $y[cm]$ $v[cm\ s^{-1}]$ $\mathcal{H}[J]$ $time[s]$.

Magnets	y_1	$y_{2\to n}$	v_1	$v_{2\to n-1}$	v_n	$\mathcal{H}$	time	step size
7	1	$static$	1	0	1	$12 \cdot 10^{-4}$	4012	$4 \cdot 10^{-3}$

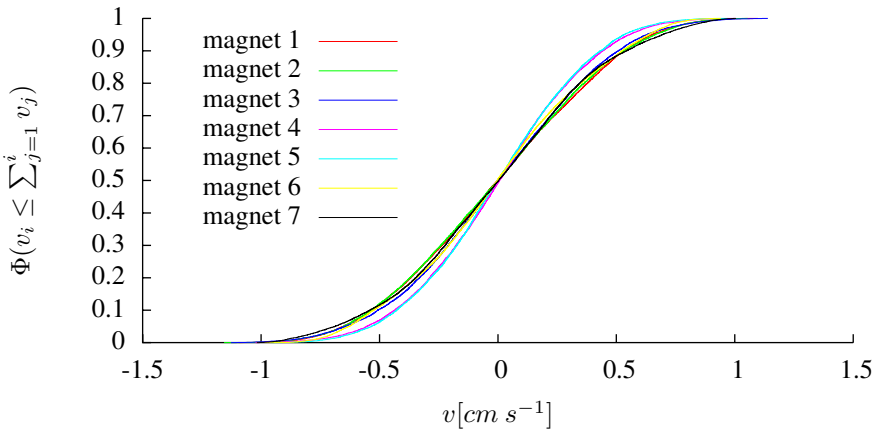

Figure 5.7: The figure shows the cumulative density curve of the system when initiated with the magnets in their static equilibrium positions and giving the top and bottom magnet a small initial momentum. It is clear that the probability of occupying a state with a given momentum is similar for all the magnets. More details about the initial conditions can be found in table (5.3).

The result in figure (5.7) shows that different initial conditions can make a significant difference to the simulation results even though the energy in the system is similar. The linear model, on the other hand, did not show this behavior when the same initial conditions were applied. It was not expected that the non linear term would cause the system to approach a state of uniformly distributed kinetic energy even for the small Hamiltonian in table (5.4). However, the cumulative probability still shows that the system does not reach an equilibrium state during the simulation.

5.4 Equilibrium simulations

The equilibrium distribution of kinetic energy can be used as an analogue to the temperature of the system. It is well established that the velocity of the particles in an ideal gas, at a given temperature, is described by the Maxwell-Boltzmann probability density function. Translated to the system in this work, this means that all of the magnets in the system must have the same probability of occupying any given velocity.

Looking back at the results in figure (5.6) this is not the case. However, the total energy of the system in the previous section was small and by increasing the energy it is reasonable that the nonlinear interactions will dominate the dynamics of the system. As shown in table (5.5), the initial conditions in the section corresponds to a higher value of the total energy. The result in figure (5.8) shows the effect the increased value has on the long time behavior of the system.

Table 5.5: Initial conditions for the static equilibrium simulation used to generate the figures in this section figure (5.8). The random momentum was chosen as follows: $p^0 = K(rand(seed) - 0.5)$. With $K = \frac{78}{\sqrt{2}}$, choosing $K = 78$ corresponds to the largest value of the Hamiltonian, according to figure (5.3). The static equilibrium positions for the rest of the magnets was calculated using equation (5.9).
The units of the table are: $y[cm]$ $v[cm\ s^{-1}]$ $\mathcal{H}[J]$ $time[s]$.

Magnets	y_1	$y_{2\to n}$	$v_{1\to n}$	$\mathcal{H}$	time	step size	seed
7	1	$static$	$random$	2	4012	$4 \cdot 10^{-4}$	581802

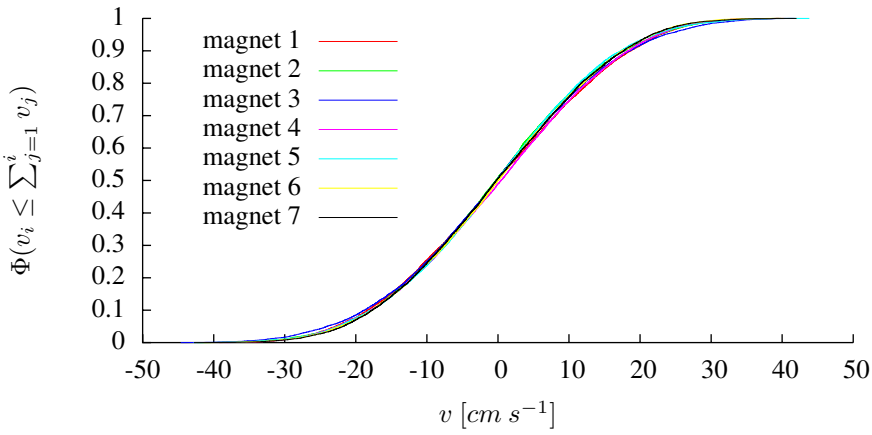

Figure 5.8: The figure shows the cumulative density curve of the system where all the magnets have approximately the same probability of being at any given state. The initial conditions in table (5.5) show that the system is initiated with a large total energy.

The cumulative distribution for all the magnets in figure (5.8) is very similar, which suggests that they can be described using the same probability density function. The density functions were estimated by dividing the velocity range into 57 bins of equal width and the results were collected in their respective bins. Figure (5.9) was obtained from the same results that produced the cumulative distribution in figure (5.8).

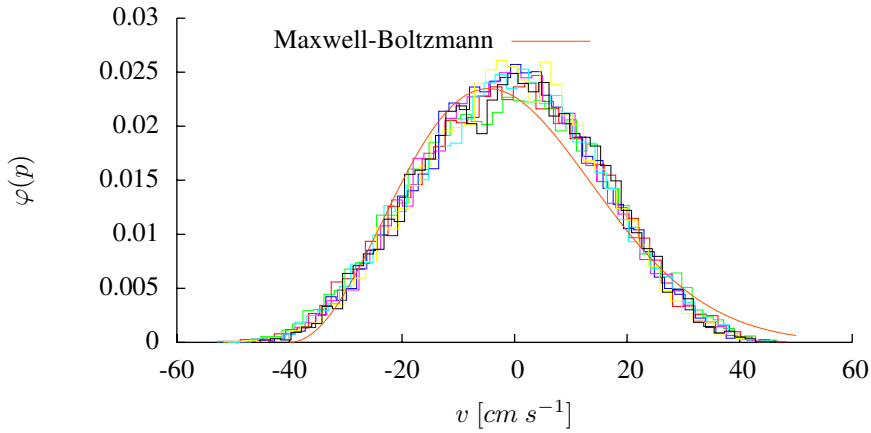

Figure 5.9: The figure shows the probability density curve for the magnets whose cumulative distribution is shown in figure (5.8). The figure also shows that the Maxwell-Boltzmann density function can be fitted to describe the density function for all the magnets.

Figure (5.9) shows that the density functions for the momentum are the same for all the magnets and that the Maxwell-Boltzmann distribution function can be fitted reasonably well. This suggests that the equipartition theorem can be applied.

5.5 Equipartition

The equipartition theorem is a general formulae from classical statistical mechanics which states that at the energy of a system at thermal equilibrium is shared equally within the components of the system. The theorem relates the kinetic energy with the thermodynamic energy as the following general formulae:

$$\bar{E_k} = \frac{1}{2} m v_{RMS}^2 = \frac{3k_B}{2} T$$

Where $\bar{E_k}$ is the average kinetic energy of all the components, T is the thermodynamic temperature, k_B is the Boltzmann constant and m is the mass of the system.

Based on the results presented in this work, the most likely candidate for equipartition is the result from the simulations in figure (5.5) and (5.8), the latter was used to make figure (5.10). The figure shows the average kinetic energy for each magnet in the system that, according to the equipartition theorem, is uniform.

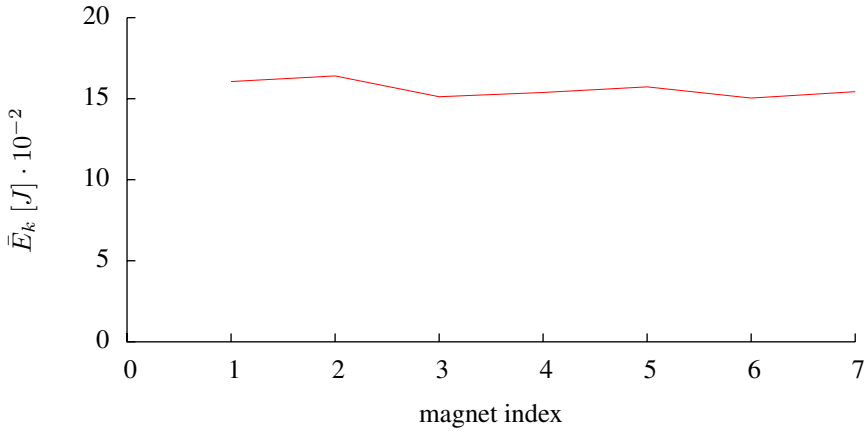

Figure 5.10: Plot of the average kinetic energy for each magnet in the stack based on the results from figure (5.8).

The trend from the figure shows that the average kinetic energy is constant throughout the system. On the basis of equipartition it can therefore be concluded that the temperature is uniform. However, the result in this section is obtained under the assumption that the system is ergodic as shown in section (5.6).

5.6 Ergodic hypothesis

The ergodic hypothesis states that the probability of a component in a system to be in a microstate within the phase space region bounded by the total energy is uniform. The ergodic was an embedded assumption in the conclusion based on the equipartition theorem in section (5.5). It was assumed that by simulating the system over a long period of time and taking the average of the mechanical state variable was the same as the statistical ensemble.

An example of a system that is not ergodic is shown in figure (5.11). The figure shows a phase plot of the microstates that was occupied throughout the simulation based on the simulation result from figure (5.6). This system can therefore not be ergodic, since it is only the states of magnet seven that can be found towards the edge of the phase space. The trend in the figure is that there is a color shading from the center of the circle, i.e. the high energy states towards the edge of the region bounded by the Hamiltonian can not be reached by the magnets at the bottom of the stack.

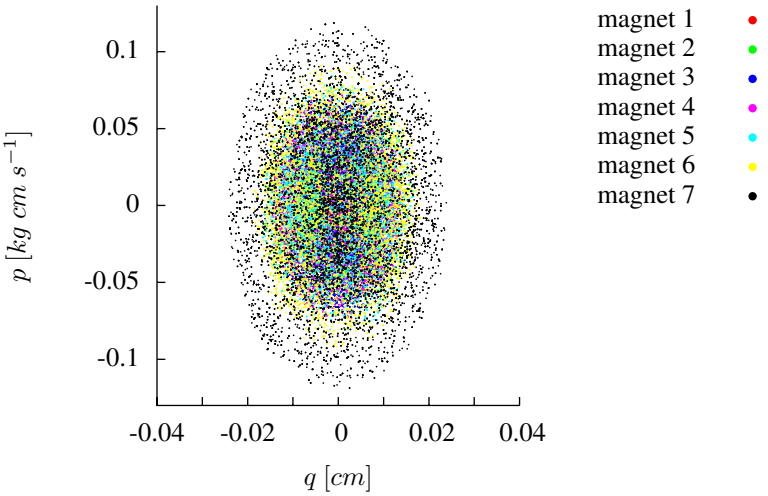

Figure 5.11: The figure shows randomly selected microstates that was occupied by each magnet in the system from the simulation in figure (5.6).

The results from the simulation in figure (5.11) shows that the system is not ergodic, however, the microstates for each individual magnet can still be individually uniformly distributed. The reason for this is that the system obeys Liouville's theorem.

Liouville's theorem is related to the ergodic hypothesis. It states that the probability density is uniform along the phase space trajectory of the system. That is, when the system is in any given state, the neighboring states all have the same probability. The data analysis in this work, as explained in section (5.3.1), was performed by choosing random states

using a uniform distribution. The reason why this assumption was introduced was that the initial conditions in table (5.5) were chosen from a uniformly distributed function, i.e. the initial states was uniformly distributed. Consequently, they will according to Liouville's theorem remain uniformly distributed throughout the simulation interval.

The system from figure (5.8) was found to have constant kinetic energy in section (5.10), consequently it should therefore be ergodic. Figure (5.12) shows the phase space microstates that was occupied during the simulation.

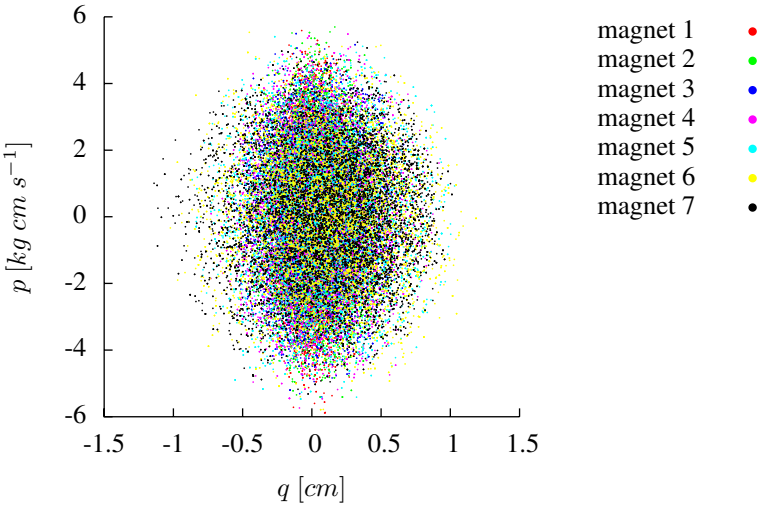

Figure 5.12: The figure shows randomly selected microstates that was occupied by each magnet in the system from the simulation in figure (5.8).

The results in figure (5.12) shows a very different trend than figure (5.11). The microstates towards the centre of the phase space are, as expected, most probable. However, by looking at the "cloud" of states it is clear that the microstates towards the edge of the region bounded by the total energy can be populated by any of the magnets. The ergodic hypothesis states that the phase space region should be completely covered. Even though this is not the case in figure (5.12) the trend suggests this can be accomplished by running the simulations longer. The conclusion is therefore that the system of magnet is ergodic and Liouville if the initial energy is large enough and the time interval is sufficient.

5.7 Pressure dependence

The pressure dependence of the system is analyzed based on the fact that the top magnet only exerted the force of gravity on the stack, i.e. the magnetic force excerpted by magnet n of the top magnet is in the static case equal to the weight. This means that any force that is greater than the weight of the top magnet can be interpreted as the pressure of the atmosphere.

From the ideal gas law it is clear that the pressure of an ideal gas is proportional to the temperature (dT) of the gas for a closed system ($dN = 0$) at a constant volume ($dV = 0$).

$$dp = \frac{\partial p}{\partial T}dT + \frac{\partial p}{\partial V}dV + \frac{\partial p}{\partial N}dN \quad ; \frac{\partial p}{\partial T} = \frac{NR}{V}$$

The result from section (5.5), stating that the temperature is proportional with the average kinetic energy, was used in order to increase the thermodynamic temperature of the system of magnets. The expression in equation (5.1) was subsequently used in order to calculate the force on the top magnet, the average of this value was interpreted as the pressure. Note that the statistical value of the state is assumed to be related to the thermodynamic pressure under the ergodic assumption.

The simulations where carried out using the initial conditions from table (5.5) and changing the parameter K in order to increase the total energy of the system without changing the distribution of the initial state. The reason for this is that the same ”seed” was used for the probability distribution that determined the initial velocities.

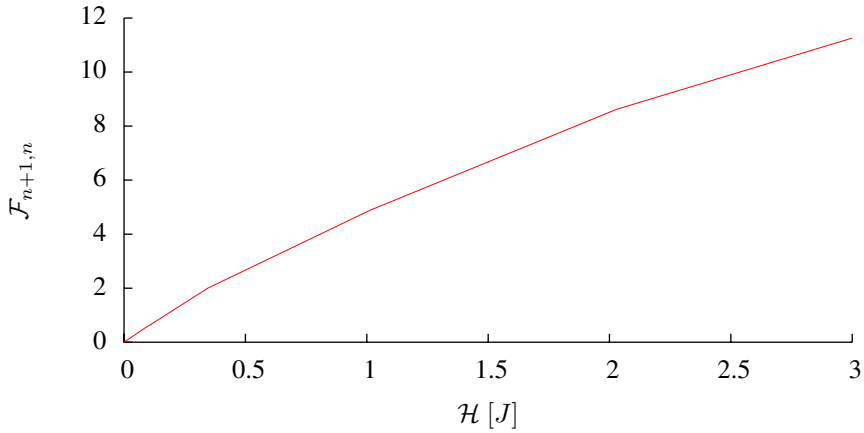

Figure 5.13: Plot of pressure against the kinetic energy in the system

The figure shows that the magnetic force affecting the top magnet increases linearly with respect to the total energy of the system. Analog to a thermodynamic system, the pressure increases linearly with respect to the temperature.

Chapter 6

Discussion

The goal of this work was to study a mechanical system of vertically stacked magnets as an analogy to an atmosphere of an ideal gas by studying the long time behavior of the system. This discussion chapter is divided into three sections that are intended to discuss the results in this work as well as suggesting topics for future work.

6.1 The symplectic integrators

Chapter (2) introduced the theory necessary to understand the background of the symplectic integration methods in this work based on canonical transformations from classical Hamiltonian mechanics. Special attention was given to the development of the integration methods in chapter (3). Note that the methods in this work were chosen such that they could be understood based on the theory that is presented in this work, but there are higher order methods such as the sixth order method in Calvo et al. (2009) available. These methods are often based on the more mathematical approach of group theory and a different name for a symplectic integration that is commonly used is ”geometric integration”.

The basic properties of the symplectic methods were shown in section (4.1) using low order methods to integrate the simple harmonic oscillator. Figure (4.1) shows how the explicit and implicit Euler methods both diverge from the analytical solution whereas the symplectic method closes the phase space trajectory. Even though the symplectic Euler method was able to close the phase space trajectory, it was consistently not exactly equal to the analytical trajectory. When the second order methods Leapfrog and SERKN were applied to the same problem, the result in figure (4.4) shows that the phase space trajectory is equal to the analytical solution. However, the numerical solution is not equal to the analytical solution, even though the phase space trajectory suggests this. According to Sanz-Serna (1992) a characteristic feature of symplectic integrators is that the value of the Hamiltonian oscillates. This is shown in figure (4.3) for the symplectic Euler method and the Leapfrog and SERKN methods figure (4.5). The literature search did not reveal an explicit explanation to why the symplectic integrators have this property. However, it was

expected that the symplectic methods could not conserve the Hamiltonian and the phase space structure of the ODEs simultaneously. Since the analytical solution has no degrees of freedom, the numerical method will never be able to exactly reproduce all the properties of the solution. On the other hand, from the figures that show the Hamiltonian as a function of time, it is clear that the amplitude of the oscillations depends on several factors.

In figure (4.3) it is clear that the amplitude of the oscillation is dependent on the step size of the method. Since none of these methods in the figure resulted in phase space trajectories exactly equal to the analytical solution, it can be concluded that the the amplitude of the Hamiltonian must be smaller than 10^{-3}, which is the amplitude of the most accurate method. When the order of the numerical methods is increased in figure (4.5), the amplitude of the oscillations is significantly decreased. The amplitude is 10^{-5} for both the Leapfrog and SERKN methods and they produce the same phase space trajectory even though the solutions are not identical. By looking at the oscillation of the Hamiltonian, it is clear that they oscillate around a different equilibrium point and the phase is shifted π $[rad]$ with respect to each other. The exponentially fitted and symplectic method seems to oscillate around the true value of the Hamiltonian, but the symplectic oscillates around a point close to the true value. From these figures it was concluded that the largest oscillation that should be allowed for the Hamiltonian was 10^{-5}. Furthermore, it was concluded that the order of the method or step size could be used in order to achieve the desired accuracy.

The harmonic chain was chosen as the system of ODEs in section (4.2). Unlike the harmonic oscillator, the ODEs in the harmonic chain interacts , which is similar to the system of magnets. Both because of the nonlinearity of the stack of magnets and in order to study the exponentially fitted techniques, it would be desirable to perform the numerical experiments on a nonlinear system. However, due to lack of knowledge about the analysis of nonlinear dynamics this was not considered in this work. and the linear system is assumed to be sufficient. This is admittedly a drawback of this work because the stack of magnets was represented by a highly nonlinear system of equations. On the other hand, the equations of motion in this work are not stiff and the assumption is therefore that the nonlinearity can be dealt with using exponential fitting techniques.

The results from the numerical experiments are shown in table (4.2) and (4.3). The tables respectively show the results of three simulations using different step sizes for a harmonic chain of five and thirteen mass points. In order to ensure the generality of the results, the same initial conditions were never used twice. The system was instead initiated in different configurations (e.g. zero velocity and random positions or equilibrium positions and random velocity) and then scaled to have the same total energy. The simulations clearly showed that the order of the method significantly influences the long time accuracy of the integration. The "$ode45$" method from MathWorks performed consistently well, however this was because the error tolerance ($AbsTol$ and $RelTol$) was set to 10^{-10} using the function $odeset()$. This was necessary in order to produce results even remotely close to what the symplectic integrators could achieve using a step size in the order of 10^{-4}. This made the integration very slow and combined with the low accuracy and and

adaptive stepping it was therefore not considered for the system of magnets. The methods that where specifically derived for this work, however showed much better accuracy and both of the tables mentioned in the beginning of the paragraph show that the order of the method is a significant factor in this work. For instance it is clear that the fourth order standard RKN method shows very similar results as the third order symplectic and trigonometric RKN (STRKN) method. The regular RKN method is also consistently better than the third order exponential RKN (ERKN) method. Even though the second order Leapfrog and SERKN methods fall short compared with the higher order methods, they show some interesting properties. The error of these methods is of the same order in all of the simulations apart from one. However, the amplitude of the Hamiltonian is consistently lower in the exponentially fitted SERKN method. The fourth order RKN and third order STRKN shows a similar trend in both tables and the latter was ultimately preferred because it should perform better when applied to a nonlinear oscillatory system. The system of magnets was therefore only considered using the STRKN method.

However, for a single second order ODE the SERKN should be considered. The reason for this is that it only require one function evaluation, whereas all the other methods require two or more. The SERKN method will consequently save a significant amount of computational time.

6.2 Simulation of a model of a one dimensional system of magnets oscillating in a gravitational field

The examples in chapter (2) showed the methodology for deriving the model of the system of magnets in chapter (5). The only difference is that the assumption that the magnets are ideal dipoles implies that the force field between the magnets is inversely proportional with the squared distance between the magnets. This force model produced nonlinear equations of motion and the static equilibrium distribution in section (5.2.1) could consequently only be obtained explicitly through an approximation. The static initial conditions required that the height of the first magnet must be set and the total height of the column along with the force constant would then be determined by the number of magnets in the system. Section (5.3.1) summarizes the parameters that were constant throughout all the simulations in this work. It also shows how the linearized model from section (5.1.2) could be used in order to determine the appropriate step size and when to start the sampling as previously discussed.

6.2.1 Model validation

The simulations in section (5.3.2) were designed in order to validate the static equilibrium conditions. Figure (5.4) shows that the system remains static when the static distribution is used as the initial conditions in the equations of motion. This confirms that the distribution from (5.2.1) is the static equilibrium of the magnets. The second simulation was designed to show that the magnets continue to oscillate around the static equilibrium conditions when they are initiated away from equilibrium. Figure (5.5) shows that prob-

ability density for the positions of all the magnets. The densities are centered around the static equilibrium values and they do not overlap. Moreover, the width of the probability density function varies along the height of the stack. This suggests that the amplitude of the top magnets must be larger at the top than at the bottom. This can be interpreted as the density of an atmosphere of a gas and the density is consequently highest at the bottom of the atmosphere.

By looking at the force model of the magnets it is reasonable to assume that the magnets will never occupy the same position because the force between the magnets will become infinite in the limit where the distance becomes zero. The total energy of the system in this simulation was also of the same order of magnitude that figure (5.3) defines as the maximum value. It is therefore reasonable to assume that this result is valid for all the simulations in this work. Even though the magnets do not overlap according tho the mathematical model, it does not account for the size of the magnets. This is obviously something which must be accounted for if the model is built.

The second part of the model validation is shown in section (5.3.3) and considers the diffusion of kinetic energy. The first simulation in figure (5.6) shows how the kinetic energy is shared between the magnets when only the top magnet is given an initial velocity. However, the energy is so small that the system never reaches an equilibrium state. Instead, it shows the same behavior as the linear model and is divided into eigenfrequencies whose velocity displacement probability distribution is equal to that of the linearized force model. The reason for this can be that the initial perturbation sends a wave through the system which is simply absorbed by the other magnets in the system, and consequently leads to harmonic oscillations.

6.2.2 Thermodynamic interpretation of statistic variables

The vertical stack of magnets is not a truly thermodynamic system, i.e. the number of magnets is too small compared with a thermodynamic system which has an infinite number of components. However, as shown in section (5.12) the system behaves thermodynamically when the total energy of the system is large enough. The microstates of the system are equally accessible; i.e. the system is ergodic, and the phase space distribution around a specific state is uniformly distributed, i.e. the system obeys Liouville's theorem.

The validity of the statistical interpretation of the state variables in this work is entirely dependent on the argument that figure (5.12) implies that the system is ergodic. However, the system was also shown to not have ergodic properties in figure (5.11). A much better argument could possibly be constructed on the basis of a statistical mechanic analysis of an ensemble of magnets. The ideal gas, on the other hand, is rigorously shown in Volkovysskii and Sinai (1971) to be an ergodic system. Note that this work does not suggest any direct connection between the ergodic property of the system of magnets and the fact that the ideal gas is ergodic. Instead it is observed that the trend in the simulations indicate that the model shows several properties which resemble that of an ideal gas, which is ergodic.

The average kinetic energy, analogue to the temperature, distribution in the system was shown in figure (5.10) to be uniform. This is supported by the simulations in figure (5.9) that show the probability density for the velocity displacement of all the magnets can be approximated using a single Maxwell-Boltzmann density function. The article Velasco et al. (1996) shows that this is the case for an atmosphere of an ideal gas using an analysis based on statistical mechanics. Furthermore, the width of the probability density for the position displacement was shown in figure (5.5) to increase along the height of the column. The latter result supports the first because it implies that the frequency of the bottom magnets is higher than those towards the top of the stack. Analogue to an atmosphere of a gas, this implies that the density of the gas is largest at the bottom.

This interpretation of the pressure of the system was adopted from a similar system in Ibsen et al. (1997). It was interpreted as the absolute magnetic force excerpted on the top magnet, i.e. the magnetic force that exceeds the necessary amount needed in order to support the weight of the magnet. The interesting question was wether the pressure dependence is linear with respect the total energy, analogous to the thermodynamic ideal gas pressure dependence with respect to temperature. The results in figure (5.13) suggests that this is the case for the system of magnets as well.

The results from the simulations indicate that the vertical stack of oscillating magnets behaves similar to an ideal gas when using appropriate initial conditions, i.e. initial conditions corresponding to a total energy that makes the nonlinear terms of the model interact. However, the results in this work can not tell why this happens. Moreover, it is curious that a system consisting of only seven elements can be used as a description of an infinite thermodynamic ensemble. Moreover, as recently demonstrated in the discussion between well known academics in Brenner et al. (2013) and Felderhof (2013), one should take care when basing conclusions contradicting theoretical results based on simulations.

6.3 Suggestions for future work

The model that was presented in this work is somewhat of a ”sandbox”. It can be turned inside out, upside down, linearized and analyzed. This work focused on the development of symplectic numerical methods in order to obtain accurate results. The model was also derived and the statistical interpretation from the simulations was used to determine the thermodynamic properties of the system. There are several subjects that are interesting in order to continue this work. The following two sections suggests future topics based on continuing or extending this work.

6.3.1 Continuation of this work

The most obvious continuation is to build the model and verify the simulations by measuring the root mean squared velocities as well as the force on the top magnet.

The validation of the model can also be performed using frequency analysis of the low-energy simulations of the non-linear and the linearized model. The frequency analysis can

then be used in order to study the transition from the non-linear to the linear domain of the nonlinear model. This transition is of significant interest because if the model can be studied analytically in the linear domain, whereas the numerical results will always be an approximation.

6.3.2 Extension of this work

A powerful extension of this work would be to perform a rigorous statistical mechanic analysis of the system. The results in this work were based on results from statistical mechanics, however the theory was at no point studied in detail.

Another interesting property which was not considered in this work is the entropy of the system. The ideal gas has an analytic thermodynamic expression for the entropy and Landsberg et al. (1994) considers the entropy of an ideal gas using a canonical ensemble from statistical mechanics.

Chapter 7

Conclusion

This work set out to answer whether a vertical system of magnets oscillating in a gravitational field could be used as a model of an atmosphere of an ideal gas.

In order to obtain accurate numerical results, this work also considered methods that guaranteed that the simulation stayed on the energy surface, i.e. symplectic methods. In chapter (4) it was found that using exponential fitting techniques in addition to the symplectic requirement gave the best results. Moreover, it was found that choosing a step size that reflects the dynamics of the system is important. Consequently, since high energy simulations have fast oscillations the step size must be reduced, often significantly, in order to capture the smallest frequencies. However, as long as the value of the Hamiltonian was conserved to order $\mathcal{O}(10^{-5})$ all the frequencies were captured accurately by the integration methods.

The statistical interpretation of the mechanical state variables from the simulations was considered in chapter (5). The simulations in section (5.7), that were analogous to the pressure dependence with respect to temperature, showed that the pressure increases linearly. Moreover, the average kinetic energies for the magnets in the system, analogue to the thermodynamic temperature, was found to be constant in section (5.5). The analogy to density also seems to be decreasing along the height of the column in section (5.3.2). The validity of the statistical interpretation of the simulation results was supported by the fact that the phase space microstates; shown in section (5.6), obeys the ergodic hypothesis.

The final conclusion is therefore that a model consisting of a finite system of seven idealized dipole magnets stacked vertically in a gravitational field behaves thermodynamically equivalent to an atmosphere of an ideal gas.

Bibliography

Berghe, G. V., De, H. M., Daele, M. V., and Hecke, T. V. (1999). Exponentially-fitted explicit runge-kutta methods. *Computer Physics Communications*, 123(13):7 – 15.

Brenner, H., Dongari, N., and Reese, J. (2013). A molecular dynamics test of the navier-stokes-fourier paradigm for compressible gaseous continua. *arXiv:1301.1716 [physics.flu-dyn]*.

Calvo, M., Franco, J. M., Montijano, J. I., and Rández, L. (2009). Sixth-order symmetric and symplectic exponentially fitted runge-kutta methods of the gauss type. *J. Comput. Appl. Math.*, 223(1):387–398.

Coombes, C. A. and Laue, H. (1985). A paradox concerning the temperature distribution of a gas in a gravitational field. *American Journal of Physics*, 53(3):272–273.

D'Ambrosio, R., Paternoster, B., and Santomauro, G. (2014). Revised exponentially fitted runge-kutta-nyström methods. *Applied Mathematics Letters*, 30(0):56 – 60.

Felderhof, B. U. (2013). Comment on "proposal of a critical test of the navier-stokes-fourier paradigm for compressible fluid continua". *Phys. Rev. E*, 88:027001.

Franco, J. (2004). Exponentially fitted explicit runge-kutta-nyström methods. *Journal of Computational and Applied Mathematics*, 167(1):1 – 19.

Goldstein, H., Poole, C. P., and Safko, J. L. (2014). *Classical Mechanics 3.rd ed.* Pearson Education Limited. ISBN: 0321-188977.

Hairer, E., Lubich, C., and Wanner, G. (2002). *Geometric Numerical Integration. Structure-Preserving Algorithms for Ordinary Differential Equations*. Springer.

Hairer, E., Nørsett, S., and Wanner, G. (1993). *Solving Ordinary Differential Equations I, Nonstiff problems*. Springer-Verlag.

Ibsen, J., Cordero, P., and Tabensky, R. (1997). Hard rods in the presence of a uniform external field. *The Journal of Chemical Physics*, 107(14):5515–5523.

Kalogiratou, Z. and Simos, T. (2002). Construction of trigonometrically and exponentially fitted runge-kutta-nyström methods for the numerical solution of the schrödinger equation and related problems method of 8th algebraic order. *Journal of Mathematical Chemistry*, 31(2):211–232.

Karolius, S. (2014). Matlab directory. Directory containing implementations and simulations of a linear harmonic chain and a one dimensional system of oscillating magnets using various integration techniques. `http://folk.ntnu.no/sigveka/Master_Thesis/MatLab/`.

Landsberg, P. T., DunningDavies, J., and Pollard, D. (1994). Entropy of a column of gas under gravity. *American Journal of Physics*, 62(8):712–717.

Lyche, T. (1972). Chebyshevian multistep methods for ordinary differential equations. *Numerische Mathematik*, 19(1):65–75.

Monovasilis, T., Kalogiratou, Z., and Simos, T. (2013). Exponentially fitted symplectic runge-kutta-nystroem methods. *Applied Mathematics and Information Sciences*, 7(1):81–85.

Paternoster, B. (1998). Runge-kutta(-nyström) methods for odes with periodic solutions based on trigonometric polynomials. *Applied Numerical Mathematics*, 28(2-4):401 – 412.

Ruth, R. D. (1983). A canonical integration technique. *IEEE Transactions on Nuclear Science*, 30(4):2669–2671.

Sanz-Serna, J. (1992). Symplectic integrators for hamiltonian problems: an overview. *Acta Numerica*, 1(1):243–286.

Simos, T. and Aguiar, J. (2003). Exponentially-fitted symplectic integrator. *Physical Review*, 67(1):1–8.

Simos, T. b. (2002). An exponentially-fitted runge-kutta-nystroem method for the numerical solution of initial-value problems with oscillating solutions. *Applied Mathematics Letters*, 15:217–225.

Van de Vyver, H. (2005). A symplectic exponentially fitted modified rungekuttanystrm method for the numerical integration of orbital problems. *New Astronomy*, 10(4):261–269.

Velasco, S., Romon, F., and White, J. (1996). On a paradox concerning the temperature distribution of an ideal gas in a gravitational field. *European Journal of Physics*, 17(1):43.

Volkovysskii, K. and Sinai, Y. (1971). Ergodic properties of an ideal gas with an infinite number of degrees of freedom. *Functional Analysis and Its Applications*, 5(3):185–187.

Warberg, T. (2013). Vibrating spring analogies to ideal gas. Notes and derivations of a nonlinear and linear one dimensional system of magnets in a gravitational field.

Weyl, H. (1946). *The classical groups : their invariants and representations. 2.ed*. Princeton University Press. ISBN: 0691-079234.

Wu, X., You, X., and Wang, B. (2013). *Structure-Preserving Algorithms for Oscillatory Differential Equations*. Springer (jointly with; Science Press Bejing). ISBN: 978-3-642-35338-3.

Zhao, M. and Zhu, W.-J. (1991). Canonical runge-kutta-nyström methods for second order ordinary differential equations. *Computers. Math. Applic.*, 22(9):281–297.

Appendix A

Magnets equilibrium distribution

This appendix considers the equilibrium state of a one dimensional system of idealized dipole magnets stacked vertically in a gravitational field. The goal of the appendix is to derive analytical expressions for the vertical equilibrium distribution of the magnets (i.e. the initial positions when the velocity is equal to zero).

A.1 Static equilibrium of a vertical system of magnets

This section derives the expression describing the equilibrium distribution for the system of magnets. In order to give some background it will summarize the derivation of the equations of motion.
The magnets are described by the Lagrangian in equation (A.1), where y_i is the vertical position of a magnet.

$$\mathcal{L} = \frac{1}{2} m \dot{\mathbf{y}}^2 - mg\mathbf{y} + \sum_{i=0}^{n} \frac{k_m}{(y_{i+1} - y_i)} \tag{A.1}$$

The equations of motion for the system is obtained by minimizing the action integral of the Lagrangian. The minimization results in the following Euler-Lagrange equation. The equation is a requirement that any trajectory which follows a path of minimized action must satisfy.

$$\frac{\partial \mathcal{L}}{\partial y} - \frac{d}{dt}\frac{\partial \mathcal{L}}{\partial \dot{y}} = 0$$

By applying the Euler-Lagrange equation to the Lagrangian in equation (A.1) the equations (A.2) for the trajectory of the system is obtained:

$$m\ddot{y}_i = -mg + \frac{k_m}{(y_i - y_{i-1})^2} - \frac{k_m}{(y_{i+1} - y_i)^2} \tag{A.2}$$

There is one equation of motion for each magnet in the system.

The equilibrium distribution of the magnets is found by setting the derivative equal to zero. The equations shown below represent the first (bottom), all the inner and the last (top) magnet in the system respectively.

$$\begin{aligned} \frac{1}{(y_1 - y_0)^2} &- \frac{1}{(y_2 - y_1)^2} = \frac{mg}{k_m} \\ \frac{1}{(y_i - y_{i-1})^2} &- \frac{1}{(y_{i+1} - y_i)^2} = \frac{mg}{k_m} \quad ; i = 2 \dots n-1 \\ \frac{1}{(y_n - y_{n-1})^2} &- \frac{1}{(y_{n+1} - y_n)^2} = \frac{mg}{k_m} \end{aligned} \tag{A.3}$$

$$\mathbf{Bz} = -z_0 \mathbf{e}_1 + \frac{mg}{k_m}\mathbf{e} \quad ; \mathbf{B} = \begin{bmatrix} -1 & & & \\ 1 & -1 & & \\ & \ddots & \ddots & \\ & & 1 & -1 \end{bmatrix} \tag{A.4}$$

The following definition was used in equation (A.4).

$$\mathbf{z} = \begin{bmatrix} \frac{1}{(y_2^0 - y_1^0)^2} & \frac{1}{(y_3^0 - y_2^0)^2} & \cdots & \frac{1}{(y_{n+1}^0 - y_n^0)^2} \end{bmatrix}^T \qquad z_0 = \frac{1}{(y_1^0 - y_0^0)^2}$$

When the matrix equation is solved for z_i the following expression is obtained

$$z_i = z_0 - i\frac{mg}{k_m} \quad ; i = 1 \dots n \tag{A.5}$$

The following expression is obtained when substituting back for y_i^0 in equation (A.5).

$$y_{i+1}^0 - y_i^0 = \sqrt{\frac{1}{\frac{1}{(y_1^0 - y_0^0)^2} - i\frac{mg}{k_m}}} \quad ; i = 1 \dots n \tag{A.6}$$

It is necessary to find a suitable expression for the magnetic force field constant (k_m). This constant will be to determined using the ratio (α), which is defined as the ratio between the of the height of a single magnet hovering above a fixed ground state and the bottom magnet in the stack. The bottom magnet will need to hold the entire weight of the stack whereas the single magnet only needs to support its own weight. Either way, the force balance must be satisfied and for the single magnet it is expressed as shown in equation (A.7).

$$\frac{k_m}{(y_{eq}^0)^2} = mg \tag{A.7}$$

By combining equation (A.6) and (A.7) and setting the position of the bottom magnet $y_0^0 = 0$ the following expression is obtained.

$$\boxed{y_{i+1}^0 - y_i^0 = y_1^0\sqrt{\frac{1}{1 - \alpha i}} \quad ; \alpha \hat{=} \left(\frac{y_1^0}{y_{eq}^0}\right)^2 \quad ; i = 1 \dots n} \tag{A.8}$$

The equations are expanded below and the position of the top magnet is set to be the height of the system (L) (i.e. $y_{n+1} = L$).

$$y_2^0 - y_1^0 = y_1^0\sqrt{\frac{1}{1-\alpha}}$$
$$y_3^0 - y_2^0 = y_1^0\sqrt{\frac{1}{1-2\alpha}}$$
$$\vdots$$
$$y_n^0 - y_{n-1}^0 = y_1^0\sqrt{\frac{1}{1-(n-1)\alpha}}$$
$$L - y_n^0 = y_1^0\sqrt{\frac{1}{1-n\alpha}}$$

These equations can be condensed into a single nonlinear equation in y_1^0 as shown in equation (A.9)

$$\boxed{L - y_1^0 = y_1^0 \sum_{i=1}^{n} \sqrt{\frac{1}{1-i\alpha}} \quad ;\alpha \hat{=} \left(\frac{y_1^0}{y_{eq}^0}\right)^2} \tag{A.9}$$

The equilibrium distribution of all the magnets can now be obtained using the recursive relation in equation (A.8). However, the nonlinear equation (A.9) describing the position of the first magnet must be solved first.

A.2 Equilibrium distribution

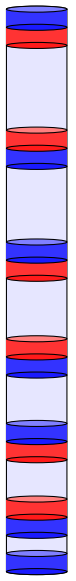

This section considers the case when all the magnets are of equal mass. In this case, the top magnet will float on top of the stack without exerting any extra force other than the force of gravity. This is referred to as the relaxed state of the system. An illustration of the expected equilibrium distribution is shown in the illustration. The sum in equation (A.9) is approximated by the integral shown below in order to obtain an approximated solution to the position of the first magnet.

$$\int \frac{1}{\sqrt[p]{ax+b}}dx = \frac{p}{a(p-1)}(ax+b)^{1-\frac{1}{p}} + C \quad ;p > 1$$

When this approximation is used on the sum in equation (A.9) the following expression in obtained

$$\int_1^n \sqrt{\frac{1}{1-\alpha x}}dx = \frac{2}{\alpha}\left(\sqrt{1-\alpha} - \sqrt{1-\alpha n}\right)$$

In order to continue, it is necessary to introduce a couple of assumptions. First, the number of magnets will always be greater than one and as a general statement it an be assumed

$n \gg 1$. Furthermore, it can be stated that the force excerted by the top magnet is exactly equal to the force of gravity. This means that magnet $n+1$ does not exert any force on magnet n other than the force of gravity and thereby simply floats on top of the stack of magnets. The result of these assumptions simplifies the integral as shown below.

$$\int_1^n \sqrt{\frac{1}{1-\alpha x}}dx \approx \frac{2}{\alpha}\left(\sqrt{1-\alpha}\right) \approx \frac{2}{\alpha}\left(1-\frac{\alpha}{2}\right) = 2(n+1)-1 \quad ;\sqrt{1-x} \approx 1-\frac{x}{2}+\mathcal{O}(x^2)$$

When this approximation is used in the original integral the expression in equation (A.10), the position of the first magnet is obtained.

$$\boxed{y_1^0 \approx L\left[1+\sum_{i=0}^{n}\sqrt{\frac{1}{1-\alpha i}}\right]^{-1} \quad ;\alpha = \frac{1}{n+1}} \tag{A.10}$$

Now it is a trivial task to obtain the equilibrium positions for the rest of the magnets. This is done by using the position of the first magnet in equation (A.8).

$$\boxed{y_{i+1}^0 \approx y_i^0 + \frac{L}{2(n+1)}\sqrt{\frac{1}{1-\alpha i}} \quad ;i = 0\ldots n} \tag{A.11}$$

The final solution is the static initial condition for the relaxed system of magnets. It is clear that the distance between the magnets will increase with the height of the column. The total height can also be estimated using the expression for the equilibrium position of the first magnet in equation (A.10).

$$L \approx 2y_i^0(n+1)$$

It is expected that if the system is started using the relaxed equilibrium positions and zero velocity, it will not move when integrated over time.

In order to solve the equations of motion, it is necessary to find an expression for the force field constant. This can be obtained by combining equation (A.7) and (A.8). The result is shown in equation (A.12).

$$\boxed{k_m = \frac{mg(y_1^0)^2}{\alpha}} \tag{A.12}$$

The static equilibrium of the system is now described by the ODEs in equation (A.2) and the initial conditions in equation (A.10) with zero velocity.

A.3 Compressed equilibrium distribution

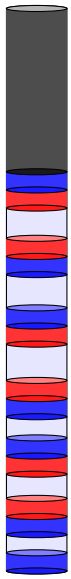

This section considers the solution of equation (A.9), which describes the position of the first magnet, when the stack of magnets is compressed (e.g. by adding mass on the top magnet). An illustration of this case is shown in the illustration.

Assuming $n \gg 1$ and $1 \gg \alpha$ while still $1 \gg n\alpha$. The sum in equation (A.9) can now immediately be expressed as shown below:

$$\sum_{i=1}^{n} x = \frac{n(n+1)}{2}$$

The square root can be approximated as follows:

$$\sqrt{\frac{1}{1+\alpha x}} \approx 1 + \frac{\alpha x}{2} + \mathcal{O}(x^2)$$

The approximation leads to the final expression for the static equilibrium that is shown below.

$$L - y_1^0 = y_1^0 \sum_{i=1}^{n} \sqrt{\frac{1}{1-\alpha i}} \approx y_1^0 \sum_{i=1}^{n} \left(1 + \frac{\alpha i}{2}\right) = y_1^0 \left(n + \frac{\alpha n(n+1)}{4}\right) \tag{A.13}$$

The last term in the parentheses disappears because of the assumption $1 \gg n\alpha$. The following expression can therefore be found for the equilibrium position of the first magnet.

$$y_1^0 = \frac{L}{n+1}$$

This expression is linear and the position of all the magnets can therefore be obtained directly from the recursive relation in equation (A.8).

$$y_{i+1}^0 = y_i^0 + \frac{L}{n+1} \qquad ; i = 0 \ldots n$$

Note that the position of the bottom particle is defined to be zero (i.e. $y_0^0 = 0$).

A.4 Linearized relaxed model

The equilibrium state is characterized by the balancing of the forces between the magnets. The force due to gravity is already linear; however, the magnetic force between the magnets can be expressed as follows.

$$\mathcal{F}_{i+1,i} = \frac{k_m}{(y_{i+1} - y_i)^2}$$

Consider the recursion relationship for the equilibrium distribution of the relaxed model in equation (A.11) in order to describe the distance between the magnets. The representation of the recursion relation shown below was obtained using the definition of α.

$$y^0_{i+1} - y^0_i = \frac{L}{2n+1}\sqrt{\frac{n+1}{n+1-i}}$$

The formulae is an approximate relationship that is limited by the approximations in section (A.1). However, it allows for an approximate relationship to be formulated for the inverse squared equilibrium distance between the magnets.

$$\frac{1}{\left(y^0_{i+1} - y^0_i\right)^2} = \frac{4(n+1)(n+1-i)}{L^2}$$

The force can now be linearized around the static equilibrium using $\Delta y_{i+1,i} \hat{=} (y_{i+1} - y_i)$.

$$\mathcal{F}_{i+1,i} \approx \frac{k_m}{\left(\Delta y^0_{i+1,i}\right)^2} - \frac{2k_m}{\left(\Delta y^0_{i+1,i}\right)^3}\left(\Delta y_{i+1,i} - \Delta y^0_{i+1,i}\right) + \mathcal{O}(\Delta y^2_{i+1,i})$$

$$\mathcal{F}_{i+1,i} \approx \underbrace{\frac{3k_m}{\left(\Delta y^0_{i+1,i}\right)^2}}_{c_{i+1,i}} - \underbrace{\frac{2k_m}{\left(\Delta y^0_{i+1,i}\right)^3}}_{k_{i+1,i}} \Delta y_{i+1,i}$$

The force is now linearized by a straight line with slope $k_{i+1,i}$ and intercept $c_{i+1,i}$. However, the force field constant is not known. Instead of trying to express the force constant explicitly, the force terms can be viewed as a linear system of equations. For one magnet i there will be two force terms. Because the system is linear, the ratio of the equations describing the forces can be considered instead of evaluating each equation separately. This reveals a simple expression for the ratio of the intercepts.

$$\frac{c_{i+1,i}}{c_{i,i-1}} = \left(\frac{\Delta y^0_{i,i-1}}{\Delta y^0_{i+1,i}}\right)^2 = \frac{N+1-i}{N+2-i}$$

Furthermore, as shown below, the ratio between the intercepts can be used in order to express the ratio of the slopes.

$$\frac{k_{i+1,i}}{k_{i,i-1}} = \left(\frac{\Delta y^0_{i,i-1}}{\Delta y^0_{i+1,i}}\right)^3 = \left(\frac{c_{i+1,i}}{c_{i,i-1}}\right)^{\frac{3}{2}}$$

The Lagrangian for the linear model can now be formulated based on the standard expressions for the gravitational potential energy and kinetic energy.

$$U^{(m)} = c_{i,i-1}(y_i - y_{i-1}) - \frac{k_{i,i-1}}{2}(y_i - y_{i-1})^2 \quad ; i = 1 \dots n$$

The equations of motion are derived using the Euler-Lagrange equation from the beginning of section (A.1). The equations of motion for the linearized Lagrangian are shown in equation (A.14).

$$-m\ddot{y}_i - mg + c_{1,i-1} - k_{i,i-1}(y_i - y_{i-1}) - c_{i+1,i} + k_{i+1,i}(y_{i+1} - y_i) = 0 \quad \text{(A.14)}$$

The following vector ($\mathbf{c}$) and tridiagonal metric ($\mathbf{T}$) are defined in order to write the equations of motion in matrix form.

$$\mathbf{c} = \begin{bmatrix} c_{2,1} - c_{1,0} & \dots & c_{i+1,i} - c_{i,i-1} & \dots & c_{n+1} - c_n \end{bmatrix}^T$$

$$\mathbf{T} = \begin{bmatrix} t_{1,1} & t_{1,2} & & & & & \\ t_{2,1} & t_{2,2} & t_{2,3} & & & & \\ & \ddots & \ddots & \ddots & & & \\ & & t_{i,i-1} & t_{i,i} & t_{i,i+1} & & \\ & & & \ddots & \ddots & \ddots & \\ & & & & t_{n,n-1} & t_{n,n} & t_{i,n+1} \end{bmatrix}$$

The elements of the matrix are a function of the index i, however the matrix is still symmetric. The following equations can be used to determine the elements in the matrix.

$$t_{i,i} = k_{i,i-1} + k_{i+1,i}$$
$$t_{i,i+1} = t_{i+1,i} = -k_{i+1,i}$$

The matrix representation of the equations of motion can now be written in matrix form.

$$m\ddot{\mathbf{y}} = -\mathbf{T}\mathbf{y} + k_{1,0}y_0\mathbf{e}_1 + k_{n+1,n}y_{n+1}\mathbf{e}_n - \mathbf{c} - mg\mathbf{e} \quad \text{(A.15)}$$

Where the following vectors have not yet been defined:
$\mathbf{e}_1 = [1, 0, \dots, 0]^T$,$\mathbf{e}_n = [0, \dots, 1]^T$,$\mathbf{e}_1 = [1, \dots, 1]^T$.
Note that this equation is linear and that all the terms that are multiplied by a vector $\mathbf{e}$ are constant.

The goal is to simplify the equation of motion even further by removing the constant terms. In order to do this, the steady state solution of the equation of motion shown below is used.

$$\mathbf{y}^0 = \frac{k_{n+1,n}y^0_{n+1}}{m}\mathbf{T}^{-1}\mathbf{e}_n - m^{-1}\mathbf{T}^{-1}\mathbf{c} - g\mathbf{T}^{-1}\mathbf{e}$$

In order to simplify the equation of motion in equation (A.15), the steady state solution is used to define a new variable ($\mathbf{q}$).

$$\mathbf{q} \hat{=} \mathbf{y} - \mathbf{y}^0$$

When this variable is introduced into the equation of motion, the constant terms cancel and the final equation of motion is obtained.

$$\ddot{\mathbf{q}} = -m^{-1}\mathbf{T}\mathbf{q} \quad \text{(A.16)}$$

Appendix B

Euler-Lagrange equations from calculus of variations

This appendix is intended to serve as a short refresher of the ideas behind calculus of variations. In addition to providing a detailed derivation of the Lagrange equations of motion, it provides a deeper insight into the properties of functionals.

The starting point for this derivation is the generic functional $\mathcal{J}[y(x)]$ shown in equation (B.1). By looking back at equation (2.4) it can bee seen that the functional has the same form as the action functional in the previous chapter.

$$\mathcal{J}[y(x)] = \int_a^b f(y, y', x)dx \quad ; y = y(x) \quad y' = \frac{dy}{dx} \tag{B.1}$$

Figure (B.1) helps to visually introducee the idea behind the process. The left plot in the figure shows the actual solution $\bar{y}(x)$ over an integration interval $a \to b$. The second function shown is in the vicinity of the solution but is shifted from the actual solution by a second function $\eta(x)$ which in turn is scaled by a constant ϵ. However, the area beneath the actual solution and the shifted solution is the same because the function $\eta(x)$ is chosen such that it vanishes at the endpoints of the integration interval. The strategy that is used as illustrated in the left picture in figure(B.1) is that instead of considering the actual solution, a special function in the vicinity of the solution will be considered. The actual solution can now implicitly be obtained by considering the limit when the scaling constant ϵ goes to zero, as shown in the right picture in the figure.

This must now be formulated mathematically. Equation (B.2) is the mathematical representation of the left picture in figure (B.1). This equation defines the actual solution as the solution to the minimization of the shifted functional.

$$\frac{d}{d\epsilon}\mathcal{J}[\bar{y}(x) + \epsilon\eta(x)]\Big|_{\epsilon=0} = 0 \tag{B.2}$$

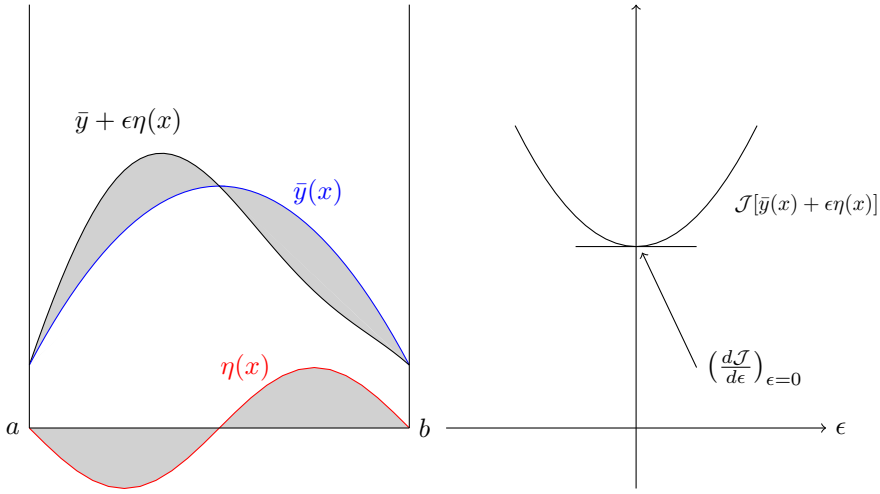

Figure B.1: The figure illustrates the idea behind calculus of variations. The goal is to find the function $\bar{y}(x)$ that minimizes a functional $\mathcal{J}[y(x)]$ over the integration interval $a \rightarrow b$. The left figure shows that if the solution is shifted by a function $\eta(x)$ and scaled by a constant ϵ the area underneath the curved, hence the integral is the same. Instead of minimizing the functional directly with respect to the actual solution, the shifted solution $\mathcal{J}[\bar{y}(x) + \epsilon\eta(x)]$ can alternatively be used without changing the value of the functional. The right figure then suggests that the optimal solution, representing the minimum of the functional, can implicitly be found by considering the limit of the functional with respect to the shifted solution at the limit $\epsilon \rightarrow 0$.

In order to continue, the expression for the functional from equation (B.1) must be used. The representation in equation (B.3) was obtained using the shifted solution along with the minimization requirement from equation (B.2).

$$\frac{d}{d\epsilon}\mathcal{J}[\bar{y}(x) + \epsilon\eta(x)]\Big|_{\epsilon=0} = \frac{d}{d\epsilon}\int_a^b f(\bar{y} + \epsilon\eta, \bar{y}' + \epsilon\eta)dx = 0 \tag{B.3}$$

The next steps are purely mathematical operations. Note that the dependence on the variable x, will no longer be written for the $y(x)$ or $\bar{y}(x)$. The first step involves the differential of the integral in equation (B.2).

$$\int_a^b \left(\frac{\partial f}{\partial y}\frac{dy}{d\epsilon} + \frac{\partial f}{\partial y'}\frac{dy'}{d\epsilon}\right)dx \quad ; y = \bar{y} + \epsilon\eta(x) \quad y' = \frac{dy}{dx} = 0$$

This expression can be expanded further by using the dependence on ϵ. And further by integrating the resulting expression using integration by parts and the limits $\eta(a) = \eta(b) =$

0 as the integration limits.

$$\int_a^b \Big(\eta(x)\frac{\partial f}{\partial \bar{y}} + \overbrace{\eta'(x)}^{v'}\overbrace{\frac{\partial f}{\partial \bar{y}'}}^{u}\Big)dx = 0$$

$$\downarrow \text{Integration by parts}$$

$$\int_a^b \eta(x)\Big\{\frac{\partial f}{\partial \bar{y}} - \frac{d}{dx}\frac{\partial f}{\partial \bar{y}'}\Big\}dx + \cancelto{0}{\Big(\eta(x)\frac{\partial f}{\partial \bar{y}'}\Big)\Big|_a^b} = 0$$

The final result is an integral that must be equal to zero over the integration interval.

$$\int_a^b \eta(x)\Big\{\frac{\partial f}{\partial \bar{y}} - \frac{d}{dx}\Big[\frac{\partial f}{\partial \bar{y}'}\Big]\Big\}dx = 0$$

From this expression it can be concluded that in order to guarantee that the integral is equal to zero, the function $y(x)$ must satisfy the differential equation (B.4).

$$\frac{\partial f}{\partial y} - \frac{d}{dx}\Big[\frac{\partial f}{\partial y'}\Big] = 0 \tag{B.4}$$

Even though this was a tedious derivation is is now clear that the Euler-Lagrange equation can be applied to any functional.

Appendix C

The Hamiltonian function as the total energy

The Hamiltonian and Lagrangian functions represents two different representations of the same mechanical problem. As illustrated below they are connected through the Legendre transform:

$$\mathcal{L}(\mathbf{q},\dot{\mathbf{q}}) \overset{\mathcal{H}\hat{=}\dot{\mathbf{q}}\mathbf{p}-\mathcal{L}}{\Longleftrightarrow} \mathcal{H}(\mathbf{q},\mathbf{p}) \qquad ;p\hat{=}\frac{\partial \mathcal{L}}{\partial \dot{q}}$$

However, even though the representations are equivalent with respect to describing the physics of the system, they must obviously be interpreted differently. In order to study what the Hamiltonian function represents this appendix considers a Hamiltonian function which is generated from a general form of the kinetic as a homogeneous function with respect to the velocity of degree zero, one and two as shown below.

$$T = \frac{1}{2}T^{(2)}(q,t)\dot{q}^2 + T^{(1)}(q,t)\dot{q} + T^{(0)}(q,t) \tag{C.1}$$

Note that the homogeneous properties of equation (C.1) is supported by Euler's theorem for homogeneous functions [1]. If the kinetic energy only includes the second order term it is equivalent to the systems that have been studied throughout the examples in this work. Further more, it is assumed that if the kinetic energy can be described up to order two with respect to velocity, the potential energy can equivalently be described as homogeneous of order zero and one.

$$U = U^{(1)}(q,t)\dot{q} + U^{(0)}(q,t) \tag{C.2}$$

[1] If a function is homogeneous of degree "k" with respect to the variables $\mathbf{x}$ it must satisfy the following relation $f(\lambda x_1,\ldots,\lambda x_n,\xi_1,\ldots,\xi_n) = \lambda^k f(x_1,\ldots,x_n,\xi_1,\ldots,\xi_n)$ Three relations is found by considering the total differential of the homogeneous function. In this work the interesting relation is the following: $\left(\frac{\partial f}{\partial \mathbf{x}}\right)_{\boldsymbol{\xi}} \mathbf{x} = kf$ The relation support the claim that the kinetic energy is homogeneous with respect to the degrees mentioned.

The Lagrangian takes the form shown in equation (C.3) when the expressions for the kinetic and potential energy from equation (C.1) and (C.2) is used.

$$\mathcal{L} = \frac{1}{2}T^{(2)}(q,t)\dot{q}^2 + T^{(1)}(q,t)\dot{q} + T^{(0)}(q,t) - U^{(1)}(q,t)\dot{q} - U^{(0)}(q,t) \tag{C.3}$$

The canonical momentum can now be derived obtaining the expression shown in equation (C.4).

$$p = \frac{\partial \mathcal{L}}{\partial \dot{q}} = T^{(2)}(q,t)\dot{q} + T^{(1)}(q,t) - U^{(1)}(q,t) \tag{C.4}$$

As described in section (2.2.1) the expression for the momentum in equation (C.4) must be inverted.

$$\dot{q} = [T^{(2)}(q,t)]^{-1}\left(p - T^{(1)}(q,t) + U^{(1)}(q,t)\right) \tag{C.5}$$

The result of the inversion of the momentum shown in equation (C.5) can now be used in order to derive the expression for the Hamiltonian.

$$\mathcal{H} = p\dot{q} - \left[\frac{1}{2}T^{(2)}\dot{q}^2 + T^{(1)}\dot{q} + T^{(0)} - U^{(1)}\dot{q} - U^{(0)}\right]$$

This expression has the same form as equation (C.6). The latter can be found on page 339 in Goldstein et al. (2014) in the context of an equivalent discussion on the interpretation of the Hamiltonian. The subscripted numbers in the latter equation represents the homogeneity of the Lagrangian functions making up a total Lagrangian equivalent to the expression in equation (C.3).

$$\mathcal{H} = \dot{q}_i p_i - \mathcal{L} = \dot{q}_i p_i - \left[\mathcal{L}_0(q_i,t) + \mathcal{L}_1(q_i,t)\dot{q}_j + \mathcal{L}_2(q_i,t)\dot{q}_j\dot{q}_k\right] \tag{C.6}$$

Confident that the derivation is consistent with literature the expression for the Hamiltonian is expanded as shown below. This reveals the expression in equation (C.7) as the expression for the corresponding Hamiltonian for a Lagrangian function that is made up by the general expressions for kinetic and potential energy in equation (C.1) and (C.2).

$$\mathcal{H} = \frac{1}{2}[T^{(2)}]^{-1}\left(p - T^{(1)} + U^{(1)}\right)\left(p + T^{(1)} - U^{(1)}\right) - T^{(0)} + U^{(0)} \tag{C.7}$$

This work only considers Lagrangian functions that are homogeneous of second order with respect to kinetic energy and zero with respect to potential energy. In this case, the expression in equation (C.7) reduces to the expression in equation (C.8).

$$\mathcal{H} = \frac{1}{2}[T^{(2)}]^{-1}p^2 + U^{(0)} \qquad ; p \hat{=} T^{(2)}\dot{q} \tag{C.8}$$

The final expression for a general Hamiltonian function that describes the systems that are being studied in this work can now be written as shown in equation (C.9).

$$\boxed{\mathcal{H} = T(q,t)\dot{q}^2 + U(q,t)} \tag{C.9}$$

The result of this derivation shows that the Hamiltonian functions for systems with respectively second and first order dependence on velocity in the kinetic and potential energy is equal to the total energy of the system.

Appendix D

The harmonic oscillator

This appendix is aimed at providing a deeper insight into the derivation and solution of the simple harmonic oscillator and the chain of interacting oscillators. Moreover, it considers the analytical solution of linear, first order, homogeneous ODE systems.

D.1 Solving first order linear homogeneous ODE systems using eigenvalue / eigenvector decomposition

This section considers the analytical solution of linear, homogeneous first order ODEs, i.e. systems that can be written as follows:

$$\dot{\mathbf{y}} = \mathbf{A}\mathbf{y} \tag{D.1}$$

The solution is obtained using the similarity transform which diagonalizes $\mathbf{A}$ using the eigenvector ($\mathbf{S}$) and eigenvalue matrix (Λ). $\mathbf{A} = \mathbf{S}\Lambda\mathbf{S}^{-1}$

$$\Lambda \hat{=} \begin{bmatrix} \lambda_1 & 0 & 0 \\ 0 & \ddots & 0 \\ 0 & 0 & \lambda_n \end{bmatrix} \qquad \mathbf{S} \hat{=} \left[\begin{array}{c|c|c} & & \\ \boldsymbol{\nu}_{\lambda,1} & \cdots & \boldsymbol{\nu}_{\lambda,n} \\ & & \end{array}\right]$$

The first step is to decouple the equations. This corresponds diagonalizing the coefficient matrix using the eigenvalue matrix, Λ, and eigenvector matrix, $\mathbf{S}$, to express the coefficient matrix as $\mathbf{A} = \mathbf{S}\Lambda\mathbf{S}^{-1}$.

$$\dot{\mathbf{y}} = \mathbf{S}\Lambda\mathbf{S}^{-1}\mathbf{y}$$

Using, $\mathbf{S}\mathbf{S}^{-1} = \mathbf{I}$, we obtain.

$$\cancel{\mathbf{S}}\mathbf{S}^{-1}\dot{\mathbf{y}} = \cancel{\mathbf{S}}\Lambda\mathbf{S}^{-1}\mathbf{y}$$

Using the transformation, $\mathbf{S}^{-1}\mathbf{y} \hat{=} \boldsymbol{\chi}$, the variables are changed and the equations are now decoupled.

$$\dot{\boldsymbol{\chi}} = \Lambda\boldsymbol{\chi}$$

Each equation now has the solution, $\chi_i(t) = e^{\lambda_i t}\chi_{0,i}$, which can be expressed in matrix notation using the matrix exponential, $\exp(\Lambda t)$.

$$\boldsymbol{\chi}(t) = \exp(\Lambda t)\boldsymbol{\chi}_0$$

However, the solution must be transformed back to the original variables.

$$\mathbf{S}^{-1}\mathbf{y}(t) = \exp(\Lambda t)\mathbf{S}^{-1}\mathbf{y}_0$$

Multiplying both sides by $\mathbf{S}$ yields the actual solution

$$\boxed{\mathbf{y}(t) = \mathbf{S}\exp(\Lambda t)\mathbf{S}^{-1}\mathbf{y}_0} \tag{D.2}$$

This is a general solution that is valid for any homogeneous system of first order differential equations with constant coefficients and initial conditions $\mathbf{y_0}$.

D.2 The simple harmonic oscillator

This section derives the solution of the harmonic oscillator using the result from section (D.1). The Lagrangian for the harmonic oscillator has the following form:

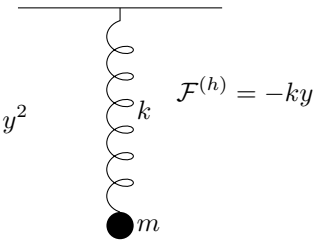

$\mathcal{F}^{(h)} = -ky$

$$\mathcal{L} \hat{=} \frac{1}{2}mv^2 - U(y) = \frac{1}{2}mv^2 - \frac{1}{2}ky^2 \quad ; U = \int_0^y k\gamma d\gamma = \frac{1}{2}y^2$$

The equations of motion are derived using the Euler-Lagrange equation shown below.

$$\frac{d}{dt}\frac{\partial \mathcal{L}(x,\dot{x})}{\partial \dot{x}} - \frac{d\mathcal{L}(x,\dot{x})}{dx} = 0$$

The result is a second order ODE that is immediately expressed as a system of first order equations such that it can be put into the framework from section (D.1).

$$\ddot{y} = -\omega_0^2 y \Leftrightarrow \begin{bmatrix}\dot{y}\\ \dot{v}\end{bmatrix} = \begin{bmatrix}0 & -1\\ \omega_0^2 & 0\end{bmatrix}\begin{bmatrix}y\\ v\end{bmatrix} \quad ; \omega_0 = \sqrt{\frac{k}{m}}$$

$$\mathbf{x} \hat{=} \begin{bmatrix}q\\ v\end{bmatrix} \qquad \dot{\mathbf{x}} \hat{=} \begin{bmatrix}\dot{q}\\ \dot{v}\end{bmatrix} \qquad \mathbf{A} \hat{=} \begin{bmatrix}0 & 1\\ -\omega_0^2 & 0\end{bmatrix}$$

The eigenvalues for the system is found by solving the following eigenvalue problem:

$$\begin{aligned}\det(\mathbf{A} - \lambda\mathbf{I}) = 0 \Leftrightarrow \det\begin{bmatrix}-\lambda & 1\\ -\omega_0^2 & -\lambda\end{bmatrix} = 0\\ \lambda^2 + \omega_0^2 = 0\\ \lambda = \pm i\omega_0\end{aligned} \tag{D.3}$$

It was expected that the resulting eigenvalues in equation (D.3) would be purely imaginary since the harmonic oscillator is a purely oscillatory system.

The matrix exponential of the eigenvalue matrix can now be expressed as follows:

$$\exp(\Lambda t) = \begin{bmatrix} e^{\lambda_1 t} & 0 \\ 0 & e^{\lambda_2 t} \end{bmatrix} = \begin{bmatrix} e^{i\omega_0 t} & 0 \\ 0 & e^{-i\omega_0 t} \end{bmatrix}$$

There is one eigenvector ($\boldsymbol{\nu}_i$) for each eigenvalue (λ_i). This means that each eigenvalue must satisfy the following equation:

$$\mathbf{A}\boldsymbol{\nu}_i = \lambda_i \boldsymbol{\nu}_i \Leftrightarrow \begin{bmatrix} 0 & 1 \\ -\omega_0^2 & 0 \end{bmatrix} \boldsymbol{\nu}_i = \lambda_i \boldsymbol{\nu}_i$$

The results are the two eigenvectors shown below.

$$v_1 = \begin{bmatrix} \imath \\ -\omega_0 \end{bmatrix} \quad ; \lambda_1 = \imath\omega_0$$

$$v_2 = \begin{bmatrix} -\imath \\ -\omega_0 \end{bmatrix} \quad ; \lambda_2 = -\imath\omega_0$$

The eigenvector matrix ($\mathbf{S}$) and the inverse can now be found:

$$\mathbf{S} = \begin{bmatrix} \imath & -\imath \\ -\omega_0 & -\omega_0 \end{bmatrix}$$

$$\mathbf{S}^{-1} = \frac{1}{2} \begin{bmatrix} -\imath & -\frac{1}{\omega_0} \\ \imath & -\frac{1}{\omega_0} \end{bmatrix}$$

The eigenvector and eigenvalues can now be used in the general solution from equation (D.2) and the solution is obtained in terms of exponential functions.

$$\mathbf{x}(t) = \begin{bmatrix} \imath & -\imath \\ -\omega_0 & -\omega_0 \end{bmatrix} \begin{bmatrix} e^{\imath\omega_0 t} & 0 \\ 0 & e^{-\imath\omega_0 t} \end{bmatrix} \begin{bmatrix} -\frac{\imath}{2} & -\frac{1}{2\omega_0} \\ \frac{\imath}{2} & -\frac{1}{2\omega_0} \end{bmatrix} \mathbf{x}_0$$

$$\mathbf{x}(t) = \frac{1}{2} \begin{bmatrix} e^{\imath\omega_0 t} + e^{-\imath\omega_0 t} & -\frac{\imath}{\omega_0}(e^{\imath\omega_0 t} - e^{-\imath\omega_0 t}) \\ \imath\omega_0(e^{\imath\omega_0 t} - e^{-\imath\omega_0 t}) & e^{\imath\omega_0 t} + e^{-\imath\omega_0 t} \end{bmatrix} \mathbf{x}_0$$

In order to obtain a more familiar formulation, the solution can be rewritten using the following trigonometric relations:

$$2\cos(x) = e^{\imath x} + e^{-\imath x} \qquad 2\imath\sin(x) = e^{\imath x} - e^{-\imath x}$$

The final result is the classic solution of the harmonic oscillator shown below.

$$\mathbf{x}(t) = \begin{bmatrix} \cos(\omega_0 t) & \frac{1}{\omega_0}\sin(\omega_0 t) \\ -\omega_0 \sin(\omega_0 t) & \cos(\omega_0 t) \end{bmatrix} \mathbf{x}_0$$

$$\Updownarrow$$

$$\boxed{\begin{bmatrix} q(t) \\ v(t) \end{bmatrix} = \begin{bmatrix} q^o \cos(\omega_0 t) + v^o \frac{1}{\omega_0}\sin(\omega_0 t) \\ v^o \cos(\omega_0 t) - q^o \omega_0 \sin(\omega_0 t) \end{bmatrix}}$$

D.3 Horizontal chain of n-coupled oscillators

This section considers a chain of coupled harmonic oscillators as shown in the figure below.

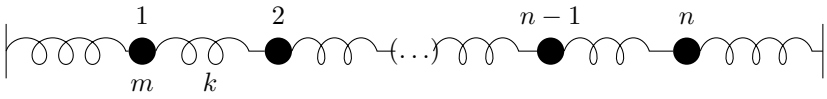

In order to obtain the analytical solution to this system, however, it is necessary to perform an analysis on the equations of motion. Subsection (D.3.1) expresses the equations of motion for the system as a homogeneous system of second order ODEs. This system can be solved using the strategy from section (D.1), however, since the eigenvalue problem involves solving a polynomial equation the system quickly turns into a numerical problem. On the other hand, as shown in subsection (D.3.2) the solution of the second order ODE can be obtained analytically for systems of any size by assuming small angles.

D.3.1 Rewriting a non-homogeneous system as a homogeneous system using the static equilibrium

The potent energy that is stored in each spring, which makes the total potential energy take the form of a sum and the Lagrangian is formulated as shown below.

$$\mathcal{L} = \frac{1}{2}m\dot{\mathbf{x}}^T\dot{\mathbf{x}} - \sum_{i=0}^{n} k\frac{1}{2}(x_{i+1} - x_i)^2 \quad ; U = \int_{x_i}^{x_{i+1}} k\xi d\xi = \sum_{i=0}^{n} k\frac{1}{2}(x_{i+1} - x_i)^2$$

Note that the left and right wall are included in the summation, such that when the Euler-Lagrange equations are applied they must be treated separately from the internal mass points. The result is the following system of n second order ODEss:

$$\begin{aligned}
\ddot{x}_j &= \frac{k}{m}(x_2 - x_1) - \frac{k}{m}(x_1 - x_0) \\
\ddot{x}_j &= \frac{k}{m}(x_{j+1} - x_j) - \frac{k}{m}(x_j - x_{j-1}) \quad ; j = 2 \dots n-1 \\
\ddot{x}_j &= \frac{k}{m}(x_{n+1} - x_n) - \frac{k}{m}(x_n - x_{n-1})
\end{aligned}$$

By using the tridiagonal matrix defined below, the system can be expressed in matrix notation shown in equation (D.4).

$$\mathbf{T} = \begin{bmatrix}
2 & -1 & & & \\
-1 & 2 & -1 & & \\
 & -1 & 2 & -1 & \\
 & & \ddots & \ddots & \ddots \\
 & & & -1 & 2
\end{bmatrix}$$

$$\ddot{\mathbf{x}} = -\omega_0^2 \mathbf{T}\mathbf{x} + \omega_0^2(x_0\mathbf{e}_1 + x_{n+1}\mathbf{e}_n) \quad ;\omega_0 = \sqrt{\frac{k}{m}} \tag{D.4}$$
$$\mathbf{e}_1 = [1\ 0\ \ldots]^T \quad \mathbf{e}_n = [0\ \ldots\ 1]^T \quad \mathbf{y} = [y_1\ \ldots\ y_n]^T$$

This system in equation (D.4) is not homogeneous, however by considering the static equilibrium ($\ddot{\mathbf{x}} = 0$) shown below it can be rewritten as a homogeneous system.

$$\mathbf{x}^0 = x_0\mathbf{T}^{-1}\mathbf{e}_1 + x_{n+1}\mathbf{T}^{-1}\mathbf{e}_n$$

The system is set to have length $L = x_{n+1}^0$ and consequently the position of the left wall becomes: $x_0^0 = 0$. The static solution now becomes:

$$\mathbf{x}^0 = x_{n+1}\mathbf{T}^{-1}\mathbf{e}_n \quad ;\mathbf{T}^{-1}\mathbf{e}_n = \frac{j}{N+1}$$

The recursive relation above defines the elements of the inverted tridiagonal matrix and it leads to the following analytical expression for the static equilibrium distribution of the mass points:

$$\mathbf{x}^0 = L\frac{j}{N+1} \quad ;j = 1\ldots n \tag{D.5}$$

From the recursive expression in equation (D.5) is s clear that the distance between the mass points are equal throughout.

In order to express the system in equation (D.4) as a homogeneous ODE system it is expressed using the deviation from the equilibrium, i.e. the following variable is introduced:

$$\mathbf{q} \hat{=} \mathbf{x} - \mathbf{x}^0$$

The equation below shows what happens when the deviation variable is introduced in the non homogeneous system in equation (D.4).

$$\ddot{\mathbf{q}} = -\omega_0^2\mathbf{T}\mathbf{q} + \omega_0^2\mathbf{T}(\underbrace{x_0\mathbf{T}^{-1}\mathbf{e}_1 + x_{n+1}\mathbf{T}^{-1}\mathbf{e}_n}_{\mathbf{x}^0} - \mathbf{x}^0)$$

The final expression in equation (D.6) is the homogeneous version of the equations of motion for the harmonic chain.

$$\boxed{\ddot{\mathbf{q}} = -\omega_0^2\mathbf{T}\mathbf{q}} \tag{D.6}$$

Note that it is a requirement that the walls are stationary, i.e. $v_0 = v_{n+1} = 0$. This assumption was introduced very silently when the equations of motion were derived from the Lagrangian.

D.3.2 Analytical solution of the harmonic chain for small angles

Equation (D.6) is a system of n-coupled, linear, homogeneous, ordinary differential equations. The solution for one oscillator was derived in section (D.3). The basis for the solution of the coupled system is that the colluded system can be approximated as the harmonic solution with the eigenvalue (ω_p).

$$q_j = A_j e^{\imath\omega_p t} \quad ; j = 1 \dots n \tag{D.7}$$

If the elements of the tridiagonal matrix are stratified, the solution the relationship between the harmonic and the coupled solution must be expressed as a linear combination shown below for one equation.

$$-\omega_p^2 A_j = \omega_0^2 (A_{j-1} - 2A_j + A_{j+1}) \tag{D.8}$$

At the boundary, i.e. the left wall $q_0 = 0$, a solution satisfying the equation for the coefficients is the following:

$$A_j = a_j \sin(j\theta) \quad ; j = 0, \dots, n+1$$

The solution can be adapted to obey the second boundary as well by determining θ such that the function is equal to zero when $j = n + 1$.

$$\begin{gathered} \sin([n+1]\theta) = 0 \\ \Downarrow \\ [n+1]\theta = p\pi \quad ; p = 1, \dots, n \\ \theta = \frac{p\pi}{n+1} \end{gathered}$$

The harmonic coefficient (ω_p) can now be found using equation (D.7) and the assumed solution as shown below.

$$q_j = a_j \sin(j\theta) e^{\imath\omega_p t} \quad : \ddot{q}_j = \omega_0^2 \Big(q_{j+1} + q_{j-1} - 2q_j \Big)$$

By differentiating the solution the following expression is obtained:

$$-\omega_p^2 a_j sin(j\theta) = \omega_0^2 \Big\{ a_j \sin([j-1]\theta - 2a_j \sin(j\theta)) + a_j \sin([j+1]\theta) \Big\}$$

This expression can be rewritten with the result shown below by successively using the trigonometric relations before demanding that the harmonic coefficient must be positive.

$$\omega_p = 2\omega_0 |\sin\left(\frac{\theta}{2}\right)| \quad ; \quad \begin{matrix} \sin(x \pm y) = \sin(x)\cos(y) \pm \sin(y)\cos(x) \\ 2\sin^2(x) = 1 - \cos(2x) \end{matrix}$$

The reason why the harmonic coefficient must be positive can be understood from the eigenvalue problem of the harmonic oscillator. In order to ensure that the eigenvalues are always imaginary, the coefficient in the eigenvalue problem must be positive.

The final expression for the harmonic coefficient is simply found by inserting the requirement that satisfied the solution right boundary, i.e. $\theta = \frac{p\pi}{n+1}$.

$$\omega_p = 2\omega_0 |\sin\left(\frac{p\pi}{2(n+1)}\right)| \qquad ; p = 1, \ldots, n \tag{D.9}$$

The expression for ω_p in equation (D.9) is known as a harmonic series. This means that the solution is a series of super positioned harmonic waves, i.e. a linear combination of solutions of the harmonic oscillator. The number of harmonic frequencies p are conveniently chosen to be the same number as the number of oscillators on the chain. This leads to the following preliminary solution satisfying the boundaries $q_0 = q_{n+1} = 0$.

$$q_j^{(p)} = a_j^{(p)} \sin(j\frac{p\pi}{n+1}) e^{\imath\omega_p t} \qquad ; p = 1 \ldots n \qquad ; j = 0, \ldots, n+1$$

In order to ensure that the solution is real, the coefficients $a_j^{(p)}$ and $e^{\imath\omega_p t}$ are expressed as trigonometric functions.

$$\begin{aligned} a_j^{(p)} &= \bar{a}_j^{(p)}(\cos(\alpha^{(p)}) + i\sin(\alpha^{(p)})) \\ e^{\imath\omega_p t} &= \cos(\omega_p t) + \imath\sin(\omega_p t) \end{aligned}$$

The real part of the coefficients can now be extracted according to $\mathbb{R}(x+\imath y) = \frac{1}{2}(x+\imath y + x-\imath y)$. Finally, the general form of the solution is obtained using yet another trigonometric relation:

$$\cos(a \pm b) = \cos(a)\cos(b) \mp \sin(a)\sin(b)$$

$$q_j^{(p)} = \bar{a}_j^{(p)} \sin\left(j\frac{p\pi}{n+1}\right) \cos(\omega_p t + \alpha^{(p)}) \qquad ; p = 1, \ldots, n$$

The solution has two degrees of freedom $\bar{a}_j^{(p)}$ and $\alpha^{(p)}$, corresponding respectively to amplitude and phase shift. To summarize the solution for the j-th term of the series with the corresponding eigenfrequency are:

$$\boxed{\begin{aligned} q_j^{(p)} &= \sum_{p=1}^{n} \bar{a}_j^{(p)} \sin\left(j\frac{p\pi}{n+1}\right) \cos(\omega_p t + \alpha^{(p)}) \\ \omega_p &= 2\omega_0 |\sin\left(\frac{p\pi}{2(n+1)}\right)| \qquad ; p = 1, \ldots, n \end{aligned}} \tag{D.10}$$

Appendix E

MatLab: Symplectic Integrators

```
function SymplecticIntegration

%  /|         m       k                          |\
%  /|----O----O----O----(...)----O----O----O-----|\
%  /|    1                                 n     |\
%
%% Summary:
% Slow function simulating a horisontal chain of
% harmonic oscillators using various integration techniques.
% Integration algoritm is selected "on/off" using "Integration"
%
% Note that the form of this script has no output function.
% This script serves as an example of the implementation of
% symplectic methods, however they are functional and can be
% used by following the intstruction under 'NOTE'.
%
% The following url contains a complete and faster implementation
% http://folk.ntnu.no/sigveka/Master_Thesis/MatLab/Magnets/
%
%% Author:       Sigve Karolius
%% Organization: Department of Chemical Engineering, NTNU, Norway
%% Contact:      sigveka@stud.ntnu.no
%% license:      GPLv3
%% requires:     MatLab R2013a or higher
%% since:        June 2014
%% NOTE:
% The integration methods can be used on other problems using
%      'CTRL+c' the desired method -> 'CTRL+v' in your script
%
% The input to the integrators must be the following:
% int      : t_max maximum integration
% scalar   : h     step size
% scalar   : nu=h
% c-vector: y_0   initial conditions
%
% However, the problem MUST be Hamiltonian and on the form:
%      dot(y)  = v
%      dot(v)  = f(y) ;where f(y) = dv = - dLdy
%
% The only ODE that the integrator can then be formulated as:
% function [dvdt] = dv(y)
%    dvdt = *some-function*
% end
```

```
44
45  Integration = struct( ... % Turn integration algoritms on  or off
46            'SymplecticTrigonometricRKN', 'off', ... % 3.rd order
47              'SymplecticExponentialRKN', 'off', ... % 2.nd order
48                      'ExponentialRKN'  , 'off', ... % 3.rd order
49                      'SymplecticRKN'   , 'off', ... % 3.rd order
50                      'StandardRKN'     , 'off', ... % 4.th order
51                      'Leapfrog'        , 'off', ... % 2.nd order
52                      'Ruth'            , 'off'  ... % 3.rd order
53                      );
54
55  t_max  = 1000;  % time
56  m      = 0.12;  % mass
57  k      = 16.25; % 'Spring' constant
58  K      = 0.1 ;  % scale step size (h = K * 1/lambda_min)
59  N      = 7;     % Number of oscillators
60  L      = 1;     % Langth
61
62  %-------------------Static equilibrium -------------------------%
63  y_eq = zeros(N,1);
64  for i = 1 : N
65      y_eq(i) = L * ( i/(N+1) );
66  end
67  w        = sqrt(k/m); % Ratio used in the equations of motion
68  %.............................................................%
69
70  %------------------- Linear     system -------------------------%
71  dHdp  = eye(N);
72  dHdq  = w^2*(2*diag(ones(1,N))...
73         -diag(ones(1,N-1),-1)  ...
74         -diag(ones(1,N-1),1));
75  z     = zeros(N);
76  A     = [z,dHdp;-dHdq,z];
77  [S,D] = eig(A);
78  s     = inv(S);
79  eigen = D*ones(2*N,1);
80  %.............................................................%
81
82  %------------------ Integration Interval ----------------------%
83  h      = K/max(abs(eigen));% step size: 1% of maximum frequency
84  t_samp = 5/min(abs(eigen));% start sampling
85  Nstep  = t_max/h;
86  t_span = [0 t_max]; % Demanded by ode15s and ode45
87  nu     = h;         % exponential approximation
88  %.............................................................%
89
90  %------------------ Initial conditions -------------------------%
91  levels = linspace(0,L,N+2)';
92  % equilibrium positions & zero velocities
93  %y_0 = [y_eq(1:end); zeros(N,1)]
94  % equidistant positions & random velocities
95  %y_0 = [levels(2:N+1); 0.5*(rand(N,1)-0.5)];
96  % random positions & random velocities
97  %y_0 = [sort(L*rand(N,1)); 0.5*(10.5*rand(N,1)-0.5)] %H=3
98  % random positions & zero velocities
99  %y_0 = [sort(L*8*rand(N,1)); zeros(N,1)]
100 %y_0 = [sort(L*32*rand(N,1)); zeros(N,1)]
101 % equilibrium positions & random velocities
102 y_0  = [y_eq;rand(N,1)]
103 %.............................................................%
104
105 %---- ODE and function describing the change wrt. position -----%
106 function [ dvdt ] = dv(q) % dv = - dHdq
107     dHdq = -w^2*( diff([0;q;L]));
108     dvdt  = dHdq(1:end-1) - dHdq(2:end);
109 end
110 %.............................................................%
111
```

```
%%%%%%%%%%%%%%%%%%%%%%%%%%%%%%%%%%%%%%%%%%%%%%%%%%%%%%%%%%%%%%%%%%%%%%%
%                           Integrators                                  %
%%%%%%%%%%%%%%%%%%%%%%%%%%%%%%%%%%%%%%%%%%%%%%%%%%%%%%%%%%%%%%%%%%%%%%%
% In all algorithms:
%
%            q1 ... qn | p1 ... pn
%           ___________|___________
%        t1|
%        t2|
%    y = . |
%        . |
%        . |
%        tn|
%
% q_temp,v_temp: c-vector [Nx1] overwritten in integration step
% t            : c-vector [length(t_span) x 1]
% count        : counter
%
%--------------------------------------------------------------------%
%% Symplectic Trigonometric RKN (Third order)
if strcmpi(Integration.SymplecticTrigonometricRKN, 'on')
    y    = zeros(length(h:h:t_max),2*N);
    t    = zeros(length(h:h:t_max), 1 );
    % Coefficients
        bb2 = [-0.18799161879915978201;   ...
                0.014823031830119705447;  ...
               -0.000656763569898881967 4; ...
                0.000050089992619037566 59;...
               -2.2837596032644413e-6;    ...
                1.6950437269127458e-7];
        bb3 = [ 0.635066644920623115;     ...
               -0.014823031830119705 45;  ...
               -0.001438399281608581791;  ...
                0.000082794662707730077 7; ...
               -1.4655145815655087e-6;    ...
                2.9118114430067654e-8];
        cc3 = [ 0.731669904218240075 04;  ...
               -0.011642558630267127 75;  ...
               -0.000347727955728088 74;  ...
               -0.000025007793862487023 2; ...
               -5.568816130391094e-7;     ...
               -5.801982609741059e-8];
        c3=0;
        b2=0;
        b3=0;
        c = 1; % counter to access element in coefficient vector
        for u = 0 : 2 : 10
            z     = (nu*h)^u;
            b2    = b2 + bb2(c)*z      ;
            b3    = b3 + bb3(c)*z      ;
            c3    = c3 + cc3(c)*z      ;
            c = c+1;
        end
        c1  = 0;
        c2  = -0.18799161879915978201;
        b1  =  0.552924973878536667  ;
        B1  = b1;
        B2  = b2*(1-c2);
        B3  = b3*(1-c3);
        a21 = b1*c2;
        a31 = b1*c3;
        a32 = b2*(c3-c2);
    % Preparing Integration
      count = 1;
      y(count,:) = y_0;
      q_temp = y_0(1:N);
      v_temp = y_0(N+1:2*N);
    % Integrate
```

```
    for T = h : h : t_max;
        % Determine coefficients
        k1 = dv(q_temp);
        k2 = dv(q_temp + h*c2*v_temp+ h^2*a21*k1);
        k3 = dv(q_temp + h*c3*v_temp+ h^2*(a31*k1+a32*k2));
        % Perform numerical step
        q_temp = q_temp + h*v_temp + h^2*(B1*k1 + B2*k2 + B3*k3);
        v_temp = v_temp + h*             (b1*k1 + b2*k2 + b3*k3);
        % Save
        t(count)    = T        ;
        y(count,:) = [q_temp',v_temp'];
        count      = count + 1;
    end
    Analyze(y_0,y,t,'SymplecticTrigonometric_RKN');
    % Free memory
    clear t qp Y1 Y2 B1 B2 b1 b2 c2 alpha32 alpha31 alpha21  ...
         k1 k2 k3 q_temp v_temp c3 B3 b3
end
%
%.....................................................................%
%---------------------------------------------------------------------%
%% Symplectic and Exponential RKN
if strcmpi(Integration.SymplecticExponentialRKN, 'on')
    y    = zeros(length(h:h:t_max),2*N);
    t    = zeros(length(h:h:t_max), 1 );
    % coefficients
    if abs(nu*h) <= 0.1
        Alpha = [1/2;              ...
                 1/24;             ...
                 1/720;            ...
                 1/40320;          ...
                 1/3628800;        ...
                 1/479001600;      ...
                 1/87178291200;    ...
                 1/20922789888000];
        Gamma = [1;                ...
                 1/6;              ...
                 1/120;            ...
                 1/5040;           ...
                 1/362880;         ...
                 1/39916800;       ...
                 1/6227020800;     ...
                 1/1307674368000];
        bb2   = [1/2;              ...
                -1/24;             ...
                 1/240;            ...
                -17/40320;         ...
                 31/725760;        ...
                -691/159667200;    ...
                 5461/12454041600; ...
                -929569/20922789888000];
        gamma = 0 ;
        b2    = 0 ;
        alpha = 0 ;
        c = 1; % counter to access element in coefficient vector
        for u = 0 : 2 : 14
            z     = (nu*h)^u          ;
            gamma = gamma  + Gamma(c)*z;
            b2    = b2     + bb2(c)*z  ;
            alpha = alpha + Alpha(c)*z ;
            c = c+1                   ;
        end
    else
        gamma = sinh(nu*h)/(nu*h) ;
        b2    = sinh(nu*h)/(nu*h*(cosh(nu*h)+1));
        alpha = (cosh(nu*h)-1)/(nu*nu*h*h) ;
    end
    B1 = alpha;
```

```
248     B2 = 0    ;
249     g1 = 1    ;
250     g2 = gamma;
251     g3 = 1    ;
252     c2 = 1    ;
253     b1 = b2   ;
254     % Variables used by the integrator
255     count = 1;
256     q_temp = y_0(1:N);
257     v_temp = y_0(N+1:2*N);
258     k2 = dv(0,q_temp);
259     for T = h : h : t_max;
260         % Evaluate coefficients
261         k1 = k2; % FSAL assumption
262         k2 = dv(q_temp+c2*gamma*h*v_temp+h^2*alpha*k1);
263         % Perform numerical step
264         q_temp = g1*q_temp +g2*h*v_temp + h^2*(B1*k1+B2*k2);
265         v_temp = g3*v_temp +h*(b1*k1+b2*k2);
266         % Save current step
267         t(count)    = T               ;
268         y(count,:)  = [q_temp',v_temp'];
269         count       = count + 1       ;
270     end
271     Analyze(y_0,y,t,'Symplectic_Exponential_RKN');
272     % Free memory
273     clear t qp Y1 Y2 g1 g2 g3 B1 B2 b1 b2 c2 alpha Alpha ...
274           q_temp v_temp Gamma gamma BB2
275 end
276 %
277 %.....................................................................%
278 %---------------------------------------------------------------------%
279 %% Exponential RKN (Third order)
280 if strcmpi(Integration.ExponentialRKN, 'on')
281     y    = zeros(length(h:h:t_max),2*N);
282     t    = zeros(length(h:h:t_max), 1 );
283     c2   = 2/3;
284     % Coefficients
285         Alpha = [2/9;                          ...
286                  2/243;                        ...
287                  4/32805;                      ...
288                  2/2066715;                    ...
289                  4/837019575;                  ...
290                  4/248594813775;               ...
291                  8/203599152481725;            ...
292                  2/27485885585032875];
293         Gamma = [1;                            ...
294                 2/27;                          ...
295                 2/1215;                        ...
296                 4/229635;                      ...
297                 2/18600435;                    ...
298                 4/9207215325;                  ...
299                 4/3231732579075;               ...
300                 8/3053987287225875];
301         bb1 = [1/4;                            ...
302               -1/144;                          ...
303                11/38880;                       ...
304               -731/58786560;                   ...
305                589/1058158080;                 ...
306               -471953/18856376985600;          ...
307                14913991/13237176643891200;     ...
308               -307687339/6065033662291968000];
309         bb2 = [3/4;                            ...
310                 1/144;13/38880;                ...
311                -709/58786560;                  ...
312                 587/1058158080;                ...
313                -471487/18856376985600;         ...
314                 14910353/13237176643891200;    ...
315                -3384354151/667153702852116480];
```

```
316         BB1 = [1/4;                          ...
317                -17/2160;                     ...
318                 55/163296;                   ...
319                -13231/881798400;             ...
320                 117673/174596083200;         ...
321                -780698467/25738954585344000;...
322                 34511669/25270973592883200; ...
323                -1046191876349/17012419422728970240000];
324         BB2 = [1/4;                          ...
325               -13/2160;                      ...
326                271/816480;                   ...
327               -1877/125971200;               ...
328                23497/34919216640;            ...
329               -780383783/25738954585344000; ...
330                379590131/277980709521715200;...
331               -95105958011/1546583583884451840000];
332         gamma  =0;
333         b1     =0;
334         b2     =0;
335         B1     =0;
336         B2     =0;
337         alpha  =0;
338         c = 1; % counter to access element in coefficient vector
339     for u = 0 : 2 : 14
340         z     = (nu*h)^u;
341         gamma = gamma  + Gamma(c)*z;
342         b1    = b1 + bb1(c)*z      ;
343         b2    = b2 + bb2(c)*z      ;
344         B1    = B1 + BB1(c)*z      ;
345         B2    = B2 + BB2(c)*z      ;
346         alpha = alpha + Alpha(c)*z ;
347         c = c+1;
348     end
349
350     % Variables used by the integrator
351     count = 1;
352     y(count,:) = y_0;
353     % Integration
354     q_temp = y_0(1:N);
355     v_temp = y_0(N+1:2*N);
356     for T = h : h : t_max;
357         % evaluate coefficients
358         k1 = dv(T,q_temp);
359         k2 = dv(T,q_temp+h*gamma*c2*v_temp+h*h*alpha*k1);
360         % perform numerical step
361         q_temp = q_temp + h * v_temp + h*h*( B1 * k1 + B2 * k2 );
362         v_temp = v_temp + h* ( b1 * k1 + b2 * k2 );
363         % Save step
364         t(count)    = T        ;
365         y(count,:)  = [q_temp',v_temp'];
366         count      = count + 1;
367     end
368     Analyze(y_0,y,t,'Exponential_RKN');
369     % Free memory
370     clear t Y1 Y2 g1 g2 g3 B1 B2 b1 b2 alpha Alpha Gamma  ...
371           BB1 BB2 c z c2 q_temp v_temp y gamma bb1
372 end
373 %
374 %.....................................................................%
375 %---------------------------------------------------------------------%
376 %% Third order symplectic RKN (Third order)
377 if strcmpi(Integration.SymplecticRKN, 'on')
378     y    = zeros(length(h:h:t_max),2*N);
379     t    = zeros(length(h:h:t_max), 1 );
380     c2 = 2/3;
381     c3 = 0;
382     b1 = 7/24;
383     b2 = 3/4;
```

```
    b3 =-1/24;
    B1 = 7/24;
    B2 = 1/4;
    B3 =-1/24;
    a21= 7/36;
    a31= 0;
    a32=-1/2;
    count = 1;
    y(count,:) = y_0;
    q_temp = y_0(1:N);
    v_temp = y_0(N+1:2*N);
    for T = h : h : t_max;
        % Determine coefficients
        k1 = dv(T,q_temp);
        k2 = dv(T+c2*h,q_temp+ h*c2*v_temp+ h^2*a21*k1);
        k3 = dv(T+c3*h,q_temp+ h*c3*v_temp+ h^2*(a31*k1+a32*k2));
        % Perform numerical step
        q_temp = q_temp + h*v_temp + h^2*(B1*k1 + B2*k2 + B3*k3);
        v_temp = v_temp + h*              (b1*k1 + b2*k2 + b3*k3);
        % Save
        t(count)    = T;
        y(count,:) = [q_temp',v_temp'];
        count      = count + 1;
    end
    Analyze(y_0,y,t,'SymplecticTrigonometric_RKN');
    % Free memory
    clear t qp Y1 Y2 B1 B2 b1 b2 c2 alpha32 alpha31 alpha21  ...
         k1 k2 k3 q_temp v_temp c3 B3 b3
end
%
%.....................................................................%
%---------------------------------------------------------------------%
%% Standard RKN (fourth order)
if strcmpi(Integration.StandardRKN, 'on')
    % Create solution vectors
    y    = zeros(length(h:h:t_max),2*N);
    t    = zeros(length(h:h:t_max), 1 );
    % Coefficients
    c2 = 0.5;
    c3 = 1;
    alpha21= 1/8;
    alpha31= 0;
    alpha32=1/2;
    B1 = 1/6;
    B2 = 1/3;
    B3 = 0  ;
    b1 = 1/6;
    b2 = 4/6;
    b3 = 1/6;
    % Initiate integration
    count  = 1;
    q_temp = y_0(1:N);
    v_temp = y_0(N+1:2*N);
    for T = h : h : t_max;
        %Determine coefficients
        k1 = dv(T,q_temp);
        k2 = dv(T+c2*h,q_temp+h*c2*v_temp+h^2*alpha21*k1);
        k3 = dv(T+c3*h,q_temp+h*c3*v_temp+h^2*(alpha32*k2));
        % Perform numerical increment
        q_temp = q_temp + h * v_temp + h *h* (B1*k1+B2*k2+B3*k3);
        v_temp = v_temp + h * ( b1*k1 + b2*k2 +b3*k3);
        % Save
        t(count)    = T        ;
        y(count,:)  = [q_temp',v_temp'];
        count       = count + 1;
    end
    Analyze(y_0,y,t,'Standard_RKN');
    % Free memory
```

```
    clear t qp Y1 Y2 B1 B2 b1 b2 c2 alpha32 alpha31 alpha21 ...
         k1 k2 k3 q_temp v_temp c3 B3 b3
end
%
%.....................................................................%
%---------------------------------------------------------------------%
%% Leapfrog
if strcmpi(Integration.Leapfrog, 'on')
    y    = zeros(length(h:h:t_max),2*N) ;
    t     = zeros(length(h:h:t_max), 1 );
    count = 1                            ;
    y(count,:) = y_0                     ;
    q_temp = y_0(1:N)              ;
    v_temp = y_0(N+1:2*N)          ;
    for T = h : h : t_max          ;
      % Integration
      q_temp = q_temp + h *0.5 *    v_temp  ;
      v_temp = v_temp + h       * dv(q_temp) ;
      q_temp = q_temp + h *0.5 *    v_temp  ;
      % Saving the calculation and preparing for next itteration
      t(count,1)        = T              ;
      y(count,:)     = [q_temp',v_temp'];
    end
    Analyze(y_0,y,t,'Leapfrog');
    % Free memory
    clear T count y v_temp q_temp t
end
%
%.....................................................................%
%---------------------------------------------------------------------%
%% Ruth
if strcmpi(Integration.Ruth, 'on')
    y     = zeros(length(h:h:t_max),2*N);
    t     = zeros(length(h:h:t_max), 1 );
    c1 = 7/24;
    c2 = 3/4 ;
    c3 =-1/24;
    d1 = 2/3 ;
    d2 =-2/3 ;
    d3 = 1   ;
    count = 1;
    y(count,:) = y_0;
    q_temp = y_0(1:N)    ;
    v_temp = y_0(N+1:2*N);
    for T = h : h : t_max;
      % Intermediate variables
      P1 = v_temp + c1 * h * dv(q_temp);
      Q1 = q_temp + d1 * h *    P1     ;
      P2 = P1     + c2 * h * dv(Q1)    ;
      Q2 = Q1     + d2 * h *    P2     ;
      % Algoritm calculating next step
      v_temp = P2 + c3 * h * dv(Q2)    ;
      q_temp = Q2 + d3 * h *   v_temp  ;
      % Saving the calculation and preparing for next itteration
      t(count,1)        = T              ;
      y(count,:)       = [q_temp',v_temp'] ;
      count      = count + 1;
    end
    Analyze(y_0,y,t,'Ruth');
    % Free memory
    clear T count y v_temp q_temp t c1 c2 c3 d1 d2 d3 P1 P2 Q1 Q2
end
%.....................................................................%

end
```